

***Summary Results for  
Brine Migration  
Modeling Performed by  
LANL, LBNL, and SNL  
for the UFD Program***

**Fuel Cycle Research & Development**

***Prepared for  
U.S. Department of Energy  
Used Fuel Disposition Campaign  
Kristopher L. Kuhlman  
Sandia National Laboratories***

***September 25, 2014  
FCRD-UFD-2014-000071  
SAND2014-18217 R***



#### **DISCLAIMER**

This information was prepared as an account of work sponsored by an agency of the U.S. Government. Neither the U.S. Government nor any agency thereof, nor any of their employees, makes any warranty, expressed or implied, or assumes any legal liability or responsibility for the accuracy, completeness, or usefulness, of any information, apparatus, product, or process disclosed, or represents that its use would not infringe privately owned rights. References herein to any specific commercial product, process, or service by trade name, trade mark, manufacturer, or otherwise, does not necessarily constitute or imply its endorsement, recommendation, or favoring by the U.S. Government or any agency thereof. The views and opinions of authors expressed herein do not necessarily state or reflect those of the U.S. Government or any agency thereof.

Prepared by:  
Sandia National Laboratories  
Albuquerque, New Mexico 87185

Sandia National Laboratories is a multi-program laboratory managed and operated by Sandia Corporation, a wholly owned subsidiary of Lockheed Martin Corporation, for the U.S. Department of Energy's National Nuclear Security Administration under contract DE-AC04-94AL85000.



Revision 2  
12/20/2012


**APPENDIX E**

**FCT DOCUMENT COVER SHEET <sup>1</sup>**

Name/Title of Deliverable/Milestone/Revision No. Summary Results for Brine Migration Modeling Performed by LANL, LBNL, and SNL for the Used Fuel Disposition Program / M2FT-14SN0818011 / rev 0

Work Package Title and Number DR Salt R&D - SNL (FT-14SN081801)

Work Package WBS Number 1.02.08.18

Responsible Work Package Manager Christi Leigh   
(Name/Signature)

Date Submitted

Quality Rigor Level for Deliverable/Milestone <sup>2</sup>	<input checked="" type="checkbox"/> QRL-3	<input type="checkbox"/> QRL-2	<input type="checkbox"/> QRL-1 Nuclear Data	<input type="checkbox"/> Lab/Participant QA Program (no additional FCT QA requirements)
--	---	--------------------------------	---	---

This deliverable was prepared in accordance with Sandia National Laboratories  
(Participant/National Laboratory Name)

QA program which meets the requirements of  
 DOE Order 414.1     NQA-1-2000     Other

**This Deliverable was subjected to:**


Technical Review

**Technical Review (TR)**

**Review Documentation Provided**

- Signed TR Report or,
- Signed TR Concurrence Sheet or,
- Signature of TR Reviewer(s) below

**Name and Signature of Reviewers**

Ernie Hardin 

---



---

Peer Review

**Peer Review (PR)**

**Review Documentation Provided**

- Signed PR Report or,
- Signed PR Concurrence Sheet or,
- Signature of PR Reviewer(s) below

---



---

**NOTE 1:** Appendix E should be filled out and submitted with the deliverable. Or, if the PICS:NE system permits, completely enter all applicable information in the PICS:NE Deliverable Form. The requirement is to ensure that all applicable information is entered either in the PICS:NE system or by using the FCT Document Cover Sheet.

**NOTE 2:** In some cases there may be a milestone where an item is being fabricated, maintenance is being performed on a facility, or a document is being issued through a formal document control process where it specifically calls out a formal review of the document. In these cases, documentation (e.g., inspection report, maintenance request, work planning package documentation or the documented review of the issued document through the document control process) of the completion of the activity, along with the Document Cover Sheet, is sufficient to demonstrate achieving the milestone. If QRL 1, 2, or 3 is not assigned, then the Lab / Participant QA Program (no additional FCT QA requirements) box must be checked, and the work is understood to be performed and any deliverable developed in conformance with the respective National Laboratory / Participant, DOE or NNSA-approved QA Program.

## Acknowledgments

The author thanks Lupe Argüello and Frank Hansen from Sandia; Phil Stauffer and Florie Caporuscio from Los Alamos; Jonny Rutqvist and Laura Blanco Martín from Berkeley; and Jörg Mönig, Jens Wolf, and Anke Schneider from GRS for providing reports and answering questions about their recent salt-related modeling work.

The author thanks Bwalya Malama, Dave Sassani, Ernie Hardin, Frank Hansen, and colleagues at the fifth US/German Workshop on Salt Repository Research, Design, and Operation for discussions on facets of the topic of brine migration in salt. The author thanks Heeho Park and Glenn Hammond for assistance with the PFLOTRAN simulations.

Finally, the author thanks Ernie Hardin for his detailed and insightful review of the entire report.

# Summary

This report summarizes laboratory and field observations and numerical modeling related to coupled processes involving brine and vapor migration in geologic salt, focusing on recent developments and studies conducted at Sandia, Los Alamos, and Berkeley National Laboratories. Interest into the disposal of heat-generating waste in salt has led to interest into water distribution and migration in both run-of-mine crushed and intact geologic salt.

Ideally a fully coupled thermal-hydraulic-mechanical-chemical simulation is performed using numerical models with validated constitutive models and parameters. When mechanical coupling is not available, mechanical effects are prescribed in hydraulic models as source, boundary, or initial conditions. This report presents material associated with developing appropriate initial conditions for a non-mechanical hydrologic simulation of brine migration in salt. Due to the strong coupling between the mechanical and hydrologic problems, the initial saturation will be low for the excavation disturbed zone surrounding the excavation.

Although most of the material in this report is not new, the author hopes it is presented in a format making it useful to other salt researchers.

This report (FCRD-UFD-2014-000071) satisfies a Level-2 milestone (M2FT-14SN0818011) in the DOE-NE Used Fuel Disposition Campaign in work package “*DR Salt R&D – SNL*” under WBS 1.02.08.18.

This report (particularly Section 5) also satisfies a Level-4 milestone titled “Summarize current THMC modeling results supporting testing of mechanical and hydrologic behavior of the near-field host rock surrounding excavations” (M4FT-14SN0818053) in the “*Salt R&D to Support Field Studies – SNL*” work package under the same WBS.

# Contents

<b>List of Figures</b>	<b>vii</b>
<b>List of Tables</b>	<b>ix</b>
<b>Acronyms</b>	<b>xi</b>
<b>1 Introduction</b>	<b>1</b>
1.1 Brine in Salt . . . . .	2
1.2 Coupled THMC Processes in Salt . . . . .	4
<b>2 Numerical Modeling of Water in Salt</b>	<b>6</b>
2.1 Current THM, THC, and THMC numerical models . . . . .	6
2.1.1 CODE_BRIGHT . . . . .	6
2.1.2 FEHM . . . . .	7
2.1.3 TOUGH-FLAC and FLAC-TOUGH . . . . .	7
2.1.4 $d^3f$ and $r^3t$ . . . . .	8
2.1.5 SIERRA Mechanics . . . . .	8
2.1.6 PFLOTTRAN . . . . .	8
2.2 Salt-Relevant Model Benchmarking Exercises . . . . .	9
2.3 Points of Comparison for Coupled Process Models . . . . .	12
<b>3 Processes Affecting Water Movement in Salt</b>	<b>15</b>
3.1 Representative Scales in Salt . . . . .	17
3.2 Water Distribution in Intact Salt . . . . .	17
3.2.1 Intergranular brine and vapor . . . . .	18
3.2.2 Intragranular brine . . . . .	19
3.2.3 Brine in non-salt layers . . . . .	20
3.2.4 Water of hydration . . . . .	20
3.2.5 Water in run-of-mine salt vs. intact salt . . . . .	21
3.3 Water Driving Forces in Salt . . . . .	22
3.3.1 Pressure . . . . .	23
3.3.2 Hygroscopy . . . . .	25
3.3.3 Capillarity . . . . .	26
3.3.4 Gravity and density effects . . . . .	28
3.3.5 Diffusive transport . . . . .	29

3.3.6	Temperature effects . . . . .	30
3.4	Distribution of Permeability and Porosity . . . . .	31
3.4.1	Permeability of heterogeneous layers . . . . .	31
3.4.2	DRZ permeability surrounding excavations . . . . .	31
3.4.3	Salt permeability as a function of mechanical properties . . . . .	33
3.4.4	Porosity changes due to dissolution and precipitation . . . . .	38
3.4.5	Permeability changes due to variable saturation . . . . .	39
3.5	Chemical Processes in Salt and Brine . . . . .	39
3.6	Balance of Dimensionless Quantities . . . . .	40
3.6.1	Thermal characteristic time . . . . .	41
3.6.2	Hydraulic characteristic time . . . . .	42
3.6.3	Mass transport characteristic time . . . . .	42
<b>4</b>	<b>Recent Hydrologic Model Development and Lab Testing for Water in Salt</b>	<b>45</b>
4.1	Los Alamos National Laboratory . . . . .	45
4.2	Lawrence Berkeley National Laboratory . . . . .	46
4.3	Sandia National Laboratories . . . . .	47
<b>5</b>	<b>Hydrologic Initial Conditions in Salt Repositories</b>	<b>48</b>
5.1	Evolution of the DRZ Around Excavations . . . . .	49
5.2	Effect of DRZ Dry-out on Hydrologic Modeling Initial Conditions . . . . .	52
5.3	WIPP Observations of DRZ Dry-out . . . . .	56
5.3.1	MB139 water table . . . . .	56
5.3.2	WIPP small-scale mine-by . . . . .	56
5.3.3	WIPP large-scale brine inflow (Room Q) . . . . .	57
<b>6</b>	<b>Summary and Conclusions</b>	<b>64</b>
	<b>References</b>	<b>65</b>
<b>A</b>	<b>PFLOTRAN input files</b>	<b>85</b>
A.1	Saturated Initial Condition . . . . .	85
A.2	Nonuniform Saturation Initial Condition . . . . .	89

## List of Figures

1.1	Map of salt distribution in the US (Johnson and Gonzales, 1978) . . . . .	1
1.2	Intragranular brine inclusions and intergranular pore fluids in salt (Olivella et al., 1995) . . . . .	2
1.3	Cartoon representation of coupling in THMC systems (Cosenza and Ghoreychi, 1993). . . . .	4
3.1	Relation between brine types and flow mechanisms. Adapted from Shefelbine (1982) and Schlich and Jockwer (1985). . . . .	15
3.2	Proposed reduction of connectivity at constant porosity in intergranular porosity during salt reconsolidation and healing (Hansen et al., 2014a) . . . . .	18
3.3	Characteristic thermogravimetric analyses from bedded salt samples (Powers et al., 1978) . . . . .	21
3.4	Static formation pore pressures interpreted from WIPP tests (Beauheim and Roberts, 2002) . . . . .	24
3.5	Range of salt porosity and pore size (Cosenza and Ghoreychi, 1993) . . . . .	25
3.6	Salt petrofabric study results for WIPP and Asse salt (Bechthold et al., 2004). . . . .	25
3.7	Capillary pressure data from WIPP anhydrite marker bed cores (Howarth and Christian-Frear, 1997) . . . . .	27
3.8	Capillary pressure data for fine-grained crushed salt (Cinar et al., 2006); Brooks and Corey (1966) and van Genuchten (1980) model parameters indicated; MRSM = steady-state modified restored-state method, CPDM = dynamic constant pressure desaturation method . . . . .	28
3.9	Capillary pressure data for fine-grained crushed salt at 5% and 10% porosity (Olivella et al., 2011); van Genuchten (1980) model parameters indicated . . . . .	28
3.10	Correlation between intrinsic permeability and gas-threshold pressure; see Salzer et al. (2007) for references. . . . .	29
3.11	Idealized lithology of a typical non-salt component of bedded salt: MB139 (Borns, 1985) . . . . .	32
3.12	Permeability and porosity estimates from WIPP Small-scale Mine-by test (Stormont et al., 1991a); power-law model suggested by Cosenza (1996) . . . . .	33
3.13	Brine permeabilities interpreted from tests conducted at WIPP (Beauheim and Roberts, 2002) . . . . .	34
3.14	Typical macrofracturing and damage surrounding a room excavated in bedded salt (Borns and Stormont, 1988) . . . . .	34



---

3.15	Trends in permeability and porosity for dilating (orange) and healing (blue) salt (Hansen et al., 2014a) . . . . .	35
3.16	Salt permeability against net confining pressure ( $\sigma_m$ ) and octahedral shear stress ( $\tau_o$ ) (Lai, 1971). . . . .	36
3.17	Experimental results showing redistribution of porosity due to precipitation and dissolution in crushed salt, as a factor of initial salt porosity for initial saturation of 40% (left) and initial brine saturation for initial porosity of 30% (right) (Olivella et al., 2011). . . . .	38
5.1	Directional nature of damage surrounding a rectangular excavation in salt (Gramberg and Roest, 1984; Borns and Stormont, 1988). . . . .	50
5.2	Numerical prediction of damage distribution around a WIPP disposal room ( $D$ given in Equation (5.1)) (Van Sambeek et al., 1993a) . . . . .	50
5.3	Photo of <i>en echelon</i> (large aperture sub-parallel) fracturing at change in roof elevation at WIPP (Hansen, 2003), with orientation drawings at left illustrating roof geometry and rockbolts. . . . .	51
5.4	One-dimensional two-phase flow modeling in brine using PFLOTTRAN. Initial conditions starting from nearly brine-saturated and hydrostatic (6 MPa) pressure. . . . .	54
5.5	One-dimensional two-phase flow modeling in brine using PFLOTTRAN. Initial conditions from 20% brine saturation in DRZ and 100% brine saturation in intact salt, with hydrostatic (6 MPa) pressure. . . . .	55
5.6	Water table observed with shallow MB139 boreholes in the DRZ at WIPP. Modified from (Deal et al., 1995, App. E). . . . .	56
5.7	WIPP Small-scale Mine-by borehole layout (Stormont et al., 1991a) . . . . .	57
5.8	WIPP Small-scale Mine-by brine (left) and gas (right) pressures in observation boreholes before, during, and after excavation of the central borehole (Stormont et al., 1991a) . . . . .	58
5.9	WIPP Small-scale Mine-by experiment results showing extent of DRZ (blue dotted line) and desaturated zone (green dashed line); modified from Stormont et al. (1991a)	59
5.10	WIPP Room Q inflow data (Freeze et al., 1997) . . . . .	60
5.11	Room Q porosity increase predicted by SPECTROM-32 (Freeze et al., 1997) . . . . .	61
5.12	Room Q TOUGH2 baseline porosity case inflow predictions, showing constant-porosity model (dashed), variable porosity model (solid) (Freeze et al., 1997) . . . . .	62
5.13	Room Q TOUGH2 increased porosity case inflow predictions, showing baseline porosity increase (solid) and 5% and 10% additional DRZ porosity (dashed) (Freeze et al., 1997) . . . . .	63

## List of Tables

3.1	Hydrous evaporite minerals in geologic salt; upper 4 minerals more common than lower 4. See references and notes in Roedder and Bassett (1981) . . . . .	22
3.2	Values of characteristic times; characteristic length $L = 1$ m (Cosenza and Ghoreychi, 1993; Cosenza et al., 1998) . . . . .	41
3.3	Typical thermal properties for salt (Cosenza and Ghoreychi, 1993; Cosenza et al., 1998) . . . . .	41
3.4	Thermal Peclet numbers for different salt types (Cosenza et al., 1998) . . . . .	42
3.5	Typical hydraulic properties for salt (Cosenza and Ghoreychi, 1993; Cosenza et al., 1998) . . . . .	43
3.6	Typical mass-transport properties for salt (Cosenza and Ghoreychi, 1993; Cosenza et al., 1998) . . . . .	44
3.7	Transport Peclet numbers for different salt types (Cosenza and Ghoreychi, 1993) . . . . .	44

---

# Acronyms

<b>BAMBUS</b>	Backfill and Material Behavior in Underground Salt Repositories (Asse project)
<b>CODE_BRIGHT</b>	COupled DEformation, BRIne, Gas and Heat Transport (Universitat Politècnica de Catalunya THMC numerical model)
<b>DOE</b>	US Department of Energy
<b>DRZ</b>	Disturbed Rock Zone
<b>EOS</b>	Equation of State
<b>FEHM</b>	Finite Element Heat and Mass transfer (LANL THC numerical model)
<b>FLAC<sup>3D</sup></b>	Fast Lagrangian Analysis of Continua in 3D (Itasca Consulting Group geomechanical model)
<b>LANL</b>	Los Alamos National Laboratory
<b>LBNL</b>	Lawrence Berkeley National Laboratory
<b>PFLOTRAN</b>	Parallel reactive FLOW and TRANport (THC numerical model)
<b>REV</b>	Representative Elementary Volume
<b>SNL</b>	Sandia National Laboratories
<b>THC</b>	Thermal-Hydrologic-Chemical coupled modeling
<b>THM</b>	Thermal-Hydrologic-Mechanical coupled modeling
<b>THMC</b>	Thermal-Hydrologic-Mechanical-Chemical coupled modeling
<b>TM</b>	Thermal-Mechanical coupled modeling
<b>TOUGH2</b>	Transport Of Unsaturated Groundwater and Heat, version 2 (LBNL TH numerical model)
<b>TSDE</b>	Thermal Simulation of Drift Emplacement (BAMBUS in-drift heater test)
<b>US</b>	United States
<b>WIPP</b>	Waste Isolation Pilot Plant

*this page intentionally blank*

# 1 Introduction

Salt is considered a medium for radioactive waste disposal in the United States and Germany. In 1955 the US Atomic Energy Commission convened an expert panel to recommend best practices for radioactive waste disposal from the growing US nuclear weapons and power industries (Hess et al., 1957). The primary panel recommendation was to investigate direct disposal of liquid re-processing waste in salt dome cavities. Oak Ridge National Laboratory conducted liquid waste disposal tests in two Carey salt mines in Kansas (Morgan, 1959). Complications observed during these liquid waste tests related to salt cavity stability and off-gas containment led to the existing recommendation for disposal of solidified waste (Lomenick, 1996, §2.2.2). US heat-generating radioactive waste is mostly solid used or spent fuel and high-level waste comprised of liquid re-processing waste that either is or eventually will be turned into vitrified glass logs (SNL, 2014). Permanent geologic disposal of solid radioactive wastes may involve placing waste casks or canisters in vertical or horizontal boreholes or into rooms mined into stable geologic salt deposits, with or without backfill.

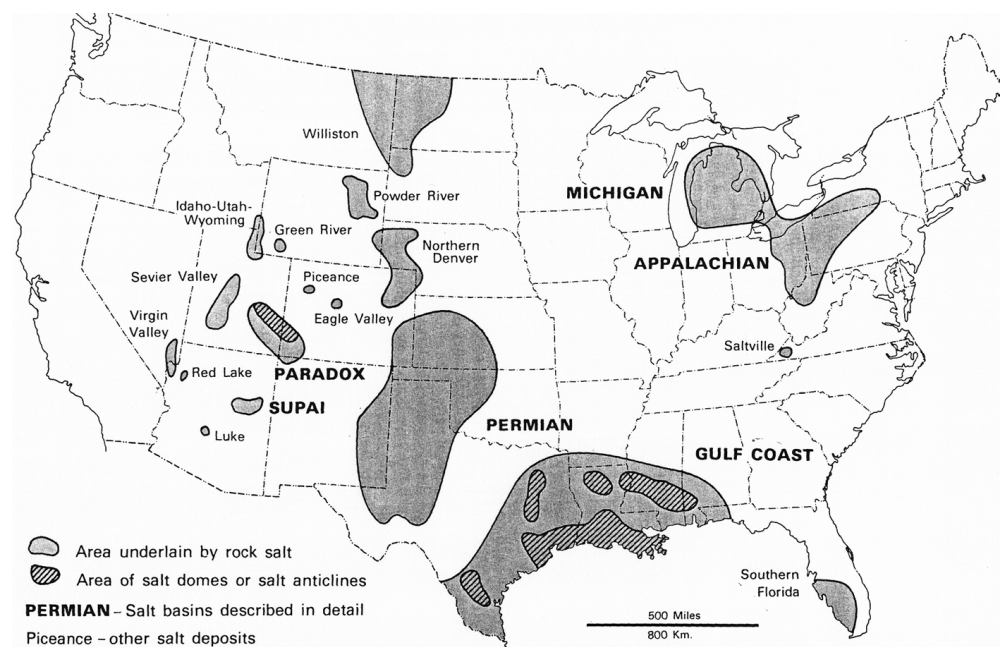


Figure 1.1: Map of salt distribution in the US (Johnson and Gonzales, 1978)

Both the US and Germany have extensive geologic salt deposits, with some in suitable areas for waste disposal (Johnson and Gonzales, 1978; Isherwood, 1981; Klinge et al., 2007; Bornemann

et al., 2008). In the US, the Waste Isolation Pilot Plant (WIPP) is the only operational deep geologic salt radioactive waste repository, but other candidate salt sites have been investigated (Lomenick, 1996), including Palo Duro Basin (Texas), Lyons (Kansas), Paradox Basin (Utah), and several Gulf Coast salt domes (Figure 1.1).

At proposed mined repository depths ( $\leq 1$  km depth) and thermal loads ( $< 10$ W to a few kW per canister; SNL, 2014) thermal, hydraulic, mechanical, and chemical processes are all relatively important. Brine flow in salt is coupled with salt geomechanical behavior, which is strongly temperature dependent. Salt is considered a candidate medium for waste disposal because:

- Salt has the unique benefit of self-healing behavior (i.e., creep under deviatoric stress) under typical repository conditions,
- Intact salt is essentially impermeable to fluids, and
- Salt has high thermal conductivity.

It is of central importance to understand and predict the long-term implications associated with brine flow in salt surrounding radioactive waste (e.g., UFD Campaign, 2012; Kuhlman and Malama, 2013; and Kuhlman and Sevougian, 2013).

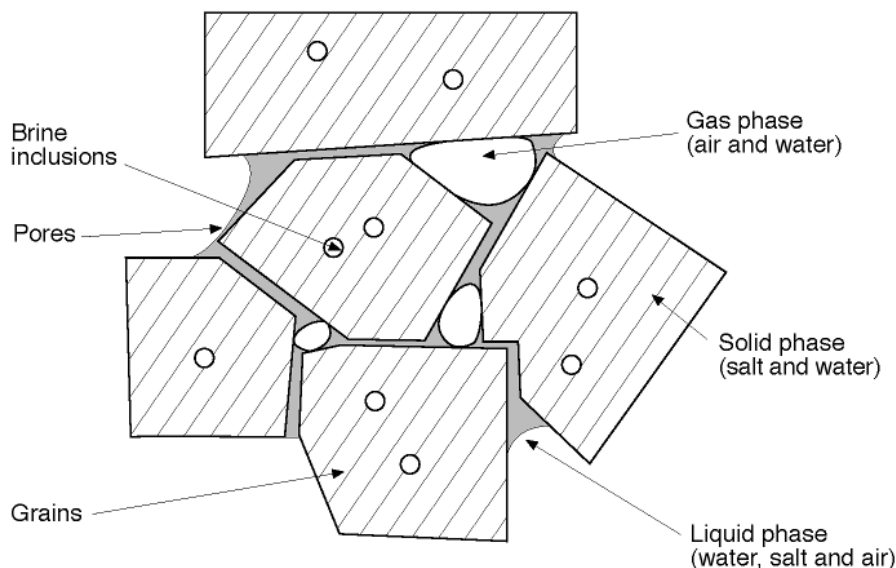


Figure 1.2: Intragranular brine inclusions and intergranular pore fluids in salt (Olivella et al., 1995)

## 1.1 Brine in Salt

Figure 1.2 illustrates two of the three primary water forms in bedded rock salt, intergranular and intragranular brine. We consider three brine types:

- Intragranular brine inclusions in salt (loosely called “negative crystals”; Figure 1.2);

- Intergranular (i.e., grain-boundary or pore) fluids (Figure 1.2);
- Water of hydration bound to hydrous minerals (Roedder and Bassett, 1981; Caporuscio et al., 2013);

Early laboratory permeability testing in the 1950s and 1960s illustrated linear Darcy-type porous media flow under a pressure gradient through salt cores from the Grand Saline salt dome mine (Reynolds and Gloyna, 1960; Gloyna and Reynolds, 1961). From the 1960s to the mid-1980s, much of the research on brine movement in salt focused on migration of intragranular fluid inclusions under temperature gradients.

Although intragranular brine inclusions are volumetrically the largest brine component in most bedded salt (aside from brine content in any secondary hydrous minerals), the significance of brine flow due to pressure gradients through connected intergranular porosity has been shown in numerous field and laboratory studies. A historic surge in brine inclusion research was fueled by field and laboratory observations made during Project Salt Vault (Bradshaw and Sanchez, 1969; Bradshaw and McClain, 1971). Data collected during project Salt Vault was fitted by Jenks (1979) using a simple exponential model, which saw wide application. Rübél et al. (2013) surmised the Jenks (1979) model was fitted to anomalous data, making most subsequent applications of this model inappropriate.

Research at Sandia National Laboratories (SNL) associated with WIPP since the mid-1970s developed experimental data to support the thermoporoelastic conceptual model for brine flow in salt (McTigue, 1986, 1990). Hadley (1982) developed an alternative conceptual model for vapor flow from an evaporation front. These models assumed liquid or vapor movement in connected intergranular porosity and discounted intragranular brine inclusions to simplify mathematical and numerical models. Olander et al. (1982) developed a conceptual model including both intergranular vapor flow and intragranular brine inclusion movement. Ratigan (1984) developed a numerical model including intragranular brine inclusions and intergranular brine flow, but it did not include thermal expansion effects on the intergranular porosity. Current numerical models for brine flow in granular salt assume a porous continuum (e.g., FEHM, TOUGH2, or PFLOTTRAN) with water moving under liquid and vapor pressure gradients. A Lattice Boltzmann numerical models has been used to simulate individual brine inclusion movement under a thermal gradient (Stauffer et al., 2013), but the latest generation of numerical models have not incorporated brine inclusions along with intergranular brine and vapor migration. Rutqvist et al. (2014) discussed plans to implement brine inclusion migration with intergranular brine and vapor flow via a dual-porosity conceptual model using TOUGH2.

The current generation of numerical models, individually introduced and discussed in Section 2.1, take three approaches to the simulation of coupled processes in salt. One group of simulators was derived from porous media mass and energy flow solutions to geothermal or radioactive waste disposal problems. They include thermal and hydraulic processes, but do not include large-deformation mechanical processes (FEHM, PFLOTTRAN, TOUGH2, and  $d^3f/r^3t$ ). The second group of simulators is derived from geomechanical models (Adagio in SIERRA Mechanics, and FLAC), requiring coupling with other models to include hydraulic and thermal convection effects. The third group of simulators include coupled thermal-hydrologic-mechanical processes relevant to salt repositories: TOUGH-FLAC and CODE\_BRIGHT. TOUGH-FLAC (and FLAC-TOUGH) externally and iteratively couples two existing programs, while CODE\_BRIGHT is a

tightly coupled simulator. The continued development and convergence of all three groups of simulators, each using different solution and coupling strategies, will eventually provide a robust and complementary set of tools to predict salt-repository relevant conditions.

## 1.2 Coupled THMC Processes in Salt

The coupled nature of Thermal, Hydrological, Mechanical, and Chemical (THMC) salt behavior has been known for over 50 years (Hess et al., 1957; Serata and Gloyna, 1959; Reynolds and Gloyna, 1960), but the details regarding the governing physical processes have only been well understood and confirmed since large-scale heated brine migration field and laboratory tests results in the 1980s at Asse, WIPP, and Avery Island (Sherer, 1987). Coupled process numerical modeling is an active area of research in repository science (Tsang, 2009), reservoir geomechanics (Prevost, 2014), and several other earth science fields (Herrera and Pinder, 2012), leading to the development of generic modeling tools for numerical simulation of coupled processes (e.g., Elmer: Lyly et al., 1999; FiPy: Guyer et al., 2009; COMSOL: COMSOL, 2012; SfePy: Rashed, 2012; and Albany: Hansen et al., 2014b).

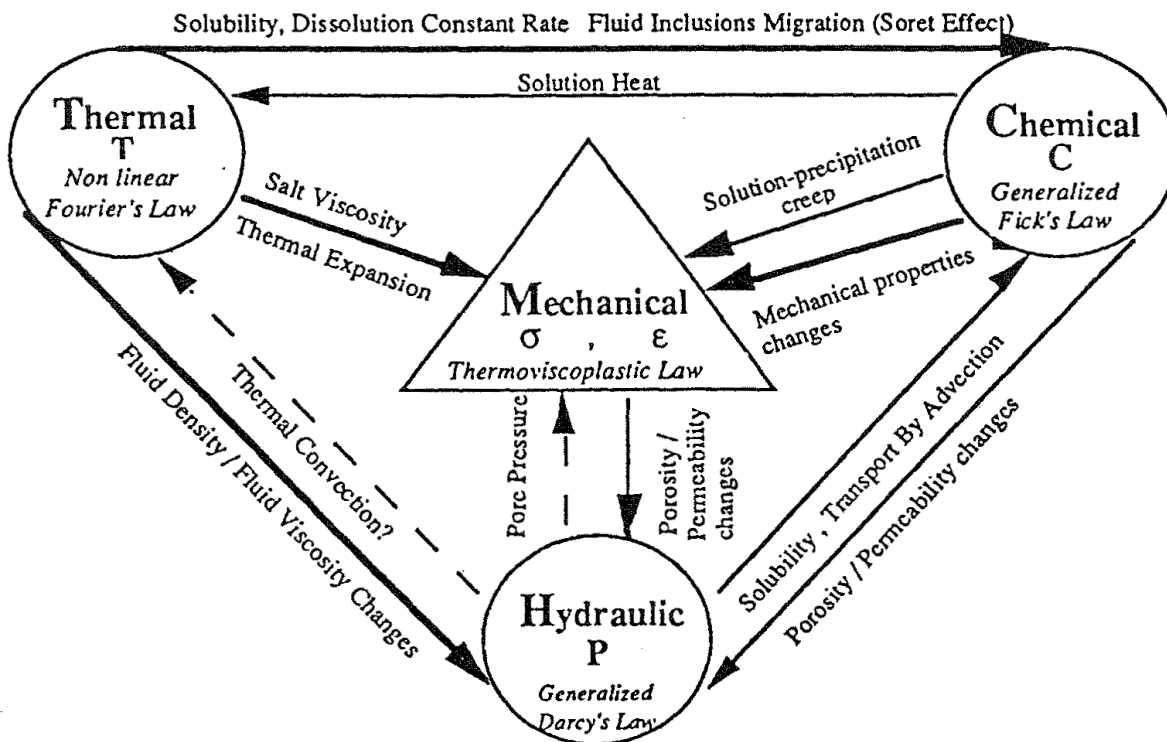


Figure 1.3: Cartoon representation of coupling in THMC systems (Cosenza and Ghoreychi, 1993).

Figure 1.3 illustrates the typical relationships between THMC processes in salt. Dashed connections in this figure show processes that may not exist in intact salt, while heavier solid arrows indicate stronger connections between processes. These four separate physical processes are coupled in salt because each process can influence the potentials and parameters of other processes. Except under restrictive circumstances, we cannot isolate a single process without significant error



and loss of physical significance. The thermal-mechanical (TM) problem in salt is characterized by the strong dependence of mechanical deformation properties on temperature; higher temperature reduces salt's effective viscosity. The thermal-hydrological-mechanical (THM) problem in salt is further characterized by the even stronger dependence of salt's hydraulic properties on mechanical deformation, along with the differential thermal expansion of salt and brine. Chemical effects can be superimposed on the THM representation, with additional coupling due to the precipitation and dissolution of salt in the pore space.

---

## 2 Numerical Modeling of Water in Salt

Analytical brine (McTigue, 1990) and vapor (Hadley, 1982) flow solutions are limited to linear constitutive models (e.g., Darcy's law or Knudsen flow for single phases), heat conduction (i.e., no free convection), and constant formation parameters (e.g., no heterogeneity or thermal effects on brine viscosity). To consider these non-linear effects, we must use gridded numerical models. In Section 2.1, we list a set of coupled numerical models useful for salt repository conditions. In Section 2.2, we list some historic and ongoing benchmarking exercises conducted under conditions relevant to salt repositories. Section 2.3 summarizes some generalities regarding the listed coupled numerical models in salt.

### 2.1 Current THM, THC, and THMC numerical models

The following numerical models allow solution of coupled non-linear equations using iterative solvers. Other numerical models exist to solve similar problems in other fields, but the following programs are noted because they have been used to simulate thermal-hydrologic-mechanical and thermal-hydrologic-chemical processes under salt-repository relevant conditions. Kuhlman and Malama (2013) summarized additional historical numerical modeling in salt, including brine inclusion migration modeling and vapor transport modeling.

#### 2.1.1 CODE\_BRIGHT

CODE\_BRIGHT ([https://www.etcg.upc.edu/recerca/webs/code\\_bright](https://www.etcg.upc.edu/recerca/webs/code_bright)) is a two-phase, variably saturated, porous medium flow, finite-element model developed at Universitat Politècnica de Catalunya to solve the poroelastic air/brine flow problem in deforming salt (Olivella et al., 1994, 1995). CODE\_BRIGHT has been used to simulate reconsolidation (Czaikowski et al., 2012) and dissolution/precipitation (Castagna et al., 2000; Olivella et al., 2011) of crushed salt.

CODE\_BRIGHT can simulate large deformations, with thermal, mechanical, hydrological (gas and liquid phases), and transport processes in a tightly coupled manner. Chemical processes are generally limited to the dissolution and precipitation of NaCl. The numerical model executables are freely available (but it is not open source) and it is typically used with the commercial GiD pre- and post-processor (<http://www.gidhome.com>). CODE\_BRIGHT is only available compiled for Windows and is limited to a single processor.

### 2.1.2 FEHM

FEHM (<https://fehm.lanl.gov>) is a two-phase, finite-volume, porous medium flow transport model considering reactive solute transport and thermal energy balance. The numerical simulator has limited (infinitesimal deformation for single-phase flow only) mechanical modeling capabilities (Zyvoloski et al., 2011). Stauffer et al. (2013) discuss recent improvements and enhancements to FEHM related to salt-repository thermal-hydrologic-chemical simulations.

FEHM solves the mass and energy balances in porous media in a tightly coupled manner for multiple components. The reactive transport portion of the program is computed sequentially at each time step following flow and energy transport calculations (Zyvoloski et al., 1999, Fig. 1). FEHM executables are freely available (under a non-commercial LANL software license) for Linux, Macintosh OS X, and Windows. The software is limited to a single processor.

### 2.1.3 TOUGH-FLAC and FLAC-TOUGH

TOUGH-FLAC is a set of iteratively coupled independent domain-specific models, which has been used in enhanced geothermal reservoir simulations, CO<sub>2</sub> sequestration, and modeling earthquake swarms (Rutqvist and Tsang, 2003; Rutqvist, 2011). TOUGH-FLAC runs each program independently: it modifies the porosity, permeability, and capillary pressure inputs to TOUGH2 based on output from FLAC<sup>3D</sup>, and modifies the pressure, temperature and saturation inputs for FLAC<sup>3D</sup> based on the output from TOUGH2 (EOS3). The coupling scheme between TOUGH2 and FLAC<sup>3D</sup> is based on the fixed stress-split method (Kim, 2010; Rutqvist et al., 2014). The flow problem is solved first, and the pore pressure and temperature are prescribed during the geomechanical calculation. Clausthal University of Technology has developed a related coupled model referred to as FLAC-TOUGH (Blanco Martín et al., 2014b). It uses a different (i.e., the drained-split and undrained-split methods (Prevost, 2014) and a hybrid of the two) coupling strategy and first solves the mechanical problem. FLAC-TOUGH is compared to TOUGH-FLAC in Rutqvist et al. (2014).

TOUGH2 (<http://esd.lbl.gov/research/projects/tough>) solves the mass and energy balance equations in porous media, allowing different equations of state (EOS) modules to be used, each bringing different capabilities to TOUGH2 (e.g., precipitation and dissolution of saline porous media). TOUGH2 is freely available for download (under a non-commercial LBNL software license) for US Government users and collaborators, but must be purchased for commercial use, and is limited to a single processor. The related TOUGH-MP simulator does allow parallel execution of TOUGH2 simulations on distributed-memory systems (Zhang et al., 2008).

FLAC and FLAC<sup>3D</sup> (<http://www.itascacg.com>) are two- and three-dimensional commercial explicit finite difference large-deformation geomechanical numerical models by Itasca Consulting Group. The models are primarily geomechanical models, with heat conduction and limited poroelastic flow capabilities. The software has the capability to implement new constitutive models not included in the main executable (i.e., the FISH language), which is used by some researchers to implement different salt creep constitutive models (Wieczorek et al., 2010; Wolters et al., 2012). All FLAC programs are only available for Windows, and only FLAC<sup>3D</sup> (version 5.01) is available as a multi-threaded shared-memory program, although constitutive models or coupling routines implemented in FISH are executed serially (Rutqvist et al., 2014). In August 2014, the Itasca website indicates future versions of all FLAC models will allow multi-core parallel execu-

tion.

### 2.1.4 d<sup>3</sup>f and r<sup>3</sup>t

GRS has developed and recently updated a density-dependent three-dimensional finite-volume flow (d<sup>3</sup>f) and solute transport (r<sup>3</sup>t) thermal-hydrologic-chemical numerical model for evaluating the stability of salt formations from the point of view of repository performance assessment (Schneider, 2012; Schneider et al., 2012). These models were developed to focus on flow and transport modeling in the geosphere rather than in the repository, but have similar capabilities to other repository simulators. The models were focused on modeling density-driven flow and radionuclide transport in overburden above a salt dome, including thermohaline convection. Although the model does not include Richards or two-phase flow, it does include free-surface flow. Free-surface flow is a useful simplification for representing a water table aquifer in a regional flow system, being less computationally expensive than two-phase flow or Richards' equation flow. The finite-volume representation can be used to discretize a porous three-dimensional solid which includes two-dimensional representations of intersecting discrete fractures.

The software is not available for non-research use outside of GRS under its current software license. The simulator has advanced multigrid solvers with distributed-memory parallel solution capabilities.

### 2.1.5 SIERRA Mechanics

SIERRA Multimechanics is a general multi-physics finite-element suite of numerical models comprised of several independent but potentially interrelated modules (Stewart and Edwards, 2003). Aria is an energy (conduction, convection, and enclosure radiation) and incompressible Navier-Stokes/porous media flow module with electrostatics and transport capabilities (Notz et al., 2007). Adagio (SIERRA Solid Mechanics Team, 2011) is a quasistatic large-deformation mechanical module (i.e., including clay layer slipping, failure, and tearing) with salt-relevant constitutive models implemented (Munson and Dawson, 1979; Callahan, 1999). The Aria and Adagio modules typically solve their respective numerical problems on different finite element meshes, which must be externally interpolated and coupled through the Arpeggio module (Kostka and Templeton, 2010). The SIERRA Mechanics suite was developed for applications outside repository sciences, but it has been used to simulate large non-isothermal deformations under salt repository conditions (Clayton and Gable, 2009; Clayton et al., 2010; Stone et al., 2010; Argüello and Rath, 2012, 2013; Argüello, 2014) as well as other geoscience-related applications (Martinez et al., 2011).

SIERRA Multimechanics is developed and used internally on Linux clusters at Sandia National Laboratories, and is not available for general distribution outside Sandia, Los Alamos, and Lawrence Livermore National Laboratories. It is configured to run in parallel on large-scale supercomputers.

### 2.1.6 PFLOTRAN

PFLOTRAN (<http://www.pflotran.org>) is a multiphase flow and reactive multicomponent transport simulator (Hammond et al., 2014; Lichtner et al., 2014). In the context of subsurface

simulation, PFLOTRAN simulates single and multiphase fluid flow (i.e., Richards' equation, air-water, CO<sub>2</sub>-water), thermal conduction/convection, and biogeochemical transport (e.g., aqueous speciation, sorption, mineral precipitation-dissolution, microbial degradation, radioactive decay and ingrowth) on structured and unstructured finite-volume grids. The structure of the software allows general inclusion of processes (e.g., electrical geophysics); an infinitesimal-strain geomechanical process is currently under development. The software is founded upon the Portable, Extensible Toolkit for Scientific Computation (PETSc) framework (Balay et al., 2014). PFLOTRAN is developed for high performance distributed memory parallel supercomputing, to simulate subsurface problems composed of billions of degrees of freedom utilizing hundreds of thousands of processor cores while still being applicable to serial batch systems or one-dimensional reactive transport using the identical executable and source code (Hammond and Lichtner, 2010).

PFLOTRAN is open-source, developed under a GNU Lesser General Public License and freely available for download from <https://bitbucket.org/pflotran/pflotran-dev>.

## 2.2 Salt-Relevant Model Benchmarking Exercises

*Verification* of a numerical model involves testing the programs for bugs or errors in its implementation of the governing equations, boundary conditions, and input/output routines. The Method of Manufactured Solutions is a general model validation approach for gridded models (Salari and Knupp, 2000). *Validation* of a numerical model requires data from an experiment or another validated model and involves reproducing observed conditions and processes. Rather than just illustrating the correctness of the implementation, validation also tests the appropriate representation and coupling of relevant physical processes in the numerical model.

Because there is a current need to verify and validate a new generation of coupled process models being developed and extended for salt repository relevant conditions, we summarize previous salt-repository relevant benchmarking exercises here to indicate the history of what has already been done, some ongoing exercises, and what validation data may be available.

- The WIPP project involved two generations of thermal-mechanical verification exercises. The first benchmarking exercise considered closure of an idealized room in homogeneous salt (Dawson, 1979), while the second exercise compared nine models, considering 27 distinct geologic layers – including 10 clay layers acting as slipping planes (Krieg et al., 1980). These modeling exercises were performed before WIPP was excavated using material properties estimated from cores. These benchmarking exercises compared alternative numerical solution approaches, and did not consider brine flow in salt. Based on experience from these two benchmarking problems, Munson and Morgan (1986) developed a general parallel calculations framework for program validation and verification exercises (Morgan et al., 1987). The Office of Nuclear Waste Isolation also began developing its own benchmarking exercises, based upon these WIPP benchmarking exercises (Wigley and Russell, 1980).
- COSA (COMputer COdes COmparison for SAlt) was a two-part European geomechanical model verification and validation exercise (1984–1988) in salt. In the first phase, two benchmark problems were simulated for verification of twelve different geomechanical finite-element models from ten European countries (Lowe and Knowles, 1986). In the second validation phase, three *in situ* experiments at Asse were used to compare the results of the

same finite-element models (Lowe and Knowles, 1989). The study found the geomechanical constitutive models had the largest impact on model results. Brine flow was not explicitly considered.

- INTRACOIN (International Nuclide TRANsport COde INtercomparison) was the first of three multi-stage projects in a Swedish-led international modeling verification effort (1981–1986). INTRACOIN validated and verified solute transport models in multiple geologies considered for radioactive waste disposal (SKI, 1984, 1986; Larsson, 1992).
- HYDROCOIN (HYDROlogic COde INtercomparison) was the second of three multi-stage Swedish-led international groundwater flow modeling verification efforts (1984–1990) (Cole, 1986; SKI, 1992), conducted as a follow-up to INTRACOIN. Similar to other stages, its three levels addressed model verification to hypothetical cases (Level 1), validation against experiments (Level 2), and model uncertainty quantification (Level 3). At Level 1, Case 5 was two-dimensional density-dependent groundwater flow above a salt dome (Konikow et al., 1997), and Case 6 was three-dimensional steady-state regional flow through a bedded salt formation, designed to resemble the Palo Duro Basin in Texas. HYDROCOIN Level 2 included simulation of both field and laboratory coupled free thermal convection (Cases 1 and 2). HYDROCOIN Level 3 (Case 3) was a refined version of Level 1 Case 6 (regional groundwater flow through Palo Duro-like evaporite sediments), and Case 4 was a refinement of Level 1 Case 5 (density dependent flow over a salt dome).
- INTRAVAL was the third Swedish-led international model benchmarking exercise, conducted as a follow-up to INTRACOIN and HYDROCOIN. Phase 2 included eleven international test cases, one being simulation of isothermal brine observed in WIPP boreholes (Beauheim et al., 1997), and another being interpretation of pumping tests in alluvial channels near the Gorleben salt dome (van Weert and Hassanizadeh, 1994). In the WIPP case, the analytical solution of McTigue (1993) and two international finite-element numerical models were matched to brine inflow data collected from the small-scale brine inflow test (Finley et al., 1992). The project essentially validated the use of Darcy's law for isothermal brine flow in salt, although they indicated in their conclusions "coupled hydrological and geomechanical models may provide a better understanding of the system" (Larsson et al., 1997).
- Freeze et al. (1997) conducted a comparison between three different modeling approaches to simulate observed results from the Room Q WIPP large-scale brine inflow experiment (Section 5.3.3). They compared the ability of two numerical models and an analytical solution (McTigue, 1993) to match observed Room Q inflow data. One numerical model computed brine inflow as a post-processing step to a mechanical damage calculation, and the other used mechanical deformation predictions from SPECTROM-32 (Callahan et al., 1989) to estimate porosity changes in an isothermal TOUGH2 simulation.
- The BAMBUS (Backfill and Material Behavior in Underground Salt repositories) project centered around the large-scale in-drift Thermal Simulation of Drift Emplacement (TSDE) test, which involved reconsolidation of crushed salt and DRZ healing during nine years of heating (Bechthold et al., 2004). The BAMBUS I report involved two-dimensional model

verification for thermal-mechanical calculations (Bechthold et al., 1999). The BAMBUS II report presented a mixture of three-dimensional and two-dimensional thermal-mechanical model validation exercises involving seven European organizations (Bechthold et al., 2004, Chap. 7). Brine flow was not explicitly considered.

- THERESA was a German geomechanical model benchmarking exercise, which mostly focused on large salt core behavior in triaxial tests modeled using FLAC (Wieczorek et al., 2010; Pudewills, 2012). Some borehole-scale tests and brine migration aspects were considered, but most models (except CODE.BRIGHT) computed brine migration using FLAC's built-in porous media flow capabilities.
- GRS is conducting a crushed salt reconsolidation constitutive model validation against three ongoing long-term (low-porosity) crushed salt oedometer experiments (Czaikowski et al., 2012). These tests are producing data for validation of salt reconsolidation constitutive models, and were designed to show the effects of multiple salt reconsolidation mechanisms subject to different loads and water contents. Intermediate data and modeling results have also been reported in the US/German workshop series (Hansen et al., 2012, 2013a).
- The “Joint Project” is an ongoing collaboration (Schulze et al., 2007; Hou et al., 2007; Salzer et al., 2012; Hampel et al., 2012, 2013) of German salt researchers and SNL to validate numerical models and their geomechanical constitutive models against repository-relevant data, including:
  - Heated borehole free convergence test at Asse (Hampel et al., 2013), using data from the original COSA project (Lowe and Knowles, 1986);
  - Long-term healing behind a cast-iron drift liner at Asse (Hampel et al., 2013), using data from the ALOHA project (Bechthold et al., 2004); and
  - Room closure in WIPP experimental rooms B (heated) and D (isothermal) (Munson et al., 1988, 1990; Argüello and Rath, 2013).

Although the drift liner validation test involves salt permeability data used to discern the extent of damage and healing behind the bulkhead, brine inflow was not explicitly considered. The progress of the Joint Project was also discussed in the 2010–2013 US/German Workshops on Salt Repository Research, Design, and Operation (Steininger, 2010; Hansen et al., 2012, 2013a,b).

Most early benchmarking efforts involved geomechanical models, while more recent validation exercises focused on validation of coupled TM or THM models. Isothermal hydro-mechanical benchmarks would be useful for testing the nature of the mechanical-hydraulic coupling (Section 3.4.3). There already exist several test data from WIPP for validation:

- Laboratory brine-injection creep experiments (Brodsky, 1990; Brodsky and Munson, 1991);
- The small-scale brine inflow experiments (Finley et al., 1992);
- The large-scale brine inflow experiment (Room Q; Jensen et al., 1993a; Jensen et al., 1993b; Section 5.3.3);

- The Small-scale Mine-by test (Stormont et al., 1991b; Section 5.3.2); and
- Mechanically instrumented brine permeability tests conducted in boreholes (Saulnier et al., 1991; Stensrud et al., 1992; Chace et al., 1998).

Obviously, thermal effects in THM simulations are important, but it would also be beneficial to isolate and test hydro-mechanical coupling separate from THM coupling.

## 2.3 Points of Comparison for Coupled Process Models

This section presents a list of some points of comparison based on observations and generalizations about the coupled numerical models discussed in the previous section.

- **Large vs. Small Strains:** Small-strain geomechanical solutions are useful in CO<sub>2</sub> sequestration, geothermal, and similar problems (Rutqvist, 2011). Salt deformation requires large-strain solution (especially heated salt), due to the relatively quick creep closure of excavations. The formulation of the mechanical problem for finite strains (Zienkiewicz et al., 1999) is more general than the traditional formulation of the infinitesimal strain problem included in FEHM and PFLOTRAN. TOUGH-FLAC recently was modified to accommodate large strains, which complicates the iterative coupling between these two independent models (Rutqvist et al., 2014). The large-strain mechanical problem is more difficult to develop and simulate; these large-strain complications were the focus of geomechanical model verification and validation exercises in the 1980s (e.g., WIPP benchmarking and the COSA project).
- **Numerical Solution Methodology:** Finite volume (or integrated finite differences) is a commonly used solution strategy in reservoir simulations (Prevost, 2014) or coupled process modeling (e.g., FEHM, PFLOTRAN, TOUGH2,  $d^3f/r^3t$ , and FiPy; Guyer et al., 2009), because the method ensures conservation of mass or energy by definition and is computationally economical. Finite element approaches are commonly used for geomechanical problems where continuity of stress and strain (proportional to the derivative of displacement) is required, especially those with large deformations (e.g., CODE\_BRIGHT, SIERRA Mechanics, and Albany; Hansen et al., 2014b). FLAC is somewhat unusual as a modern numerical model since it uses explicit finite differences; no solution matrix is formed, but very small time steps are often needed for numerical stability.

Finite volumes or integrated finite differences is a special form of the method of weighted residuals (Finlayson, 1972) using piecewise-constant weighting functions, while finite elements typically use linear or higher-order shape functions that are equivalent to piecewise linear or higher-order weighting functions (Fallah et al., 2000). Finite element simulations therefore have constant derivatives (e.g., fluxes, stresses, or strains) and linearly variable primary variables (e.g., potential, temperature, or displacement) across elements, while finite volume simulations have identically zero derivatives across elements because primary variables are constant across elements.

Ensuring mass or energy conservation in finite-element methods requires small elements and short time steps, and finite-volume methods are too low-order for large-strain mechanical problems. Due to these factors, it can be difficult to develop a single numerical model



that excels at both coupled process modeling and large-strain geomechanics, without the added complication and approximation associated with mapping from one type of discretization to another, as done in TOUGH-FLAC and FLAC-TOUGH (Kim, 2010; Prevost, 2014). CODE\_BRIGHT is the only tightly coupled THMC model presented here developed entirely using finite elements, but several general finite-element coupled process modeling frameworks exist (e.g., Albany: Hansen et al., 2014b, Elmer: Lyly et al., 1999, SfePy: Rashed, 2012, or COMSOL: COMSOL, 2012). The flexibility of finite elements (linear or higher-order basis functions and more general element shapes) can make up for disadvantages associated with mass-balance issues, but the finite-element method is more difficult to derive and implement than the finite-volume approach.

- **Physical and Numerical Coupling:** A range of coupling types exist in physical problems, and a range of coupling types may exist in numerical implementations of coupled models. Physical processes are coupled to varying degrees, from strongly coupled (e.g., effects of temperature on creep deformation) to weakly coupled (e.g., heat flux due to pressure gradients – the Dufour effect). Pairs of physical processes can be one-way coupled (e.g., fluid flow advects dilute concentrations of dissolved species, but low species concentrations do not generally impact flow) or fully coupled (e.g., free thermohaline convection – where large concentration differences impact fluid density, further driving fluid flow).

There is a range of different degrees to which physically coupled THMC processes can be simulated in a numerical model, including loosely, iteratively, and tightly coupled (Kim, 2010; Prevost, 2014). Numerical models can also be one-way or fully coupled. There is necessarily some correlation between physical and numerical coupling, but the nature of numerical coupling is also to some degree a choice of the modeler. All processes could be tightly coupled all the time, but this would make the numerical model unnecessarily complex and slow. A decision must be made to ignore certain effects or processes in a numerical implementation, due to the importance of these effects on the expected results.

When numerical models are “loosely coupled”, results are passed between models, but there is no iteration – this is typically only effective when physical coupling is one-way or weak (e.g., TOUGH2 and SPECTROM32 modeling presented in Section 5.3.3). When independent models are iteratively coupled at each time step, some state variables are free while others are fixed; parameter dependence between the models is computed in a processing step between each iteration at each time step (e.g., TOUGH-FLAC or SIERRA Mechanics). Alternatively, the tightly coupled problem can be solved by posing all the governing equations for all the degrees of freedom simultaneously, in a single matrix problem (e.g., CODE\_BRIGHT). Tight coupling is most robust way to solve the problem; iteratively coupled approaches are benchmarked against tightly coupled solutions (Kim, 2010; Prevost, 2014). Tight coupling does not require freezing state variables or iterating between models, but it requires more computer memory and the fully coupled model must be developed “from the ground up”. Existing domain-specific numerical models cannot be utilized in developing a tightly coupled model.

- **Serial vs. Parallel Execution:** Parallel computing has become very important in numerical simulation in the last 20 years. Implicit solution of three-dimensional domains with

large numbers of elements, and coupled process models with large numbers of degrees-of-freedom per element require significant computational effort. FEHM, TOUGH2, and CODE\_BRIGHT were originally developed before the latest revolution in parallel computing, and it is not simple to modify these models to allow them to execute in parallel (e.g., see Zhang et al. (2008) regarding development of TOUGH2-MP from TOUGH2). PFLOTRAN, SIERRA Mechanics, and  $d^3f/r^3t$  have been developed to allow efficient parallel simulation of physically large or complex domains using distributed memory parallelization.

Shared-memory parallelization allows several processors on the same computer to be utilized in a calculation (e.g., as done by FLAC<sup>3D</sup>), while distributed memory parallelization requires communication between computers (e.g., with the message passing interface – MPI), but works on large computational clusters. This is the approach taken by PFLOTRAN, SIERRA Mechanics, TOUGH2-MP, and  $d^3f/r^3t$ . Parallel execution is no longer a computational luxury but a requirement in modern numerical models; serial calculation times for coupled THM models are often on the order of weeks or months.

- **Closed vs. Open Source Software:** Open-source software has several possible benefits over closed-source or proprietary software models. Commercial software is often closed source and has an associated fee. Free software (no fee) may be either open-source or proprietary. While providing no-fee software increases the probable software user base, distribution of the software under a permissive open-source license has additional benefits. Open source software can often live on beyond its original intended use or developer, if others find it useful. Open-source software development is typically more transparent than closed-source software. Software developed using money from public funding sources should be typically available to the public who funded its development.
- **Radiative Transfer in Rooms:** Open excavations (i.e., rooms or boreholes without solid backfill) include more complex heat transfer processes than porous-media filled cavities. Numerical models discussed here all consider heat conduction, and most handle porous media thermal convection (of brine and vapor). Thermal convection and radiation heat transfer in the open air of drifts and boreholes are non-linear processes that significantly increase the complexity of the thermal solution over conduction. Aria in SIERRA Mechanics is the only model discussed here that can include these complicating heat-transfer effects.

Typically, air is treated as a porous medium of high permeability and it is assigned an effective thermal diffusivity, based upon assumed thermal gradients across the excavation. Radiation boundary conditions are proportional to difference in temperature to the fourth power, and free or forced (i.e., mine ventilation) convection often include very steep gradients near surfaces (i.e., boundary layers). Very hot waste will require comparisons between the effective heat conduction approach and the physically realistic radiative transfer problem. Accurate simulation of pre-closure conditions in a repository with high heat-generating waste could require these advanced processes to predict temperatures to a high level of accuracy at the waste package (Francis et al., 2003; Buscheck et al., 2002). Backfilling the entire excavated space with crushed salt simplifies the heat transfer processes required to simulate the problem (Kazan and Ghoreychi, 1996).

### 3 Processes Affecting Water Movement in Salt

In this chapter, we present a summary of brine storage and migration mechanisms, indicating to what degree they are accounted for in current numerical models (discussed in the previous chapter). Brine movement mechanisms vary by the different water types found in geologic salt (Figure 1.2). Figure 3.1 indicates the main brine migration mechanisms: their relationships are outlined in further detail below. Most current numerical models only consider all or part of the intergranular “Pore Fluid + Vapor” column of Figure 3.1, and not the other two columns.

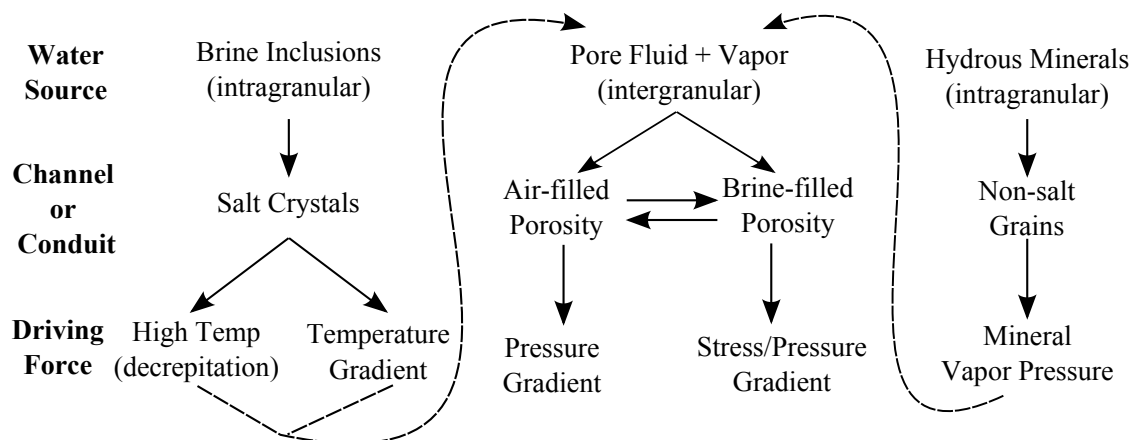


Figure 3.1: Relation between brine types and flow mechanisms. Adapted from Shefelbine (1982) and Schlich and Jockwer (1985).

GRS (Rübel et al., 2013) performed a summary of the US and German salt water-migration literature focusing on impacts to the safety case for heat-generating waste. The summary report discusses the relative importance of hydrated minerals, brine inclusion migration, large-volume brine reservoirs, and intergranular brine. Their summary is recounted here with additional discussion and references because it justifies the reasoning for only considering pressure-driven flow in a salt repository:

- Water from hydrated minerals can be avoided in a repository by keeping waste away from significant hydrated mineral deposits or keeping the peak temperature below the minerals’ dehydration temperatures.
- Large-volume brine reservoirs are associated with isolated blocks of anhydrite in domal salt (up to 1000 m<sup>3</sup> in size) or interbedded anhydrite and salt layers in bedded salt (e.g., high-

pressure brine reservoirs in the Castile Formation at WIPP; Popielak et al., 1983). They can be avoided by staying away from geologic formations associated with them. Brine migration in fractured reservoirs under thermal gradients is assumed to be inconsequential, because of their association with non-salt geology.

- Intragranular brine inclusion migration is assumed to only be important as a mechanism for creating additional intergranular water, once inclusions migrate to a “loose” grain boundary (see left dashed arrow in Figure 3.1). Brine inclusions may migrate between crystals if conditions are favorable (Schenk and Urai, 2005).
- Intergranular brine migration was considered under the end-members of only-liquid or only-vapor transport:
  - Rübél et al. (2013) contends vapor phase transport is the primary mechanism for water flow away from a receding evaporation front towards a heated borehole. Brine inflow data collected from US and German tests were compared to predictions using the vapor transport model of Hadley (1982). Rübél et al. (2013) assumed vapor flow is governed by Knudsen flow (i.e., small pores and low pressures), which is of a similar form to Darcy’s law for liquid flow; they are both viscous diffusion of pressure linearly proportional to pressure gradients.
  - Liquid phase brine movement occurs due to viscous diffusion of fluid pressure, or more likely rock stress gradients. Rock stress gradients occur due to excavations, and they dissipate due to creep of the solid salt. Stress and pressure gradients also arise due to differential thermal expansion of brine and salt. A 1% increase in volume of the salt would be due to a 100° C increase in temperature, while the same volume decrease in brine would only require a 25° C change in temperature (Rübél et al., 2013).  
Kuhlman and Malama (2013) summarize field observations supporting brine flow as a primary flow mechanism toward a heated borehole. During WIPP Room A1 brine-inflow testing there was a 4× decrease in water vapor partial pressure during the test due to reconfiguration, but no significant change in brine inflow (Nowak, 1986; Nowak and McTigue, 1987). In-borehole observations during heating in a Carlsbad potash mine show salt encrustations form along grain boundaries in quick bursts (Shefelbine, 1982).

These arguments are sometimes used to limit consideration to only intergranular brine or vapor flow, but we discuss impacts from additional relevant water types in the following sections in this chapter. Section 3.1 mentions some issues related to problem scale and fractures in salt. Section 3.2 discusses the occurrences of water relevant to salt repository systems. Section 3.3 lists the important driving forces affecting redistribution of water in salt repository systems. Section 3.4 includes the different mechanisms contributing to the wide range of permeabilities observed in a salt repository. Section 3.5 provides general discussion on geochemical processes relevant to salt repositories. Section 3.6 presents a set of relevant characteristic and dimensionless parameters illustrating the importance of coupling in the THMC problem for intact, disturbed rock zone (DRZ), and crushed salt materials.

We discuss the components of the coupled THMC problem in salt, focusing on the movement of brine. Although the thermal, mechanical, and chemical aspects of THMC are very important, they

are not discussed here in detail beyond their influence on the hydrologic flow problem. Discussion of the thermal energy flow problem (i.e., conduction, convection, and radiation) is not specific to salt, and is discussed thoroughly in many other places (e.g., Bejan and Kraus, 2003 or Nield and Bejan, 2006). The geomechanical behavior of salt is somewhat unique compared to other geomaterials due to salt's plastic behavior; it is treated elsewhere (e.g., Senseny et al., 1992; Carter et al., 1993; Cristescu and Gioda, 1994; and Urai et al., 2008). Chemical processes important in heat-generating repositories in salt are mostly related to waste-form and waste-package corrosion and actinide chemistry (see references in Kuhlman and Sevougian, 2013).

### 3.1 Representative Scales in Salt

Salt grains can be large ( $\approx 1$  cm) and grain boundaries in undisturbed salt can have very small apertures (down to  $10^{-4}$  cm), especially compared to more typical porous media like clays, silts, and sands. The large scale of salt crystals makes the representative elementary volume (REV) needed for both mechanical and hydrologic continuum modeling assumptions necessarily larger. Cores for mechanical and hydrologic testing must be several times larger than the grain size to produce meaningful results. The diameter of small boreholes may not be significantly larger than coarse salt crystals, which may lead to scaling differences between small and large boreholes or small boreholes and excavated drifts.

A series of cylindrical-excavation creep closure tests have been conducted to investigate the effect of scale on salt creep (Fuenkajorn and Daemen, 1988; Doeven et al., 1983; Munson et al., 1994, 1995b), motivated by model predictions that did not match observed room closure in early WIPP excavations (Tyler et al., 1988; Munson et al., 1989). The differences were eventually not attributed to scale, but to creep model parameters estimated from lab test data. Brine flow to boreholes in salt has also been reported across a wide range of spatial scales, including: laboratory tests (Hohlfelder et al., 1981; Hohlfelder, 1980), small-diameter boreholes (Finley et al., 1992), large-diameter boreholes (Nowak and McTigue, 1987), and drifts (Deal et al., 1995). Although some work has been done to discuss these results scaled according to borehole size (Shefelbine, 1982), the data have not been systematically analyzed for scale effects.

Large open fractures definitely impact continuum-scale modeling, but they are not accurately represented in samples or models (Stormont, 1990b). To meaningfully represent open fractures as a porous medium would require very large samples, due to the large REV associated with these features. Discrete fractures can be represented individually in some numerical models, but characterization of individual fractures can be difficult. Open fractures present at a field site may act as capillary barriers, provide fast-transport pathways, or serve as reservoirs for brine, which will likely not be characterized in data obtained from cores, or predicted by continuum THMC models.

### 3.2 Water Distribution in Intact Salt

The distribution of both liquid and vapor water in geologic salt is discussed in the following sections, indicating if and how each component is considered in numerical models (Section 2.1).

### 3.2.1 Intergranular brine and vapor

Liquid brine within intergranular porosity moves along interconnected macroscopic pores and grain-boundaries due to a combination of fluid pressure, thermal, and rock stress gradients (McTigue, 1986, 1990). The intergranular pore space is characterized at the macroscopic scale by its grain boundary apertures, porosity, and permeability. Some of this porosity appears as “intergranular brine inclusions” (Schenk and Urai, 2005; Desbois et al., 2012; Caporuscio et al., 2013), which may be the result of physical, thermal, or chemical processes concentrating or trapping brine on salt grain boundaries, without changing the total porosity (Figure 3.2). Schlich and Jockwer (1985) describe intergranular water as “adsorbed to crystal grain boundaries,” which may be consistent with intergranular brine inclusions (left part of Figure 3.2).

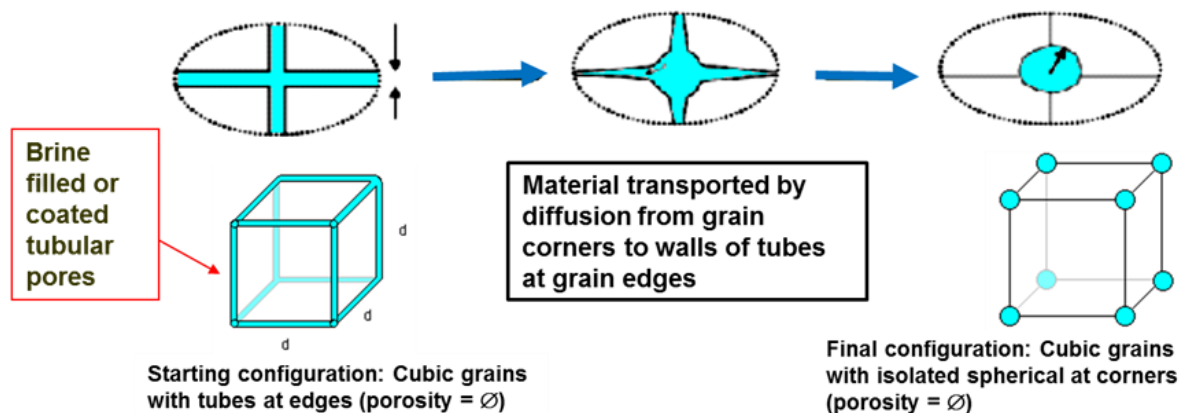


Figure 3.2: Proposed reduction of connectivity at constant porosity in intergranular porosity during salt reconsolidation and healing (Hansen et al., 2014a)

Salt intergranular permeability can vary by orders of magnitude due to changes in confining stress and damage (Sutherland and Cave, 1980; Stormont and Fuenkajorn, 1993; Stormont, 1997a). Salt damage includes microscopic fracturing (volume dilation) due to presence of deviatoric stresses near the excavation, which enhances rock permeability and porosity, and lowers brine pressure (Hansen, 2003). Section 3.4.3 discusses these effects on permeability in more detail.

Intergranular porosity most generally involves two-component flow of brine and air/vapor where dilation has increased salt porosity near the excavation. After porosity increases and air-entry pressure decreases near the excavation, a saturation front moves into the rock, sub-parallel to the excavation surface (Beauheim et al., 1994; Stormont, 1997b). Most generally, brine flow in salt is treated as a variably saturated flow problem. We may approximate the system by bounding the saturated system by a moving material boundary representing the evaporation front (Hadley, 1982) and treating vapor flow from the receding evaporation front to the excavation as a single-component vapor flow problem.

The intergranular porosity is represented in continuum Darcy flow models as a connected network of pores with an effective permeability to flow. Porous media models cannot meaningfully resolve things smaller than the relevant REV associated with the flow around the salt grains (i.e., salt grains themselves are impermeable). In intact salt, a connected network of porosity may not exist – there may not be measurable permeability (Beauheim and Roberts, 2002). Brine may be trapped in isolated porosity, such as intergranular brine inclusions (Figure 3.2).

The far-field salt (beyond the DRZ) is considered saturated with brine, because at lithostatic pressure gas would be dissolved in the brine or compressed to a very small fraction of the porosity and very high air-entry pressures are observed outside the DRZ (Stormont, 1997b). Rutqvist et al. (2014) and Blanco Martín et al. (2014a,b) considered cases with both 50% and 100% initial brine saturation in the far field. The fully brine saturated case was associated with more damage-induced permeability increase (i.e., hydrofracture) due to thermal expansion of brine from heating in the drift; in the 50% saturated case gas compressibility was able to absorb some brine and salt expansion during heating, reducing salt damage.

### 3.2.2 Intragranular brine

Intragranular brine inclusions are a significant portion of total brine content in bedded salt, but are not immediately available for flow under a stress or pressure gradient. Brine inclusions can migrate under strong thermal gradients or rupture due to high temperatures (decrepitation). Grain boundaries themselves (which can contain brine and brine inclusions) can also migrate in response to pressure and chemical gradients (Schenk and Urai, 2005; Urai et al., 2008).

Inclusions with low gas content will migrate across individual salt grains up a thermal gradient, towards a heat source (Bradshaw and Sanchez, 1969; Anthony and Cline, 1971). When brine inclusions reach the intergranular porosity between crystals, they tend to stay there, without migrating into the adjacent crystal (Olander, 1982). When inclusions have  $\gtrsim 10\%$  exsolved gas content (i.e., biphasic) they may migrate down a thermal gradient, away from the heat source (Wilcox, 1968, 1969; Anthony and Cline, 1972). As evidenced by geologic brine inclusion stability under geothermal gradients, brine inclusion movement is apparently subject to threshold temperature gradients (Gnirk et al., 1981; Krause and Brodsky, 1987).

Brine inclusion decrepitation is a form of failure due to the stress generated by the included phase's vapor pressure, and the differential thermal expansion of the salt crystal and brine inclusion (Wilcox, 1968) – brine has a much larger coefficient of thermal expansion than salt does. Upon decrepitation, intragranular brine escapes the local crystal structure, becoming intergranular brine (Figure 3.1) possibly increasing the porosity and permeability of the salt. Decrepitation temperature can vary by salt confining pressure and inclusions size. Inclusions have been shown to grow in size and gas content upon heating to temperatures just below decrepitation (Wilcox, 1968; Roedder and Bassett, 1981).

Brine inclusions can be treated in numerical models as a:

- Bulk fluid flux driven by thermal gradients (Jenks, 1979);
- Contribution (i.e., source term) to the intergranular brine flow problem (Olander, 1982; Ratigan, 1984); or
- Hybrid approach allowing communication between an overlapping brine inclusion continuum and an intergranular flow continuum (Rutqvist et al., 2014).

Most numerical models considering brine inclusion migration have followed the first approach (i.e., brine inclusions only – see Kuhlman and Malama (2013) for summary), while few have attempted the second approach (Olander et al., 1982; Ratigan, 1984). The third approach seems viable; Rutqvist et al. (2014) discussed implementing it in a future version of TOUGH2.

### 3.2.3 Brine in non-salt layers

Characteristic of bedded salt deposits, dispersed secondary (not NaCl) mineral content in Salado bedded salt at WIPP is approximately 5% (Stein, 1985). A set of 43 salt cores from the Palo Duro Basin in Texas were 0.07%–35.1% insoluble residue (mean 4.4% and median 1.7%), after dissolving crushed core samples in deionized water (Owen and Schwendiman, 1987). In addition to dispersed non-salt content, significant thickness of non-salt layers may exist in bedded salt deposits (e.g., the numbered Marker Beds in the Salado Formation halite at WIPP). These layers are typically saturated with halite brine, but may be comprised of mostly non-salt minerals like anhydrite, polyhalite, and clay. In domal salt, large-scale brine reservoirs can be associated with brittle isolated blocks of anhydrite in the salt matrix (Rübel et al., 2013).

Non-salt layers are typically higher permeability and porosity than intact salt, and do not heal or creep like salt. Brine flow through these layers is similar to intergranular brine flow in salt, but material properties may be significantly different. Brittle evaporite rocks like anhydrite or limestone may have intrinsic permeability and REV's associated with fractures, while clastic interbeds have smaller grain sizes than salt (and correspondingly smaller REV's), but clay layering may result in strong anisotropy. Clays saturated with NaCl brines may behave mechanically and chemically quite differently from clays under more “typical” fresh groundwater conditions.

These non-salt layers may behave as a porous medium in terms of flow, but their mechanical properties are different from salt, so fractures and separations may occur at bedding planes (Stormont, 1990b), leading to additional heterogeneity and effective anisotropy.

Aside from these complications associated with non-salt layers, including them in gridded numerical flow models is easy. Mechanical deformation at clay layers may include separation and displacement, which increases the complexity of geomechanical simulations. FLAC, CODE\_BRIGHT, and SIERRA Mechanics all have capabilities to allow discrete slipping or separation at specified planes in the rock associated with clay seams.

### 3.2.4 Water of hydration

Waters of hydration in non-salt hydrous minerals (Table 3.1) often constitute the largest fraction of the total water content in impure geologic evaporite deposits, up to tens of percent by weight. Powers et al. (1978) analyzed Salado Formation bedded salt cores. They performed petrographic, thermogravimetric, and crushing analysis on small samples.

They computed mass loss analysis on salt samples during sample heating up to 500° C. The mass loss was attributed to water loss from hydrated minerals and clastic interbeds. Figure 3.3 shows characteristic results for the main Salado bedded salt types encountered. Relatively pure rock salt (A) was observed to incur limited mass loss to temperatures as high as 500° C, due to low total water content (< 0.5% by weight). A significant mass-loss ( $\approx$  5% by weight) occurs at 300° C for polyhalite-bearing salt (B), and a smaller mass-loss occurs at 100° C ( $\approx$  2.5% by weight) for argillaceous salt (C).

Mineral-bound water is driven off by heating, releasing water vapor to the intergranular porosity (Figure 3.1). The release of bound water in hydrated minerals is associated with different volatilization temperatures for each mineral type (Kitagawa, 1972; Roedder and Bassett, 1981).

Table 3.1 shows clays, gypsum, and zeolites release waters of hydration at relatively low temperatures, below boiling ( $\approx$  75 – 100° C; see curve C in Figure 3.3). Bischofite and kainite can



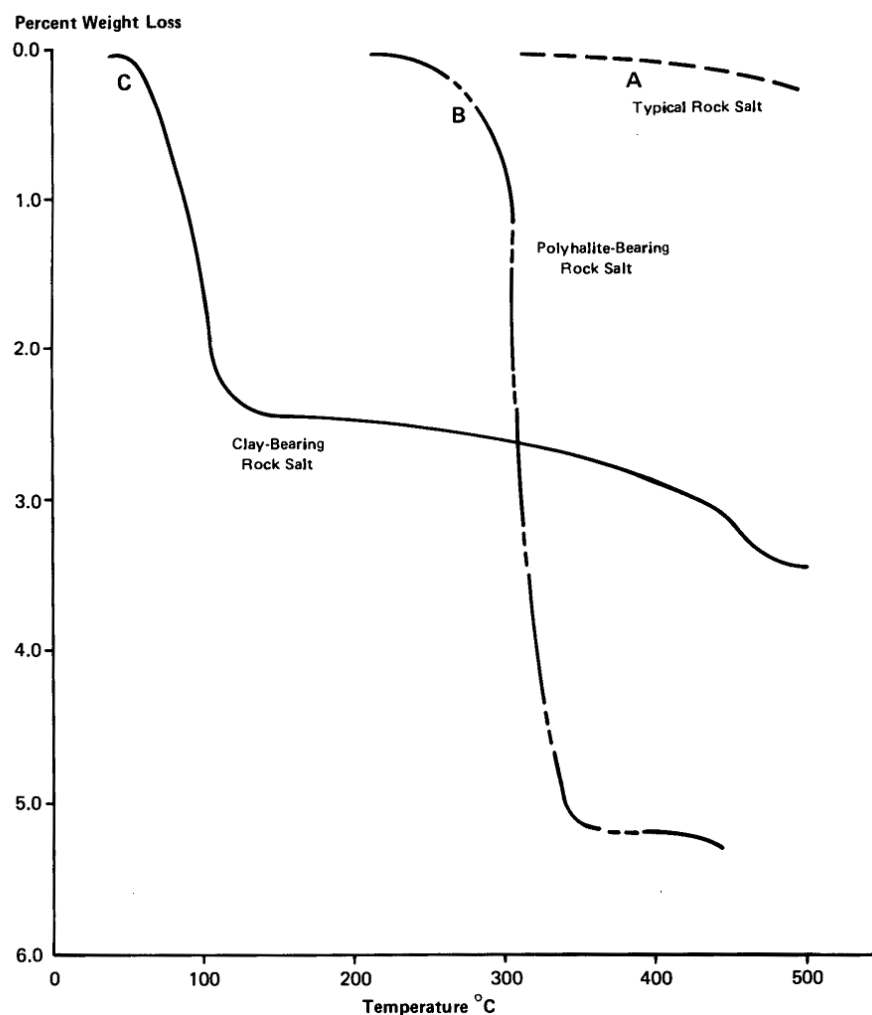


Figure 3.3: Characteristic thermogravimetric analyses from bedded salt samples (Powers et al., 1978)

release significant water at intermediate temperatures expected in a high-heat generating repository. Kieserite and polyhalite release water at temperatures above those expected under repository conditions ( $\geq 300^\circ\text{C}$ ). Roedder and Bassett (1981) report the lower dehydration temperature given for polyhalite ( $150 - 160^\circ\text{C}$ ) may be due to impurities (compare with Curve B in Figure 3.3).

This source of water can be included in the mass balance of brine flow models as a source term in the intergranular brine (similar to brine inclusions), activated at mineral-specific temperatures or ranges of temperatures. Stauffer et al. (2013) included a clay dehydration function in FEHM, based on thermogravimetric data obtained from WIPP clay samples (Caporuscio et al., 2013).

### 3.2.5 Water in run-of-mine salt vs. intact salt

The water content of mined salt is related to the intact salt from which it was mined. Run-of-mine crushed (or more simply “crushed”) salt has been proposed for use as a backfill material around

Name	Chemical Formula	% water by weight	dehydration temp. [° C]
carnallite	$\text{KMgCl}_3 \cdot 6(\text{H}_2\text{O})$	39	180 – 224
kainite	$\text{KMg}(\text{SO}_4)\text{Cl} \cdot 3(\text{H}_2\text{O})$	22	150 – 235
polyhalite	$\text{Ca}_2\text{K}_2\text{Mg}(\text{SO}_4)_4 \cdot 2(\text{H}_2\text{O})$	6	150 – 160 & 340 – 360
smectite clays		5 – 18	100 – 400
bischofite	$\text{MgCl}_2 \cdot 6(\text{H}_2\text{O})$	53	155 – 220
gypsum	$\text{CaSO}_4 \cdot 2(\text{H}_2\text{O})$	21	75 – 175
kieserite	$\text{MgSO}_4 \cdot \text{H}_2\text{O}$	13	340 – 400
zeolites		10 – 15	100 – 200

Table 3.1: Hydrous evaporite minerals in geologic salt; upper 4 minerals more common than lower 4. See references and notes in Roedder and Bassett (1981)

waste canisters in a salt repository because (Hansen et al., 2014a):

- Crushed salt is readily compacted and reconsolidated;
- Thermal, mechanical, and chemical properties of reconsolidating salt rapidly approach those of the undisturbed surrounding rock salt; and
- Reuse of mined salt in an underground facility is operationally efficient.

The components of the salt total water content associated with saturated non-salt components (i.e., clays), water of hydration (i.e., anhydrite and polyhalite), and intragranular brine inclusions may initially exist in the crushed salt in similar proportions as in the intact state. The high permeability and surface area of crushed salt compared to intact salt, means crushed salt exposed to mine ventilation may lose or take on moisture depending on the relative humidity of the ventilated air.

Crushed salt can easily be represented in porous media flow models, but the mechanical reconsolidation of crushed salt can be difficult to characterize and simulate accurately (Callahan, 1999; Olivella and Gens, 2002; Czaikowski et al., 2012). Constitutive models in mechanical deformation models for intact and crushed salt are different, as are the hydro-mechanical coupling constitutive models, due to the different pore structure in damaged and reconsolidating salt (Section 3.4.3).

### 3.3 Water Driving Forces in Salt

The driving forces and storage mechanisms which control the movement of brine in the DRZ or in crushed salt are discussed in the following subsections.

Given a distribution of porous fractured or crushed salt and available brine, the water in the intergranular porosity of a porous medium will redistribute in a variety of ways. At one end of the spectrum, single-phase liquid brine may flow under a pressure or stress gradient – assuming no movement of any gas or vapor content (e.g., McTigue, 1990 or Beauheim et al., 1997). At the other end of the spectrum, water vapor may flow as a single phase under pressure or vapor concentration gradients – assuming no movement of any brine (e.g., Hadley, 1982 or Rübél et al., 2013).

Under most variably saturated conditions, a combination of these two processes is occurring. Gas is also generally dissolving into and exsolving out of brine in response to pressure and temperature changes, changing the brine's physical properties. Either end of this "pure gas" or "pure brine" spectrum may be a valid simplification when one of the two phases (liquid water or water vapor) is essentially absent or immobile, allowing simplified linear analytical or numerical solution of the water redistribution problem (Hadley, 1982; McTigue, 1990). To explicitly consider the two-phase flow system allows for more generality and physical realism, but this increase in complexity also requires additional parameters and functional forms (i.e., capillary pressure and relative permeability relationships) not required in single-phase flow systems.

### 3.3.1 Pressure

Liquid and vapor pressures control movement of water in salt intergranular porosity. The primary driving gradient is from the far field to the excavation. If the excavation is connected to the land surface, its pressure is atmospheric (0.1 MPa). The far-field pressure in salt is considered to be lithostatic (increasing at approximately 22.6 MPa/km). Since salt creeps readily, the pressure in the far field where salt is intact and has very low-permeability is likely related to the stress in the rock, rather than a pore pressure or hydrostatic column of water.

This large pressure gradient exists over 2–5 excavation radii. Assuming Darcy's law (relating pressure gradients to flux) is valid from the far field to the excavation, the low observed brine flux into the excavation is therefore due to the large pressure gradient being applied across very low-permeability materials. The low permeability of the DRZ is due to both the low intrinsic permeability of salt and the low relative permeability of the dried-out portion of the DRZ near the excavation (where damage has increased the salt's intrinsic permeability).

The far-field ( $\geq 5$  excavation radii away) brine pore pressure has been estimated at WIPP (depth of 650 m) to be approximately lithostatic (i.e., the weight of the overlying sediments), nearly 15 MPa (Figure 3.4). Hydrostatic pressure (i.e., the weight of the column of water) would be approximately 6 MPa at a similar depth. When pore pressure approaches lithostatic pressure, it is often called "hard overpressure" (Zoback, 2007). This unique hydro-mechanical state is created under repository conditions by salt's inability to support deviatoric stresses (Wawersik and Stone, 1989).

Porous media flow models can represent the pressure driving force directly, as it is the primary one in typical groundwater and geothermal systems. Essentially single phase liquid flow due to rock stress and brine pore pressure exists from the saturation front near the drift opening, to the intact rock. Nearly single-phase vapor flow exists from the saturation front to the drift wall, in the porosity not occupied by brine. These two zones may be treated as single phase flow under some restricted conditions, but at least Richards' equation flow (i.e., infinitely mobile air phase) or two-phase flow must be considered to most generally simulate flow conditions from the excavation to the far field (Stephens, 1996; Warrick, 2003). Among the models considered in Section 2.1, CODE\_BRIGHT, FEHM, TOUGH2, and PFLOTRAN can consider two-phase flow, while  $d^3f/r^3t$  does not. Analytical solutions are limited to single-phase assumptions (Hadley, 1982; McTigue, 1986).

Brine flow and salt deformation have coupled effects on each other. Salt creep rate in cores increases after brine injection (Brodsky, 1990; Brodsky and Munson, 1991), related the poroelastic behavior of salt rock. Salt permeability increases when pressure exceeds the least principal

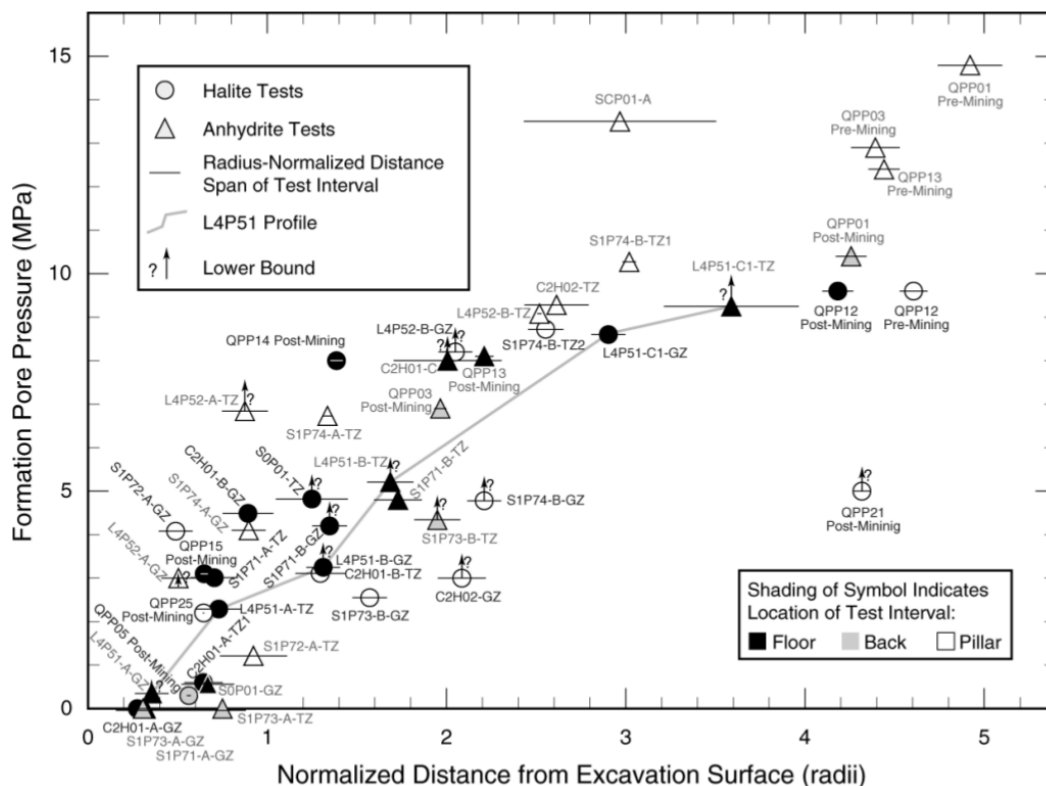


Figure 3.4: Static formation pore pressures interpreted from WIPP tests (Beauheim and Roberts, 2002)

confining stress (i.e., hydrofracture). Creep of salt can close porosity and increase pore pressure. The pressure-solution salt creep mechanism (important in both intact and crushed salt) is obviously dependent on the presence of water (Spiers et al., 1986, 1988; Urai et al., 2008), although it does not require significant amounts of water to be effective (Urai et al., 1986; Hansen et al., 2014a).

Flow through microfractured salt likely behaves like a classical porous medium. Discrete macrofractures may require a very large REV to meaningfully be represented as an effective porous medium. Significant open fractures are typically difficult to represent in most continuum models, and vapor flow through a single large-aperture fracture may dominate a flow system. Most numerical models based on the finite-volume numerical solution approach (e.g., FEHM, TOUGH2, PFLOTRAN, or  $d^3f/r^3t$ ) can simulate domains built out of an arbitrary connection of unstructured nodes and elements (i.e., not just a rectangular mesh of elements), some of which may represent fractures (Schneider, 2012; Makedonska et al., 2013).

Fracture characterization in underground excavations is difficult, requiring at least location, orientation, and aperture data for many discrete fractures. It is often too difficult to characterize or simulate discrete fractures, given the amount of available data, and a simpler porous medium approximation is typically used.

### 3.3.2 Hygroscopy

Hygroscopy is the ability of salt surfaces to attract and adsorb (or desorb) water molecules from the vapor in the atmosphere. Salt exposed to air will hold or release vapor to the air, depending on relative humidity (above or below 75% relative humidity). When dry (i.e.,  $\ll 75\%$  humidity) mine ventilation air is circulated over and through crushed salt in a salt repository, water content is lost from the exposed part of the salt and added to the ventilation air. When moist ( $> 75\%$  relative humidity) air is circulated over and through crushed salt, moisture adsorbs to the salt surface, increasing its water content. The steady-state relative humidity associated with air held in contact with a saturated salt solution is dependent on brine chemistry, but for NaCl-dominated brines, it is approximately 75% relative humidity (Potukuchi and Wexler, 1995).

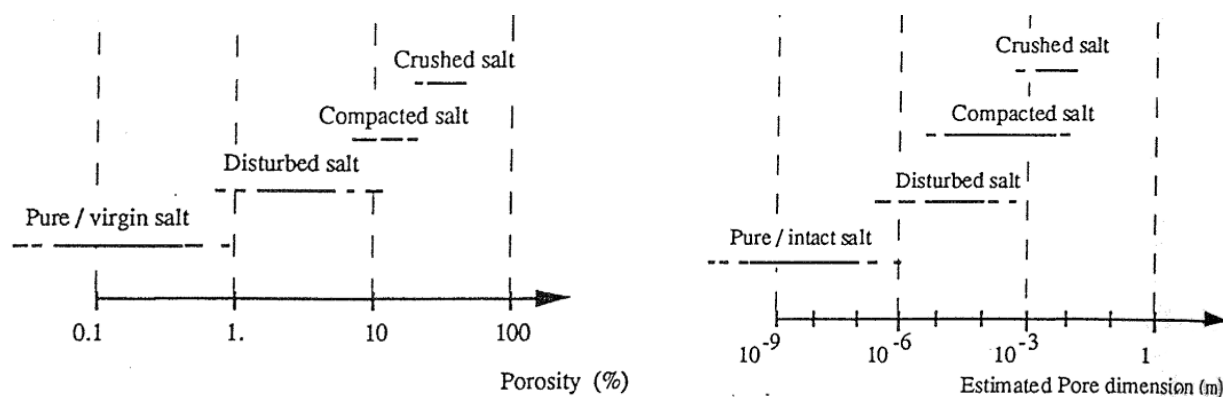


Figure 3.5: Range of salt porosity and pore size (Cosenza and Ghoreychi, 1993)

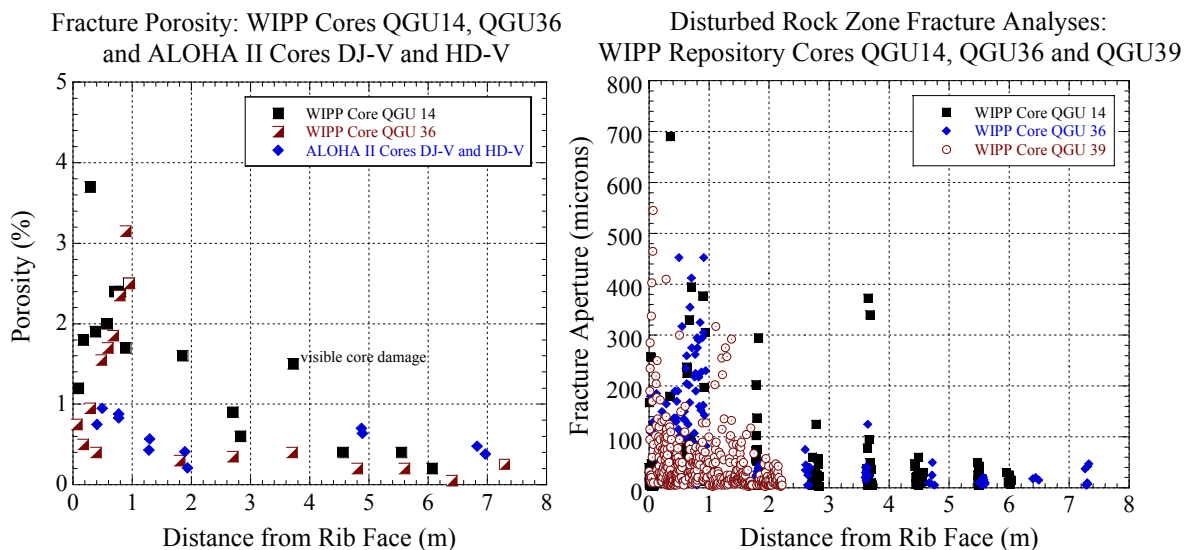


Figure 3.6: Salt petrofabric study results for WIPP and Asse salt (Bechthold et al., 2004).

The permeability and porosity of intact salt are quite low, and the permeability and porosity of unconsolidated crushed salt are orders of magnitude greater (Figures 3.5 and 3.6). This increase

in permeability and porosity allows water vapor loss to ventilation air through convection, at low pressure gradients, due to the significant increase in salt surface area exposed to air. Hygroscopy may only be a significant source or sink for water in crushed salt systems, or in significant open fractures, where air permeability and surface area are both high. Although hygroscopy may not be a significant volumetric source or sink of water, changes in humidity can be enough to affect salt creep rates (Van Sambeek, 2012).

Accurately including hygroscopic effects in numerical models requires explicit accounting for vapor-pressure lowering due to salt concentration, FEHM, CODE\_BRIGHT, and TOUGH2 (using the EWASG EOS module; Battistelli et al., 1995) have this capability, while the other numerical models considered here do not.

### 3.3.3 Capillarity

Brine is drawn into small-diameter pores or fractures through capillarity. The capillary suction ( $p_c = p_{\text{air}} - p_{\text{brine}}$ ) for immiscible fluids is inversely proportional to the pore radius or fracture aperture (Bear, 1972; Dullien, 1992). The ability of a medium to draw liquid into it below atmospheric pressure is characterized by capillary pressure or moisture release curves. Figure 3.7 shows laboratory capillary pressure data obtained from anhydrite cores taken from the DRZ at WIPP (Holcomb et al., 1995; Howarth and Christian-Frear, 1997). The high capillary pressure at brine saturation below 50% is indicative of microfractured but otherwise intact salt core.

There is not a significant amount of capillary pressure data available for either crushed or intact salt. Cinar et al. (2006) presented a study of the petrophysical properties of fine-grained crushed salt (Figure 3.8) and Olivella et al. (2011) included experimental capillary pressure data in their precipitation/dissolution laboratory modeling study (Figure 3.9). We are not aware of any capillary pressure data available for intact or damaged halite cores.

Run-of-mine salt typically used in repository operations has a very wide range of grain sizes – up to several-cm sized pieces (Brodsky, 1994), and may behave quite differently from uniform laboratory-prepared (sieved) samples used in Cinar et al. (2006) and Olivella et al. (2011).

Comparing the capillary pressure data for crushed salt (Figures 3.8 and 3.9) to the data obtained from cores of evaporites from the DRZ at WIPP (Figure 3.7) shows the capillary pressure is much lower in a material with larger pores sizes. Important parameters related to two-phase flow behavior and capillary pressure are the gas-threshold and air-entry pressures ( $P_{\text{gt}} = P_e + P_\ell$ , where  $P_{\text{gt}}$  is gas-threshold pressure,  $P_e$  is the air-entry pressure, and  $P_\ell$  is the liquid or formation pressure). Air-entry pressure is that required for air to enter a liquid-saturated sample (Davies, 1991). It can be estimated through laboratory experiments, but is often empirically related to permeability or pore/fracture aperture (Figure 3.10). Lower permeability materials tend to have high air-entry pressure, since both parameters are related to the pore radius or fracture aperture in the sample.

Undamaged salt has narrow grain-boundary and fracture apertures (Figure 3.5) and low permeability; it also has high air-entry pressure. It is difficult to force gas into undamaged brine-saturated salt. Damaged salt has larger fracture apertures and lower air-entry pressure. Compare the van Genuchten model air-entry pressure (called  $P_0$  in Figure 3.9) for the two graphs in Figure 3.9; 5% porosity corresponds to  $P_e = 0.012$  MPa and 10% porosity corresponds to  $P_e = 0.007$  MPa, while  $P_e = 0.05$  MPa in Figure 3.8. Estimates of  $P_e$  for the anhydrite cores illustrated in Figure 3.7 are  $\approx 0.04$  MPa (Howarth and Christian-Frear, 1997, Table 12).

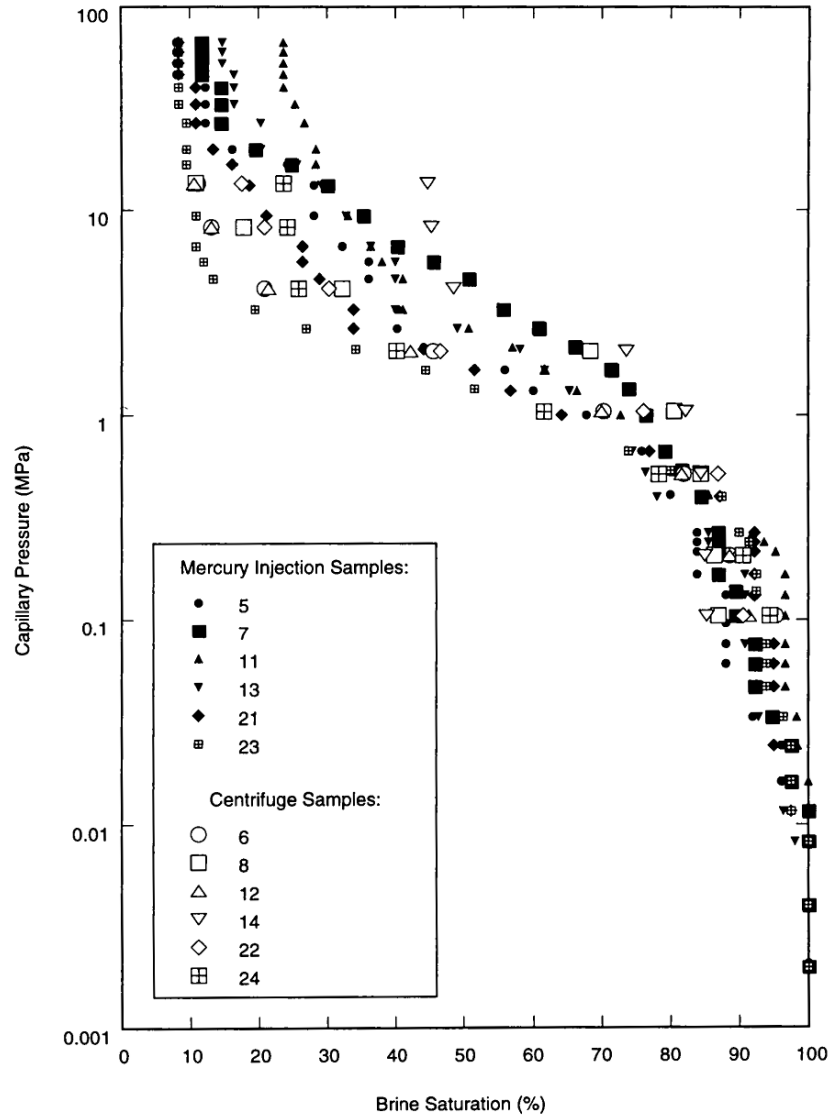


Figure 3.7: Capillary pressure data from WIPP anhydrite marker bed cores (Howarth and Christian-Frear, 1997)

Numerical models solving either the Richards' equation or the full two-phase flow problem will utilize functional models of capillary pressure/saturation relationships (e.g., Brooks and Corey, 1966 or van Genuchten, 1980) parameterized by capillary pressure data (including air-entry pressure) obtained from laboratory tests on the material of interest. Characterization of the relative permeability as a function of capillary pressure in a variably saturated medium is also required, but this is often approximated from the capillary pressure/saturation data using either the theory of Mualem (1976) or Burdine (1953) when no relative permeability data exist.

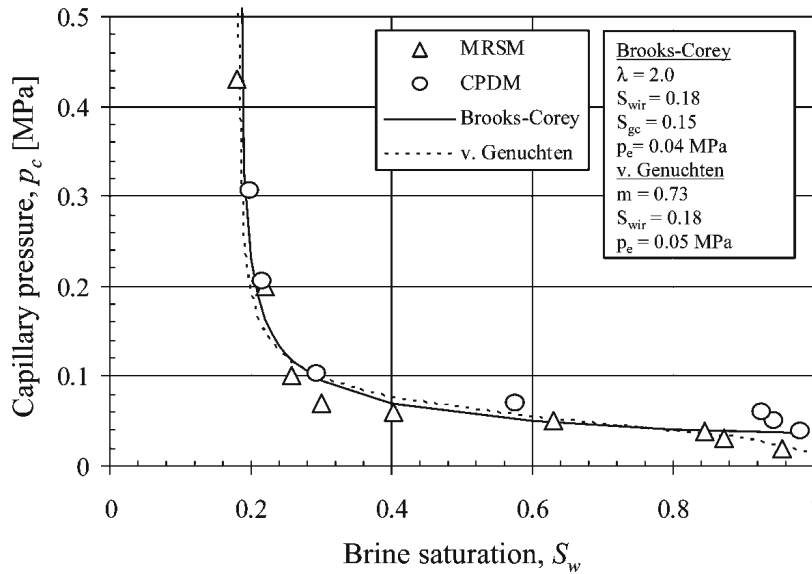


Figure 3.8: Capillary pressure data for fine-grained crushed salt (Cinar et al., 2006); Brooks and Corey (1966) and van Genuchten (1980) model parameters indicated; MRSM = steady-state modified restored-state method, CPDM = dynamic constant pressure desaturation method

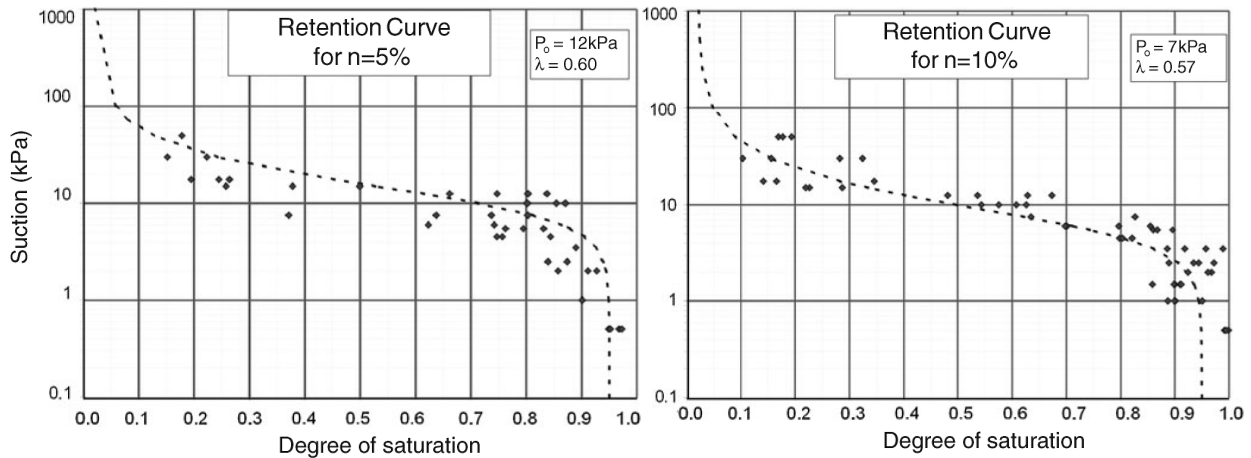


Figure 3.9: Capillary pressure data for fine-grained crushed salt at 5% and 10% porosity (Olivella et al., 2011); van Genuchten (1980) model parameters indicated

### 3.3.4 Gravity and density effects

Gravity obviously affects all fluid flow, but its effects may not be significant under all situations (e.g., horizontal constant-density flow or flow dominated by capillarity). Gravity’s effects will cause brine which flows into the DRZ to migrate towards the damaged zone associated with the floor of the room (Knowles et al., 1996; Stormont, 1997b).

In a salt repository, most water will become saturated with respect to NaCl (specific gravity of  $\approx 1.2$ ; 20% heavier than fresh water). Any fresh water due to vapor condensation will quickly



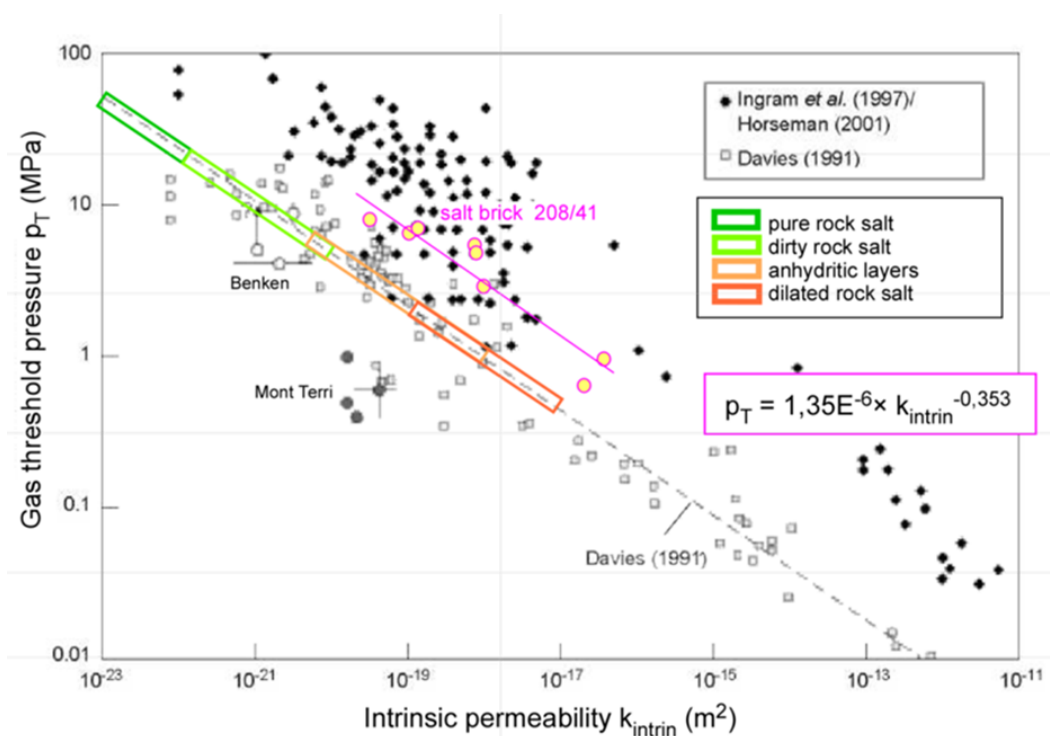


Figure 3.10: Correlation between intrinsic permeability and gas-threshold pressure; see Salzer et al. (2007) for references.

become saturated by dissolving salt. Either fresh water or less-dense brine will “float” on denser saturated brine. Density-driven convection or density stratification can also occur if brines of two different compositions develop, associated with different adjacent evaporite minerals.

To consider variable density flow in a repository requires the numerical model represent dissolved salt transport that can also change the flow properties of the system (density-dependent transport). FEHM, CODE\_BRIGHT, and  $d^3f/r^3t$  have this capability, while PFLOTRAN and TOUGH2 (EOS3) do not. The EWASG (Pruess et al., 2012) and ECO2N (Pruess, 2005) TOUGH2 EOS modules do have this capability. PFLOTRAN can simulate the transport of dissolved species in liquid water, but it currently does not update the water density.

### 3.3.5 Diffusive transport

In a liquid-dominated system, viscous brine flow occurs due to pressure gradients; solute mass transfer in the liquid can additionally occur due to concentration gradients (Bear, 1972). Similarly, in a gas-dominated system, pressure gradients lead to viscous flow, but Knudsen flow (i.e., Klinkenberg slip) may also occur under low pressures in narrow pores. Vapor concentration gradients can also drive mass transfer (Kast and Hohenthanner, 2000). Adsorbed liquids or vapors can also diffuse along pore surfaces inside a porous medium, driven by a surface liquid or vapor concentration gradients, which are related to liquid or vapor presence in pores (Satterfield, 1970).

Most numerical models considering two-phase flow will handle vapor concentration diffusion and models considering mass transport will include gradient-driven diffusion. No numerical models discussed in this report consider pore-scale flow of adsorbed liquids or gases explicitly.

TOUGH2 (using the EOS7C-ECBM module; Webb, 2011 or the REALGAS module; Moridis et al., 2012) can consider Knudsen flow of gases in small pores. Hadley (1982) and Rübel et al. (2013) considered Knudsen flow of gases primary importance in salt between the excavation and evaporation front.

In higher-permeability systems these concentration-gradient contributions are small or insignificant (flow is mostly due to viscous flow or mass advection), but in very low permeability systems (where fluid advection is negligible), diffusion can be important (e.g., see discussion on dimensionless quantities in Section 3.6).

### 3.3.6 Temperature effects

Temperature changes through time and temperature spatial gradients have two primary effects on brine flow in salt: thermal expansion of brine and migration or decrepitation of brine inclusions. As a secondary effect, salt permeability can increase several orders of magnitude during rapid cooling (Kuhlman and Malama, 2013), and accelerating creep closure during heating can heal permeability and porosity in the DRZ.

Brine and salt have very different coefficients of thermal expansion (Rübel et al., 2013). Brine expands volumetrically under an increase in temperature, and so does salt (but less so). Since a porous medium comprises both salt and brine, both components can contribute to a rise in pore pressure in response to an increase in temperature (i.e., undrained conditions). Numerical models considering thermal-hydrologic effects will account for the thermal expansion of brine (e.g., FEHM, PFLOTRAN, TOUGH2, and  $d^3f/r^3t$ ).

Single-phase brine inclusions migrate towards a heat source (up a thermal gradient), while biphasic brine inclusions can migrate away from a heat source (down a thermal gradient). This phenomenon is because the solubility of salt is strongly dependent on temperature; the difference in temperature across a brine inclusions ( $\approx 1$  mm) is enough to dissolve salt from one side of the inclusion and precipitate it on the other – effectively moving the brine inclusion. In biphasic inclusions water vapor is more mobile than dissolved salt, so evaporation and condensation produce a salinity gradient that moves the inclusion. Steep thermal gradients must be maintained to keep brine inclusions migrating; these steep thermal gradients only exist close to a heat source. In intact salt, brine inclusions may become intergranular brine or move into adjacent crystals. In crushed salt, brine inclusions would flow into the connected (typically air-filled) pore space. Increasing the temperature beyond the decrepitation point will liberate the intragranular brine through shattering of the salt crystal under the stress of expanding brine and high brine vapor pressure.

During heating, both salt and brine expand to increase rock stress and pressure. When an electric heat source is turned off, the thermal gradient in the salt reverses and rapid cooling affects the salt. Observations during the Project Salt Vault (Bradshaw and McClain, 1971), Avery Island (Krause, 1983), Salt Block II (Hohlfelder, 1980), and Asse (Rothfuchs et al., 1988) brine migration tests indicate significant pulses of brine can migrate into heater boreholes immediately following heater shut-down or decrease in heater power. This pulse of brine is likely due to the tensile microfracturing of the salt during cooling (Kuhlman and Malama, 2013). The slow decrease in heat load in a repository due to radioactive decay of waste will likely not produce this effect.

Hydraulic-mechanical constitutive models considering healing (e.g., Lux/Wolters; Wolters et al., 2012) can simulate creep closure of porosity, but most do not include increases in permeability due to tensile fracturing of salt during rapid cooling.

## 3.4 Distribution of Permeability and Porosity

Extreme variation in salt material properties may exist around an excavation. The differences between intact, damaged, and crushed salt permeability can be up to ten orders of magnitude. The porosity variation between the same types of salt can be up to three orders of magnitude (Figure 3.5), and is observed to vary at least two orders of magnitude in core samples under a microscope (Figure 3.6).

Variation in permeability and porosity in a salt repository can be due to several factors. Heterogeneity of geologic layering (Section 3.4.1) will juxtapose more and less permeable layers, while the mechanical effects of dilation and creep healing can increase or decrease permeability and porosity substantially (Sections 3.4.2 and 3.4.3). Chemical processes can influence the porosity and permeability of a salt medium through precipitation and dissolution (Section 3.4.4). Finally, a material's relative permeability to liquid or gas can be a tiny fraction of its overall intrinsic permeability (Section 3.4.5).

### 3.4.1 Permeability of heterogeneous layers

Bedded salt typically contains discrete layers of different geologic materials, including anhydrite, polyhalite, clay, and limestone. Marker Bed 139 is a 1-m thick anhydrite and clay layer at WIPP (Figure 3.11), which exists near the excavated disposal horizon. The anhydrite marker beds at WIPP have been the subject of significant laboratory (Howarth and Christian-Frear, 1997) and *in situ* hydraulic testing (Holcomb et al., 1995; Wawersik et al., 1997; Beauheim and Roberts, 2002). The contrast in both hydraulic and mechanical properties of the non-salt layers against largely pure halite layers can create preferential flow pathways through or along these layers.

Kuhlman and Malama (2014) discussed historical testing and observations supporting the possibility for flow and transport of added water in anhydrite layers within WIPP. The permeability of clay and anhydrite layers is much higher in the DRZ (especially at drift intersections) than in intact rock, essentially creating preferential pathways for brine to flow along excavated drifts, which may be dipping.

Most analytical solutions assume homogeneous material properties and simple symmetric geometries. Gridded numerical models can easily represent discrete geologic layers, representing observed heterogeneity.

### 3.4.2 DRZ permeability surrounding excavations

Using data published by Stormont et al. (1991a), Cosenza (1996) suggested a simple power-law fit to interpreted permeability data surrounding an excavated 1 m borehole (i.e., the WIPP Small-scale Mine-by test – Section 5.3.2), as a function of distance (Figure 3.12)

$$k(R) = k_1 + k_0 R^\alpha \quad (3.1)$$

where  $R = r/r_0$  is dimensionless radial distance from the center of the excavation normalized by the radius of the excavation ( $r_0$ ),  $k_1$  is the far-field (i.e., undisturbed) permeability,  $k_0$  is the permeability at the excavation face, and  $\alpha$  is a negative exponent ( $\alpha \approx -20$ ). These data suggest permeability increases exponentially towards the excavation, from approximately one excavation

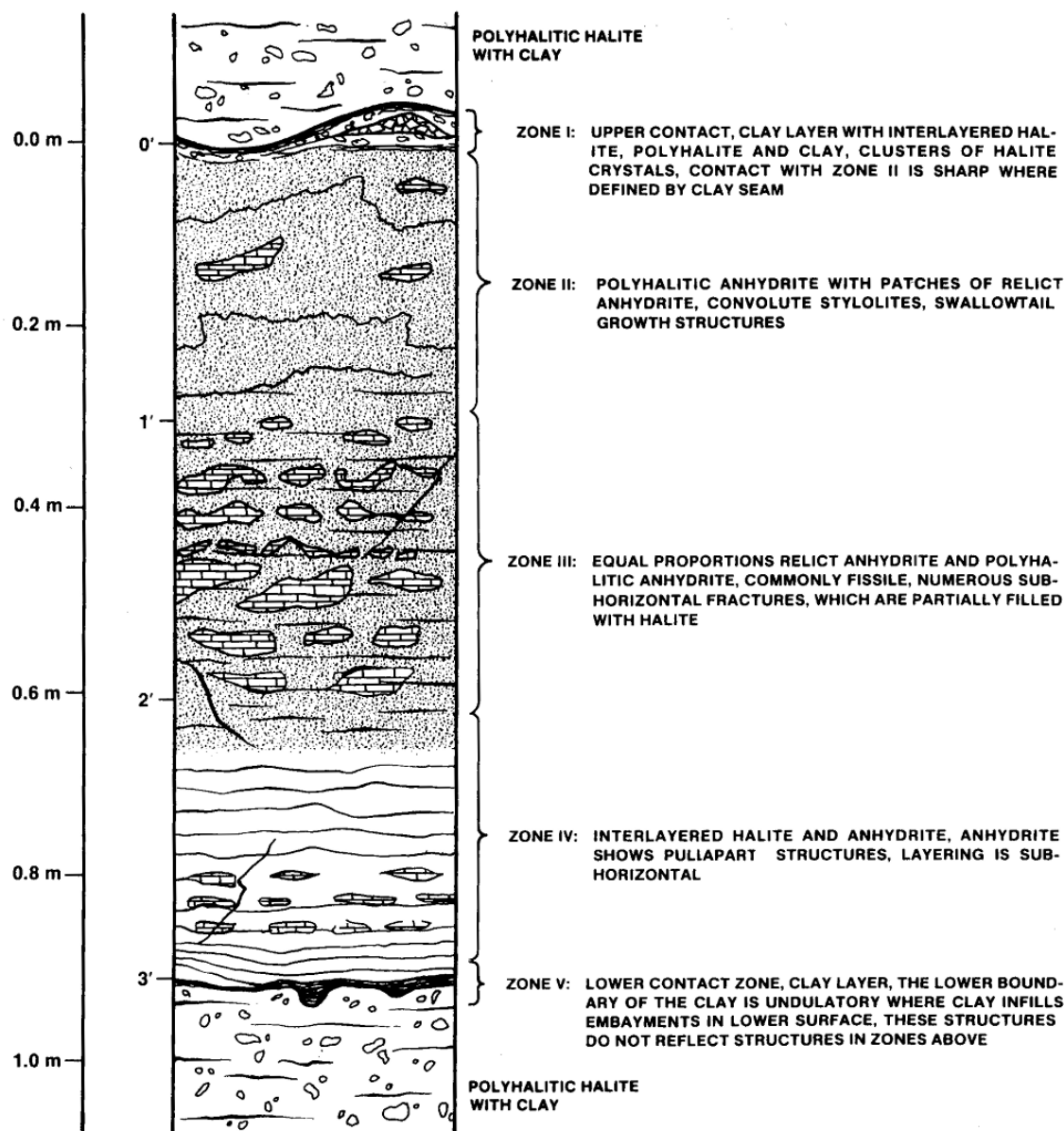


Figure 3.11: Idealized lithology of a typical non-salt component of bedded salt: MB139 (Borns, 1985)

radius into the salt ( $R = 2$ ). This relationship is only based on data from a single experiment, but it illustrates hydraulic properties in the DRZ are exponentially graded. Figure 5.9 in Section 5.3.3 shows additional results from the Small-scale Mine-by test. Stormont et al. (1987) presented similar data illustrating an increase in porosity approaching the excavation face, and Beauheim et al. (1991) discussed their brine permeability testing results in the context of the distribution of permeability surrounding an excavation in salt.

Beauheim and Roberts (2002) discussed brine permeability tests conducted in the evaporites at the WIPP site (Figure 3.13). Their data include results from multiple locations and tests, and do not show the simple behavior trend in the Small-scale Mine-by data (Figure 3.12).

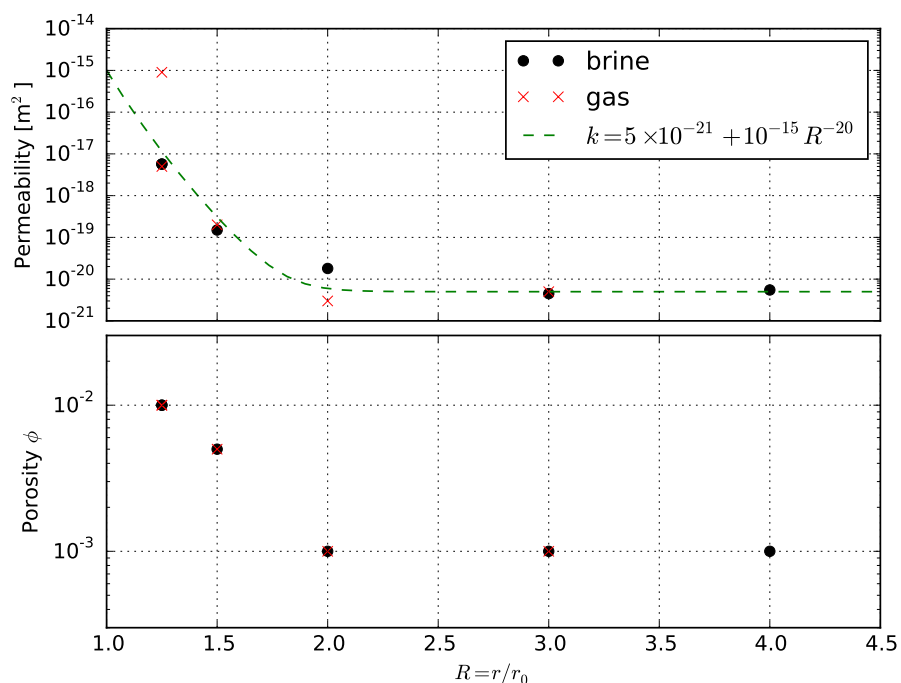


Figure 3.12: Permeability and porosity estimates from WIPP Small-scale Mine-by test (Stormont et al., 1991a); power-law model suggested by Cosenza (1996)

The DRZ has increased porosity due to microfracturing, which increases the bulk permeability of the salt. Macrofracturing also occurs, with large fractures typically being sub-parallel to the excavation and air-filled (Figure 3.14). Because they are air-filled, macrofractures are impermeable to brine flow, and they may act as reservoirs for collection of liquid brine.

The extent of damage in salt due to the excavation can be broken into two concentric zones centered on the excavation. Changes in permeability and porosity propagate approximately 1 excavation radius into the salt (Figure 3.12), while changes in pressure and rock stress propagate much further into the rock – five excavation radii or more into the salt (Figure 3.4). These are sometimes referred to as the excavation *damaged* and excavation *disturbed* zones, respectively (Davies and Bernier, 2005). Stormont et al. (1991a) referred to these regions as “major” and “minor” DRZs.

Salt permeability can be very sensitive to small amounts of dilation (Figure 3.15). First cross-hole arrivals of ultrasonic compressional waves have been used to delineate the extent of the DRZ in alcoves at WIPP (Holcomb et al., 2002) and Asse (Roest, 1987) with good success, indicating the dilation effects do impact sonic velocity through the salt.

### 3.4.3 Salt permeability as a function of mechanical properties

Brine flow is very sensitive to the relationship between intrinsic permeability ( $k$ ), porosity ( $\phi$ ), and the stress-strain state and history of the rock, but this relationship is difficult to characterize generally (i.e., across multiple experiments). Pore structure is the link between the mechanical and hydrologic responses of a porous medium (Stormont et al., 1991b). Pore structure in the

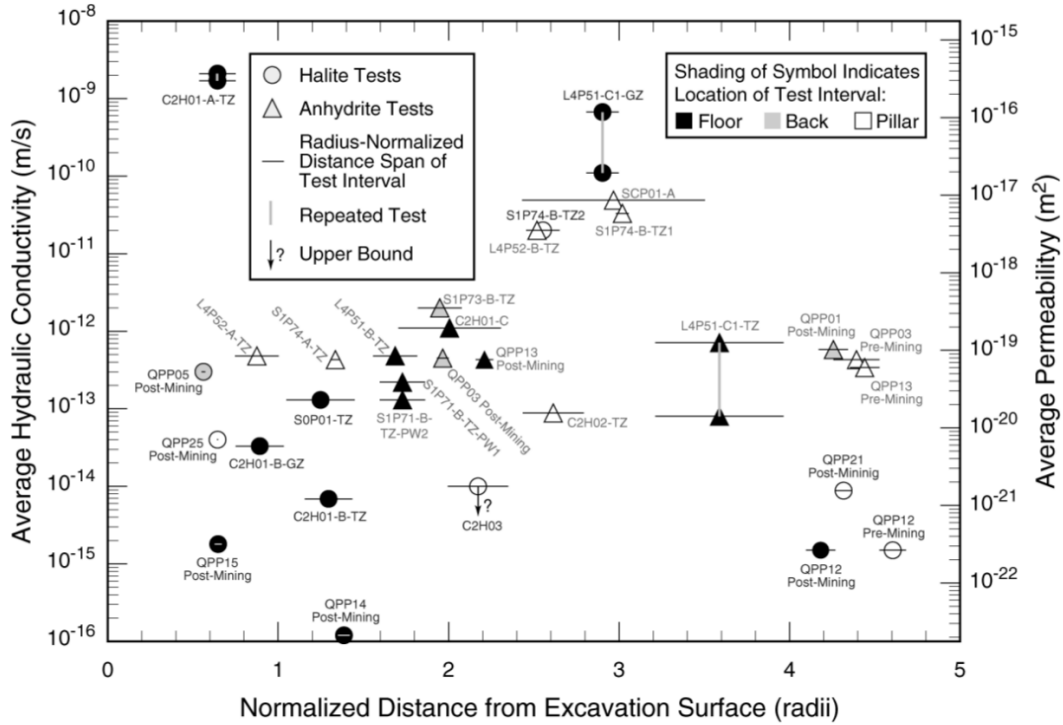


Figure 3.13: Brine permeabilities interpreted from tests conducted at WIPP (Beauheim and Roberts, 2002)

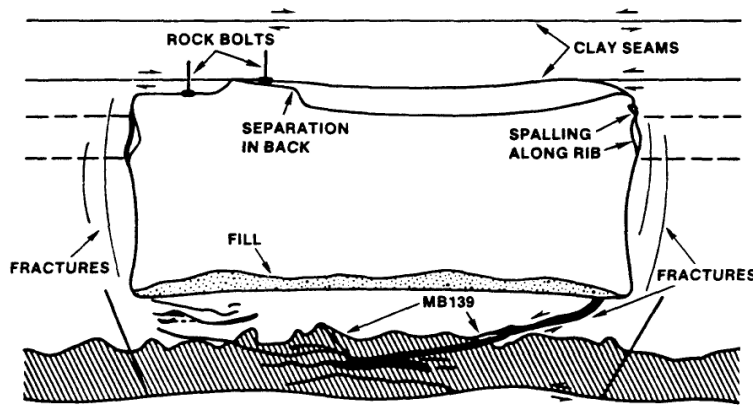


Figure 3.14: Typical macrofracturing and damage surrounding a room excavated in bedded salt (Borns and Stormont, 1988)

DRZ is different from pore structure in crushed salt or anhydrite and clay layers. Permeability would be expected to respond differently to stress and strain changes in these different materials, too. Many attempts have been made to parametrize the flow system dependence upon mechanical deformation. Most attempts fit relatively simple functions to observed field or laboratory data.

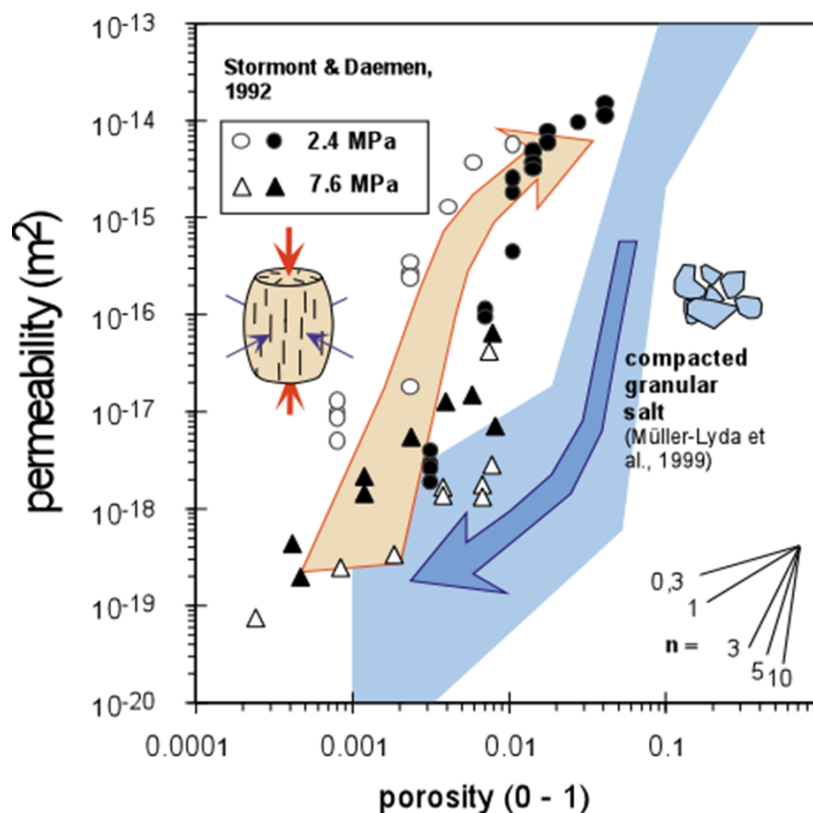


Figure 3.15: Trends in permeability and porosity for dilating (orange) and healing (blue) salt (Hansen et al., 2014a)

### Porosity-permeability relationships

The Kozeny-Karman relationship between porosity and permeability (derived for a bundle of cylindrical tubes) is typically used in crushed salt and granular media (Dullien, 1992, §3.3.1)

$$k = \frac{C\phi^3}{\Upsilon S_v(1 - \phi^2)}, \quad (3.2)$$

where  $C$  is a particle shape factor,  $\Upsilon$  is related to medium tortuosity, and  $S_v$  is medium-specific surface area. Porosity is nearly as difficult to estimate as permeability, but changes in porosity can be related to changes in rock damage.

Hansen et al. (2014a) discussed the difference in the relationship between permeability and porosity during dilation (i.e., damage) of intact salt and reconsolidation (i.e., healing) of granular salt. Figure 3.15 shows the general trends of these behaviors, and relates them to an exponent ( $n$ ) used in a power-law relationship

$$k = \phi^n, \quad (3.3)$$

indicated as labeled slopes in the corner of the figure.

Figure 3.15 shows a marked increase in permeability with small changes in porosity for dilating intact salt ( $n \geq 5$  for  $\phi \leq 0.01$ , then  $n \approx 1$  for  $\phi > 0.01$ ). The reconsolidation of crushed salt does not follow the reverse of this trend ( $n \approx 1$  for  $\phi \leq 0.05$ ), due to the very different nature of

the pore structure in reconsolidating crushed salt (isotropic porous medium) and dilating intact salt (anisotropic fractured medium). This hysteresis relationship between permeability and porosity illustrates one aspect of why it would be difficult to treat both intact and reconsolidating crushed salt with the same constitutive model.

### Stress-permeability relationships

Reynolds and Gloyna (1960) developed an empirical relationship between permeability and a combination of stress and pressure, based on fitting experimental data collected from tests on Grand Saline salt dome samples. Their relationship is

$$\log(k_L) = -21.1 - a_1 \log(\sigma_2 - p) \tag{3.4}$$

where  $\sigma_2$  is mean confining stress [psi], and  $a_1 = 0.212$ . Their  $k_L$  [m<sup>2</sup>] was “nonreactive fluid permeability”, most closely approximated through permeability tests with kerosene. Permeability estimated using brine was approximately  $k_L/3$  in their tests.

Lai (1971) determined the following empirical relationship for salt kerosene permeability

$$\log(k) = 0.62 - a_2(\sigma_2 - p) + a_3\tau_{oct} \tag{3.5}$$

where  $\tau_{oct}$  is the octahedral shear stress [psi],  $a_2 = 6.7 \times 10^{-4}$  [psi<sup>-1</sup>], and  $a_3 = 1.39 \times 10^{-3}$  [psi<sup>-1</sup>]. Equation (3.5) is illustrated in Figure 3.16, it essentially extends (3.4) beyond hydrostatic tests, to include shear stress effects on salt damage and permeability. Hydrostatic pressure decreases permeability; shear stress increases permeability.

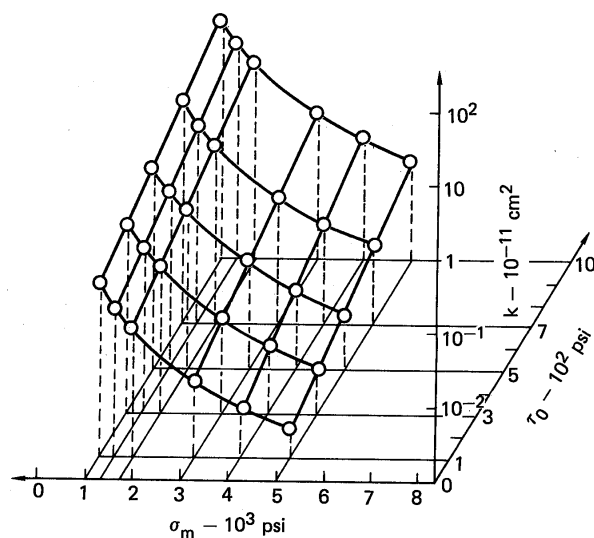


Figure 3.16: Salt permeability against net confining pressure ( $\sigma_m$ ) and octahedral shear stress ( $\tau_o$ ) (Lai, 1971).



### Stress/strain-permeability relationships

Stormont and Fuenkajorn (1993) based their permeability model upon the equivalent channel concept, developing the following relationship

$$\log(k) = \hat{A} + 2\lambda \log(\sigma_3/p) + s \log(\hat{\epsilon}_{kk}) \quad (3.6)$$

where  $\hat{\epsilon}_{kk}$  is the dimensionless dilatant volume strain,  $\lambda$  is a negative exponent,  $s$  is related to flow-path tortuosity, and  $\hat{A}$  is a constant. Figure 3.15 shows some data this model was developed to explain. Equation (3.6) is simplified form of the model presented in Stormont et al. (1992).

Chan et al. (2001) developed a two-part expression for permeability, which included contributions from salt porosity associated with the intergranular porosity, and a damage-induced microfracture network. They implemented

$$k = C_P - \epsilon_{kk}^3 + \frac{C_{CK}\phi^3}{(1-\phi)^2}, \quad (3.7)$$

where  $C_P$  and  $C_{CK}$  are coefficients to estimate from test data. The microfracture contribution ( $C_P - \epsilon_{kk}^3$ ) was based on results from percolation theory and the cubic law (Peach, 1991), while the contribution due to the inherent intergranular porosity was related to equation (3.2). When analyzing WIPP data, they found the contribution due to microfractures was more significant. Alkan (2009) developed an updated relationship between permeability and dilatancy, based upon percolation theory and the cubic law.

Blanco Martín et al. (2014a,b) present an empirical functional form (the Lux/Wolters model; Wolters et al., 2012) for the non-linear dependence of secondary damage-induced permeability, (i.e., as implemented in TOUGH-FLAC) as

$$\log_{10} \left( \frac{k_{\text{damage}}^{\text{sec}}}{k^*} \right) = \log(k_0) + \left\langle \log \left( \frac{\epsilon_{\text{vol}}}{\epsilon_{\text{vol},0}} \right) + d \exp(f\sigma'_{\perp 2}) \frac{\text{Ei}(e\epsilon_{\text{vol}}) - \text{Ei}(e\epsilon_{\text{vol},0})}{\log(10)} \right\rangle, \quad (3.8)$$

where  $\langle x \rangle = x$  if  $x > 0$  and 0 otherwise,  $k_0$  is initial permeability [ $\text{m}^2$ ],  $\epsilon_{\text{vol}} \geq 0$  is dimensionless dilatancy,  $\epsilon_{\text{vol},0} \leq \epsilon_{\text{vol}}$  is initial dilatancy,  $\sigma'_{\perp 2}$  is effective confining stress perpendicular to fractures [MPa],  $\text{Ei}(x) = \int_x^\infty \frac{e^{-u}}{u} du$  is the exponential integral,  $k^* = 1$  [ $\text{m}^2$ ], and  $\{d, e, f\}$  are dimensionless fitting parameters. Blanco Martín et al. (2014a,b) also present an expression for hydraulically induced secondary permeability increase due to increasing pore pressure (i.e., hydrofracture)

$$\log_{10} \left( \frac{k_{\text{frac}}^{\text{sec}}}{k^*} \right) = a + b \arctan [c(\sigma_3 + p)] + d \exp [e(\sigma_3 + p)], \quad (3.9)$$

where  $\sigma_3$  is the minimum principal stress [MPa], and  $\{a, b, c, d, e\}$  are experimentally determined dimensionless fitting parameters.

Relationships between mechanical and hydraulic behavior of salt are non-linear, hysteretic, and difficult to characterize. Ideally, permeability and porosity changes due to mechanical effects which characterize the disturbed zone surrounding an excavation would be included in numerical models (i.e., as done by TOUGH-FLAC and CODE.BRIGHT). Non-mechanical numerical brine flow models simply assign higher permeability or porosity to a zone surrounding the excavation – they include mechanical effects as boundary or initial conditions.

### 3.4.4 Porosity changes due to dissolution and precipitation

Olivella et al. (2011) recently presented laboratory experiment results (Figure 3.17) and numerical modeling with CODE\_BRIGHT related to crushed salt dissolution and precipitation under salt repository relevant conditions, building on related earlier work by Olivella et al. (1996) and Castagna et al. (2000). Figure 3.17 shows the distribution and evolution of porosity (determined by destructively analyzing the cylindrical samples in slices) after heating one end of the sample. The left plot shows the distribution of final porosity, as a function of the initial porosity; larger changes appear to happen in more porous crushed salt. The right plot shows how changes in initial saturation effect the results; brine content  $\geq 10\%$  saturation does not seem to magnify the dissolution and precipitation process for an initial porosity of 30%. High porosity values near the cold end include effects of large voids that developed in the salt at the end of the sample due to dissolution, and do not represent a uniform increase in porosity at the cold end.

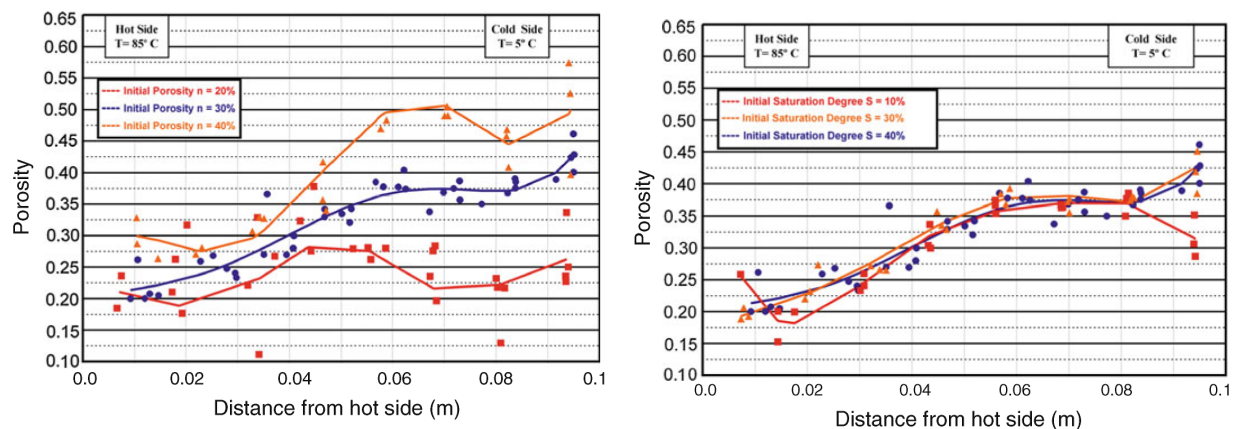


Figure 3.17: Experimental results showing redistribution of porosity due to precipitation and dissolution in crushed salt, as a factor of initial salt porosity for initial saturation of 40% (left) and initial brine saturation for initial porosity of 30% (right) (Olivella et al., 2011).

CODE\_BRIGHT and FEHM can simulate the effects that precipitation and dissolution in the porous medium have on flow. TOUGH2 has this capability with other EOS modules (EWASG and ECO2N) than those used in TOUGH-FLAC to date (EOS3). PFLOTRAN, and  $d^3f/r^3t$  do not currently have this capability. As shown by Olivella et al. (2011), significant isolated voids may develop during dissolution; these will likely not be accurately represented in a continuum-based porous media flow model.

Stauffer et al. (2013) used FEHM to simulate a drift-scale heater test in crushed salt and the precipitation-dissolution processes that occur in the material surrounding the heaters (THC). Brine is boiled away near the heaters (leading to a dry-out zone with reduced permeability from salt precipitation), vapor is efficiently transported away from the heaters and re-condenses in cooler crushed salt away from the heaters (leading to an increased porosity and permeability zone due to salt dissolution).

Little data is available on precipitation and dissolution in the DRZ. Krumhansl et al. (1991) performed post-test analysis on retrieved heaters from the WIPP Room B heater test experiments. Heater B042 was installed in a 36-inch diameter borehole without backfill, brine was removed

during heating by circulating dry nitrogen gas through weighed desiccants (Nowak and McTigue, 1987), and the heater was removed after testing by overcoring with a 37-inch bit. Analysis revealed there were two types of salt attached to the heater:

- Salt had crept into the open borehole because increased temperature effectively lowers the viscosity of salt; and
- Salt carried in by brine inflow to the borehole (35 liters total during test) had precipitated between the creeping borehole wall and the heater.

Analysis of the distribution of precipitated salt indicated the mass was consistent with the amount of brine that flowed into the borehole through salt and clay layers before the boiling ( $\approx 110^\circ\text{C}$ ) isotherm moved outside the borehole (at  $\approx 400$  days). Once boiling occurred in the DRZ, it is assumed the precipitated salt was deposited there. Reduction of permeability in damaged salt (as opposed to crushed salt) due to precipitation is likely, but the nature of these effects on salt porosity and permeability is largely unknown.

Other heated brine migration tests that achieved boiling temperatures in the DRZ (Hohlfelder, 1980; Krause, 1983; Rothfuchs et al., 1988), likely experienced this type of permeability reduction as well.

### 3.4.5 Permeability changes due to variable saturation

The intrinsic permeability of a porous or fractured medium may change due to mechanical effects, but the effective permeability to either liquid or gas is a fraction of this total, because brine or air must flow through a subset of the pore space (Dullien, 1992). Trapped air in mostly brine-saturated rock, or trapped brine in nearly air-saturated rock, result in lower effective porosities to the other component. Just as in mechanical deformation (Section 3.4.3), small changes in porosity can result in significant changes in permeability. Due to its significant compressibility, small amounts of trapped air can also increase the apparent compressibility and storage properties of the rock.

Relative permeabilities at low saturation can be very small (e.g.,  $10^{-7}$ ), essentially rendering already low permeability even more impermeable, or lowering the permeability of the DRZ below the permeability of intact salt.

## 3.5 Chemical Processes in Salt and Brine

Due to the high solubility of halite in water, the primary chemical process considered is the dissolution and precipitation of salt, which typically comprises  $\geq 95\%$  of the porous medium. The effects of these processes on the porosity and permeability of the saline porous medium are discussed in Section 3.4.4.

Among the models considered in this report with solute transport capabilities (i.e., FEHM, TOUGH2, CODE\_BRIGHT, PFLOTRAN, and  $d^3f/r^3t$ ), PFLOTRAN and FEHM include general reactive transport capabilities, while the other models have more limited chemistry simulation capabilities, requiring iterative coupling to external models (e.g., TOUGHREACT; Xu et al., 2006 or  $d^3f/r^3t$  with PHREEQC; Parkhurst and Appelo, 2013) for their geochemical modeling capabilities.

Reactive transport capabilities allow more physically realistic treatment of solute-surface reactions (i.e., sorption) and tracking of multiple interacting species and their activities, but significantly increase the data requirements for flow and transport modeling. The geochemical state of pore fluids must be characterized and the development of numerically stable geochemical initial conditions may require additional simulations. Reactive transport can allow general treatment of radionuclide transport, and the explicit treatment of transport through different regimes (e.g., from brine in salt to a fresher regional aquifer in the geosphere), which may have significant effects on the solubility and sorption of repository-relevant species.

The radioactive waste form and packaging itself (i.e., spent fuel or vitrified reprocessing waste) are evolving and degrading through time, through interim storage, transportation, and final disposal in a geologic repository. The waste form and package comprise the thermal source terms in heat-generating waste repositories. Chemical interactions between the waste form and package and the water-saturated host rock can generate gases which may pressurize a sealed repository. The thermal output, produced gas, and inventory of radionuclides are typically specified as explicit source terms in repository flow and transport models (Sassani et al., 2012, 2013). Specialized nuclear fuel performance models can be used to determine these properties for inclusion in coupled multi-physics repository simulations (e.g., Idaho National Laboratory's BISON and MOOSE simulators; <http://mooseframework.com>).

There are many potential areas for improvement and increased realism in salt repository geochemical modeling. There are significant additional requirements for process understanding and data to populate advanced reactive transport models. Reactive geochemical transport models are often best used as batch simulations (a single element) or column simulations (one-dimensional) to better understand the physics of reactions (Parkhurst and Appelo, 2013). Significant uncertainty can be associated with the spatial distribution of geochemical properties in two- and three-dimensional domains.

### 3.6 Balance of Dimensionless Quantities

The relative importance of physical processes in coupled process modeling can be roughly quantified through use of characteristic quantities. Cosenza and Ghoreychi (1993) and Kazan and Ghoreychi (1996) presented a set of characteristic times illustrating ranges of repository-relevant conditions under which the different components of THMC are important; these values are given in modified form in Table 3.2. In the following section we introduce characteristic times for intact, DRZ, and crushed salt properties from Cosenza and Ghoreychi (1993) and Cosenza et al. (1998), which could be used to define dimensionless times. Kuhlman and Malama (2013) presented dimensionless quantities illustrating the relative importance of pressure and thermal gradients on intergranular brine and thermal loading on the stress field. Schneider (2012) and Urai et al. (2008) discussed dimensionless representation of thermohaline convection problems, in the context of the salt dome stability in regional groundwater flow systems. The definitions of the different characteristic times in Table 3.2 are given in the following subsections.

Salt Type	Thermal (T)	Hydraulic (H)	Mass-transfer (C)
intact	$\tau_{Td} = 35$ days	$\tau_{Hb} = 115$ days	$\tau_{Cd} = 30$ years
DRZ	$\tau_{Td} = 35$ days	$\tau_{Hb} = 3$ hours	$\tau_{Cd} = 30$ years
	$\tau_{Tcb} = 750$ years $\tau_{Tcv} = 30$ years	$\tau_{Hv} = 2$ min	
crushed	$\tau_{Td} = 1.5$ years	$\tau_{Hb} = 10^{-4}$ sec	$\tau_{Cd} = 15$ min
	$\tau_{Tcb} = 42$ min	$\tau_{Hv} = 10^{-6}$ sec	$\tau_{Cc} = 3$ sec
	$\tau_{Tcv} = 1.7$ min		

Table 3.2: Values of characteristic times; characteristic length  $L = 1$  m (Cosenza and Ghoreychi, 1993; Cosenza et al., 1998)

### 3.6.1 Thermal characteristic time

Two characteristic thermal times ( $\tau$ ) can be related to diffusive heat transfer (Td) and forced (pressure-driven) brine convective heat transfer (Tcb);

$$\tau_{Td} = \frac{L^2}{\alpha_T} \quad \tau_{Tcb} = \frac{Lk_T}{\alpha_T C_\epsilon \mathbf{u}}$$

where  $L$  is a characteristic length [m],  $\alpha_T$  is thermal diffusivity [ $m^2/s$ ],  $\mathbf{u} = \frac{k}{\eta\phi S} \nabla p \approx \frac{k}{\eta\phi S} i$  is Darcy flow velocity [m/s],  $i$  is a pressure gradient [Pa/m],  $k$  is intrinsic permeability [ $m^2$ ],  $\eta$  is dynamic fluid viscosity [Pa·s],  $\phi$  is porosity,  $k_T$  is thermal conductivity [W/(m·K)], and  $C_\epsilon$  is volumetric fluid heat capacity at constant volumetric strain [J/( $m^3 \cdot K$ )]. A subscript b or v indicates the fluid of interest is brine or vapor. Table 3.3 lists typical values of thermal properties relevant to salt repository components ( $k$ ,  $i$ , and  $\eta$  values are listed in Table 3.5).

Property	Material	Typical Values	Units
$\alpha_T$	intact salt	$3 \times 10^{-6}$	$m^2/s$
	crushed salt	$4.8 \times 10^{-7}$	
$k_T$	intact salt	5	W/(m·K)
	DRZ salt	4.2	
	crushed salt	0.25	
$C_\epsilon$	brine	$4.2 \times 10^6$	J/( $m^3 \cdot K$ )
	air	$1.2 \times 10^6$	

Table 3.3: Typical thermal properties for salt (Cosenza and Ghoreychi, 1993; Cosenza et al., 1998)

Comparing thermal characteristic times in Table 3.2, crushed salt has much shorter characteristic times than intact or damaged salt, related primarily to the difference in efficiency between diffusion and convection processes. The characteristic time for diffusion in crushed salt is actually lower than in intact salt, due to the lower thermal conductivity of crushed salt.

The thermal Peclet number is a dimensionless quantity defined as the ratio of diffusion and convection characteristic times,

$$Pe_T = \frac{\tau_{Td}}{\tau_{Tc}}. \quad (3.10)$$

When  $Pe_T \ll 1$  heat conduction (i.e., thermal diffusion) is dominant, when  $Pe_T \gg 1$  forced brine or vapor heat convection (due to pressure gradients) is dominant (Table 3.4). Based on the computed values of  $Pe_T$ , thermal diffusion is dominant in intact salt, while thermal convection (brine or vapor) is dominant in crushed salt. There is no value for  $Pe_{Tv}$  in intact salt, because vapor saturation in intact salt is so low, this process would be ineffective.

Material	$Pe_{Tb}$	$Pe_{Tv}$
crushed salt	$2 \times 10^6$	$5 \times 10^7$
DRZ salt	$1.3 \times 10^{-4}$	$3 \times 10^{-3}$
intact salt	$5 \times 10^{-7}$	–

Table 3.4: Thermal Peclet numbers for different salt types (Cosenza et al., 1998)

The Rayleigh number is a dimensionless ratio of buoyant forces to diffusive and viscous forces (Nield and Bejan, 2006), indicating the efficacy of free convection due to thermal gradients. Values of this number can be used to characterize the importance of free vapor convection in crushed salt above different geometrical configurations of heaters, given expected heat loads.

### 3.6.2 Hydraulic characteristic time

A hydraulic characteristic time related to isothermal poroelasticity is

$$\tau_H = L^2 \frac{\eta}{kM} \frac{3K + 4G}{3K_0 + 4G} \quad (3.11)$$

where  $M$  is Biot's modulus [Pa] (the reciprocal of the constant-volume storage coefficient, which is larger than the constant-load storage coefficient commonly used in hydrology; Wang, 2000),  $K$  is the undrained bulk modulus [Pa],  $K_0$  is the drained bulk modulus [Pa], and  $G$  is the shear modulus [Pa]. For salt,  $\tau_H \approx L^2/\alpha_H$ , where  $\alpha_H = kM/\eta$  is hydraulic diffusivity [ $m^2/s$ ]; Table 3.5 lists typical values for hydraulic properties relevant to salt systems.

Table 3.2 shows the characteristic times associated with brine and vapor flow under pressure gradients. Times associated with of brine and gas are much shorter in crushed salt, than in the DRZ and intact salt. Gas/vapor flow times are shorter than associated brine flow times, due to the lower viscosity of gas.

### 3.6.3 Mass transport characteristic time

Three characteristic times can be related to dissolved mass transport of radionuclides or salt in brine (Cosenza and Ghoreychi, 1993). A characteristic time associated with mass diffusion is

$$\tau_{Cd} = \frac{L^2 \phi}{\phi D_m + \alpha_D \mathbf{u}}, \quad (3.12)$$

Property	Material	Typical Values	Units
$\eta$	brine	$1.7 \times 10^{-3}$	Pa·s
	air (25° C)	$1.9 \times 10^{-5}$	
$\alpha_H$	brine in intact salt	$10^{-7}$	m <sup>2</sup> /s
	brine in DRZ	$10^{-4}$	
	brine in crushed salt	$10^{+4}$	
$i$	disturbed rock gradient	1.5	MPa/m
	damaged rock gradient	0.3	
	crushed salt gradient	0.01	
$\phi$	intact salt	0.001	-
	DRZ salt	0.01	
	crushed salt	0.35–0.4	
$k$	intact salt	$10^{-20}$ – $10^{-22}$	m <sup>2</sup>
	DRZ salt	$10^{-18}$ – $10^{-20}$	
	crushed salt	$10^{-9}$ – $10^{-11}$	

Table 3.5: Typical hydraulic properties for salt (Cosenza and Ghoreychi, 1993; Cosenza et al., 1998)

where  $\alpha_D$  is a dispersion coefficient [m]. A characteristic time associated with dissolved mass convection in brine is

$$\tau_{Cc} = \frac{L\phi}{\mathbf{u}}, \quad (3.13)$$

and a characteristic time associated with the dissolution and precipitation of salt in brine is

$$\tau_{Cs} = \frac{V}{AR_d}, \quad (3.14)$$

where  $V/A \approx L/\zeta$  is the volume of the solution in contact with salt minerals per unit specific area of solute [m],  $\zeta$  is an empirical factor of the pore geometry in the range 2–10, and  $R_d$  is the dissolution constant [m/s]. The dissolution and precipitation of salt in water is relatively quick ( $\tau_{Cs} = 2$ –14 hours for  $L = 1$  m), due to the high solubility of NaCl in water. Table 3.6 provides typical values of relevant mass transport properties in salt.

Table 3.3 gives characteristic time associated with dissolved mass transport in brine. Characteristic times associated with diffusion- and convection-driven mass-transfer indicate mass transport occurs over much shorter time scales in crushed or damaged salt, compared to intact salt.

Two dimensionless transport Peclet numbers are defined as the ratio of diffusion to convection (Cc) and the ratio of diffusion to dissolution (Cs) (Table 3.7),

$$\text{Pe}_{Cc} = \frac{\tau_{Cd}}{\tau_{Cc}}; \quad \text{Pe}_{Cs} = \frac{\tau_{Cd}}{\tau_{Cs}}. \quad (3.15)$$

Table 3.7 illustrates diffusion processes are dominant in damaged salt, but in crushed salt convection and diffusion mass transfer are approximately balanced. When  $\text{Pe}_C \ll 1$  mass diffusion is dominant, when  $\text{Pe}_C \gg 1$  mass convection is dominant

Property	Material	Typical Values	Units
$D_m$	halite in water (20° C)	$1.3 \times 10^{-9}$	m <sup>2</sup> /s
$\alpha_D$	crushed salt	0.01	m
$R_d$	halite in water	$10^{-5}$	m/s
$V/A$	water in halite	0.1–0.5	m

Table 3.6: Typical mass-transport properties for salt (Cosenza and Ghoreychi, 1993; Cosenza et al., 1998)

Material	Pe <sub>Cc</sub>	Pe <sub>Cs</sub>
crushed salt	0.1	$10^{-5}$
DRZ salt	$10^{-6}$	$10^{-2}$

Table 3.7: Transport Peclet numbers for different salt types (Cosenza and Ghoreychi, 1993)

These characteristic times and dimensionless ratios illustrate the significant differences between flow in crushed salt and damaged (DRZ) salt or intact salt. Different processes may dominate in each part of the excavation-influenced portion of the repository, due to the nature of the material and fluid properties.



## 4 Recent Hydrologic Model Development and Lab Testing for Water in Salt

This section summarizes recent laboratory and modeling work relevant to brine flow in salt under repository conditions. Much of this work was funded by either the Department of Energy Office of Nuclear Energy (DOE-NE) Used Fuel Disposition (UFD) Campaign or the Department of Energy Office of Environmental Management (DOE-EM) related to development of the Salt Disposal Investigations (SDI; DOE, 2011) or the Salt Defense Disposal Investigation (SDDI; DOE, 2012) test plans.

### 4.1 Los Alamos National Laboratory

Stauffer et al. (2012) and Harp et al. (2014) summarize some thermal and thermal-hydrological modeling related to the proposed SDDI repository configuration performed using FEHM in FY12. Some WIPP-related benchmarking results were presented showing FEHM and the analytical isothermal and non-isothermal solutions of McTigue (1986, 1990) and Nowak et al. (1988). Thermal conduction-only simulations were made on a large three-dimensional mesh representing the SDDI test configuration (5 cylindrical heaters on the floor in two parallel drifts, covered by a trapezoidal pile of crushed salt). Finally, thermal-hydrological simulations were carried out on a smaller half-domain mesh for the SDDI test configuration. The suite of conditions explored included different thermal loads (500 W, 1000 W, and 1500 W heaters) and different initial saturation in the crushed salt.

Stauffer et al. (2013) summarizes additional modifications made to FEHM in FY13, again focusing on simulating the SDDI repository configuration. The functionality added to FEHM included:

- Crushed salt thermal conductivity dependence on porosity and temperature,
- Salt solubility in brine as a function of temperature,
- Changes in salt porosity including precipitation and dissolution of salt,
- Water vapor diffusion coefficient as a function of pressure, temperature, and porosity,
- Power-law permeability-porosity relationship,

- Water vapor pressure as a function of brine strength and temperature, and
- Temperature-dependent clay dehydration source term.

FEHM was evaluated using data from the WIPP Room Q isothermal brine inflow experiment (see Section 5.3.3 for comparison of this data with other modeling strategies). Further FEHM model comparisons were done against a single-crystal heat conduction laboratory experiment and a cone-shaped pile of crushed salt heated with a 125 W bulb.

New THC FEHM simulations were performed for the SDDI test configuration to illustrate the effects of porosity variation due to precipitation and evaporation of salt, controlled by vapor convection away from heat sources. Sensitivity analyses were done with a scaled-down two-dimensional slice model to understand the relative effect different ranges of input parameters had on maximum predicted temperatures and change in water mass across different regions of the simulation domain.

Stauffer et al. (2013) presented Lattice-Boltzmann simulations of individual brine inclusions in a single grain of salt. Single-phase brine inclusions moved up a thermal gradient, but two-phase brine inclusions did not move down the thermal gradient, as observed in numerous experiments.

Caporuscio et al. (2013, 2014) performed laboratory characterization studies related to brine content and movement in bedded geologic salt. Using thermogravimetric analysis and X-ray diffraction, they characterized brine and mineral content of clay and bedded salt samples from WIPP. Microscope-scale laboratory experiments were conducted to monitor migration of brine inclusions in single (Caporuscio et al., 2013) and multiple (Caporuscio et al., 2014) salt crystals on a heated microscope stage. Scanning electron microscopy was used to image salt crystals after brine inclusions had migrated through them under a thermal gradient, illustrating a network of small-scale brine transport tubes. Caporuscio et al. (2014) showed nuclear magnetic resonance to be a viable method for characterizing brine distribution in salt, distinguishing relative amounts of mineral-bound water, water in clays, and free water (sum of intergranular and intragranular water).

## 4.2 Lawrence Berkeley National Laboratory

Blanco Martín et al. (2014a,b) and Rutqvist et al. (2013, 2014) discuss development and recent advances of the iteratively coupled THM model TOUGH-FLAC to simulate salt repository conditions. Recently, the ability to handle large mechanical deformations was added to TOUGH-FLAC, by re-meshing the TH flow problem, while explicitly accounting for mass conservation in TOUGH2 (Rutqvist et al., 2013, 2014). They have also compared alternative coupling strategies (Berkeley's TOUGH-FLAC vs. FLAC-TOUGH by Clausthal University of Technology), where either TOUGH2 or FLAC<sup>3D</sup> is the primary model, and the other model is the secondary or slave. The TOUGH-FLAC and FLAC-TOUGH simulators have been validated against the TSDE Asse in-drift heater test (Rutqvist et al., 2014).

Rutqvist et al. (2014) presented the background and mathematics associated with an approach for simulating both intergranular and intragranular brine flow using a dual-porosity conceptualization. TOUGH2 may only require limited modifications to implement this approach.

---

### 4.3 Sandia National Laboratories

Sandia has been performing thermo-mechanical modeling of generic salt repositories using SIERRA mechanics. This modeling effort has included large-deformation modeling of room closure in hypothetical high-level waste repositories under heated conditions (Clayton and Gable, 2009; Stone et al., 2010; Clayton et al., 2012; Argüello, 2014), room closure including crushed salt reconsolidation (Clayton et al., 2010), and validating models against observed room closure at WIPP in Rooms B and D (Argüello and Rath, 2013).

Recent laboratory tests were conducted at Sandia to estimate crushed salt thermophysical properties as a function of porosity (Bauer and Urquhart, 2014; Bauer et al., 2014). WIPP crushed salt samples were consolidated to 3%–17% porosity under different loads and temperatures. Thermal conductivity, heat capacity, and thermal diffusivity were estimated for crushed salt of variable porosity and single-crystal halite.

In 2013, Sandia provided approximately 36 m of 12-inch diameter bedded salt cores from WIPP (both “clean” and “argillaceous” salt materials), which were used by several German institutions (including Institut für Gebirgsmechanik GmbH and TU Clausthal) to perform creep and triaxial strength tests (Hansen et al., 2013b). The large-diameter salt cores were sub-cored into about 150 4-inch diameter samples for testing. Preliminary results are available from some tests, while some long-term creep test are still ongoing. They will allow the German numerical modeling efforts (i.e., the Joint Project) to better parameterize their constitutive models for bedded salt, in a manner similar to what has been done for modeling domal salt. The latest validation exercise in the Joint Project involves matching thermal-mechanical model predictions to room closure in WIPP experimental Rooms B and D (Argüello and Rath, 2013; Hansen et al., 2013b).

## 5 Hydrologic Initial Conditions in Salt Repositories

The following discussion concerns development of the hydrologic state for a repository in salt, specifically its representation in hydrologic numerical models. Hydrologic conditions within and around a salt repository are strongly tied to the mechanical state and damage history of the medium (Section 5.1). We present a summary of the key processes controlling the hydrologic condition followed by results from two, one-dimensional modeling exercises to illustrate different modeling approaches (Section 5.2). Finally, supporting observations of DRZ dry-out from excavations in salt at WIPP are presented (Section 5.3).

The hydrologic state variables relevant to numerical modeling are the brine and gas pressure (i.e., two-phase or two-component flow) and the relative saturation of the porous medium with respect to each component. The relevant hydrologic properties used in a porous media flow model include the permeability and capillary pressure/relative permeability functional relationships for each simulated material.

For this discussion we consider the region of interest to be a one-dimensional “radial” slice from within an excavation, through the DRZ, out to an undisturbed portion of the native salt.

A coupled THM numerical model could, in principle, be used to determine the hydrologic properties of the salt and DRZ based solely upon their initial, undisturbed or intrinsic properties (e.g., single-phase intrinsic permeability). The extent and properties of the DRZ would be computed from the damage imparted as a result of excavation of the repository (e.g., as done by TOUGH-FLAC and CODE\_BRIGHT). With the proper constitutive relationships, this approach would be physically realistic, but computationally expensive, and would require a coupled hydraulic-mechanical model.

Hydrologic models (i.e., TH or THC – FEHM, TOUGH2, PFLOTRAN, and  $d^3f/r^3t$ ) starting with the excavated repository as their “initial condition” must specify hydraulic initial conditions without deriving them from a coupled hydrologic-mechanical model. These initial conditions for a hydrologic model must satisfy the pressure boundary conditions at either end of the one-dimensional domain:

- Far-field brine pressure is high (lithostatic)
- Excavation gas pressure is atmospheric (0.1 MPa) after excavation.

We discuss the distributions of relevant material properties and state variables in the following sub-sections.

## 5.1 Evolution of the DRZ Around Excavations

This section presents a description of the mechanical and hydrologic processes going on during development of the DRZ, from the time of first excavation to the use of the drift for disposal of heat-generating waste. These observations can either be used to specify initial conditions in TH/THC models, or as qualitative validation data for THMC/THM models.

Before any excavation occurs, a steady-state flow system in the salt is typically saturated with brine (i.e., gas only exists dissolved in the brine) at static formation pressure near lithostatic pressure, and intergranular porosity is low (e.g., 0.05%–0.1%; Figure 3.5). In pure halite an interconnected intergranular porosity or measurable permeability may not exist; only an unconnected porosity consisting of isolated brine inclusion may be present (see Figure 3.2 and Beauheim and Roberts (2002)). The salt stress state is isotropic, with no deviatoric stress and therefore no creep. These would be initial conditions for a THM model.

Once excavation occurs, rock damage begins to occur. An excavation *disturbed* zone immediately extends 2–5 excavation radii into the salt (Beauheim et al., 1991); multiple nearby interacting excavations can lead to perturbations beyond 5 excavation radii (Wawersik and Stone, 1989). This disturbed zone is characterized by reduced pore pressure and an altered (non-zero deviatoric) stress field. This change is driven by the radically altered stress state at the excavation, which enforces the following conditions:

- An atmospheric pressure boundary condition at the excavation surface;
- Very low ( $\leq 0.1$  MPa) normal stress acting perpendicular to the excavation surface; and
- No shear stress acting parallel to the excavation surface.

The excavation *damaged* rock zone extends a shorter distance into the rock, characterized by large deviatoric stresses and relatively low confining stress, which lead to salt dilation and increased porosity and permeability. Damage occurs where shear stress is large compared to confining stress – above the dilatancy boundary defined by (Van Sambeek et al., 1993b)

$$D = \sqrt{J_2} + aI_1 - C \quad (5.1)$$

$$I_1 = \sigma_1 + \sigma_2 + \sigma_3 \quad (5.2)$$

$$J_2 = \frac{1}{6} [(\sigma_1 - \sigma_2)^2 + (\sigma_2 - \sigma_3)^2 + (\sigma_3 - \sigma_1)^2] = \frac{3}{2} \tau_{\text{oct}}^2, \quad (5.3)$$

where  $\sigma$  is the stress tensor,  $I_1$  is the first stress invariant (the trace of the stress tensor – proportional to the pressure or hydrostatic stress),  $J_2$  is the second shear stress invariant proportional to squared octahedral shear stress (Jaeger et al., 2007), and  $a$  and  $C$  are constants related to the slope and intercept of the line representing the dilatancy boundary.

A near-instantaneous mechanical increase of porosity and fracture aperture (Stormont et al., 1992; Stormont and Fuenkajorn, 1993) leads to increased intrinsic formation permeability and decreased air-entry pressure. Before brine has a chance to flow and redistribute, relative brine saturation and pore pressure decrease due to the increased void volume (and relative air saturation likewise increases), which leads to a sharp decrease in *relative* salt permeability to brine. Depending on the capillary pressure distribution and intrinsic permeability of the intact salt and DRZ, the

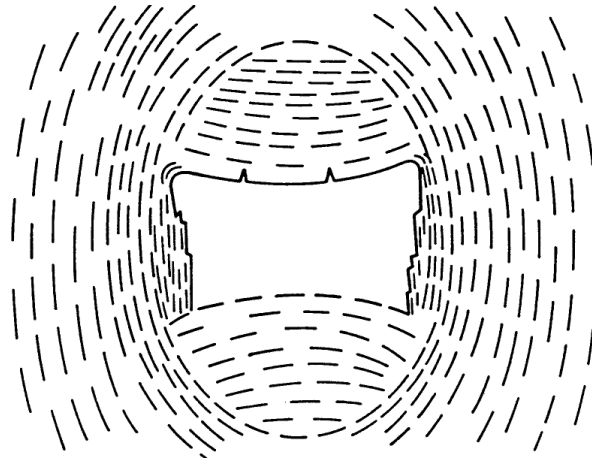


Figure 5.1: Directional nature of damage surrounding a rectangular excavation in salt (Gramberg and Roest, 1984; Borns and Stormont, 1988).

permeability of the DRZ to brine may be equal to or lower than intact salt, due to the low DRZ saturation (i.e., the DRZ may act as a capillary barrier).

The elastic response of the salt to the excavation is nearly instantaneous, but the creep response of the salt is slower and time dependent. Salt begins to creep into the excavation and the DRZ continues to deform due to deviatoric stress.

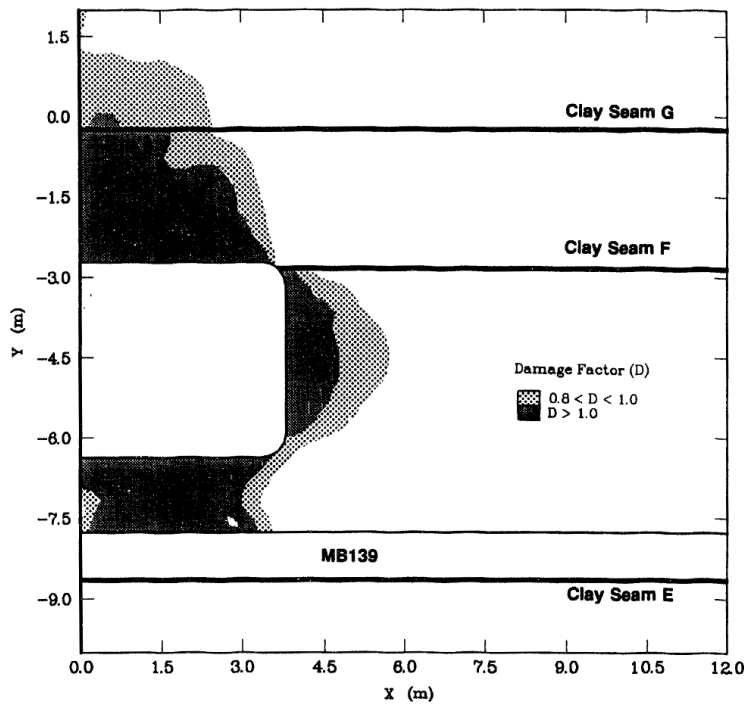


Figure 5.2: Numerical prediction of damage distribution around a WIPP disposal room ( $D$  given in Equation (5.1)) (Van Sambeek et al., 1993a)

Shortly after initial excavation, the DRZ is no longer brine saturated and is no longer at me-

chanical or hydraulic steady state. Salt porosity is highest at the excavation wall, away from room corners, and reduces to its undisturbed value approximately one excavation radius deep into the formation (for WIPP-like conditions, see Figure 5.2). Preferential fracture orientation (Figure 5.1) also leads to anisotropic dilatant permeability, enhancing brine and gas flow parallel to the excavated surface, compared to flow perpendicular to the wall. Anisotropic permeability and porosity have been confirmed in the DRZ at Asse using brine injection and electrical resistivity tomography (Jockwer and Wieczorek, 2008). Rock bolts, boreholes or other mining disturbances can create short-circuit pathways for gas flow perpendicular to the direction of maximum increased permeability (see Figure 3.14 and note presence of rock bolts in Figure 5.3).

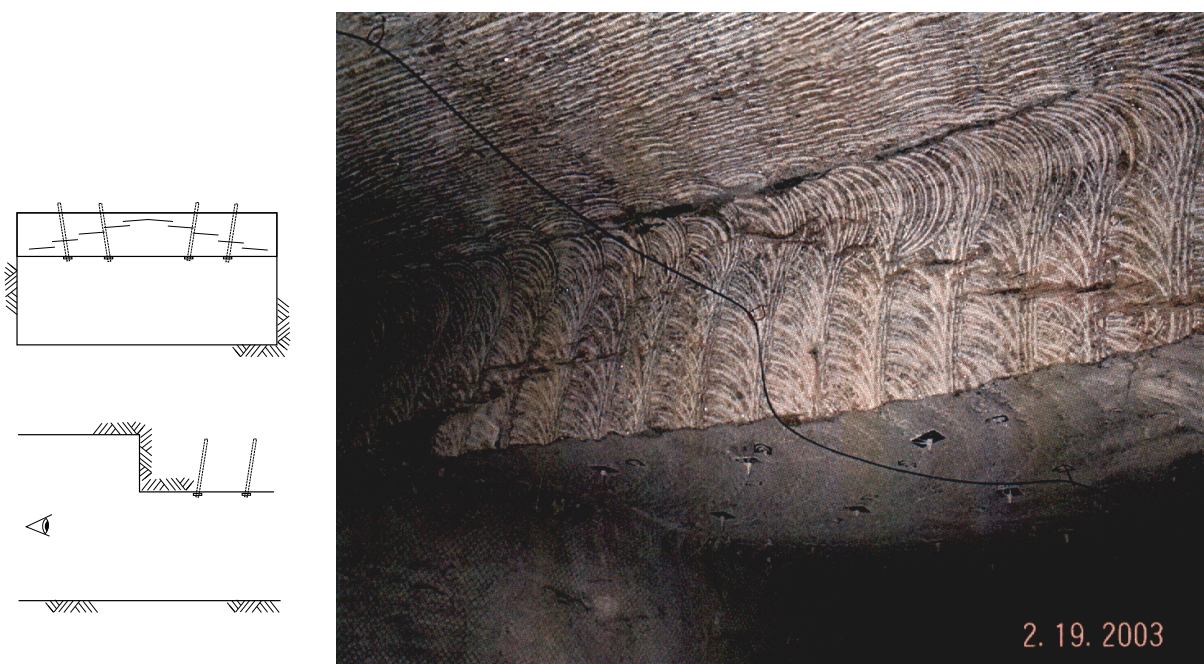


Figure 5.3: Photo of *en echelon* (large aperture sub-parallel) fracturing at change in roof elevation at WIPP (Hansen, 2003), with orientation drawings at left illustrating roof geometry and rockbolts.

The intact salt under undisturbed conditions is saturated with respect to brine. Increasing the porosity of the salt in the DRZ decreases the brine saturation. If porosity is increased by a factor of 5, brine saturation in the same material decreases from 1 to 0.2. During early-time DRZ development, brine redistributes under two-phase flow conditions. An evaporation front (i.e., a “water table”) marks the edge of a zone of saturation, controlled by capillarity, that is proximal and roughly parallel to the boundary between the DRZ and intact salt. This front which separates brine-filled salt of low permeability from pores with significant air saturation in the DRZ. Some water will flow in liquid and vapor forms towards the excavation, driven by pressure gradients, capillarity, and gravity. Brine flowing toward the excavation is apparently captured in the DRZ porosity, and does not discharge immediately to the excavation. If ventilation air humidity is low ( $\ll 75\%$ ), evaporation will occur from the DRZ or crushed salt; whereas high-humidity air ( $> 75\%$ ) can deposit adsorbed moisture on surfaces in open fractures.

Clay or anhydrite layers can also experience damage due to dilation. Their intrinsic permeabilities and porosities may be up to several orders of magnitude higher than intact salt. Sliding

and separation can occur at interfaces between salt and non-salt layers. Non-salt layers do not experience creep closure of newly opened porosity, as salt formations do.

## 5.2 Effect of DRZ Dry-out on Hydrologic Modeling Initial Conditions

The initial condition used when constructing a hydrologic model of a drift in salt must start off with low saturation ( $\leq 50\%$ ). The mechanism creating the DRZ (high permeability and porosity surrounding the excavation) also desaturates the DRZ (the same brine cannot fill the expanded porosity). The permeability of the intact halite (the primary source of liquid water) is so low the brine cannot quickly flow in from the low-permeability far-field salt to resaturate the DRZ.

This section compares two alternative initial conditions using a one-dimensional two-phase flow PFLOTRAN simulations; input files are listed in Appendix A. The point of the exercise is to quantify the difference between alternative approaches for developing the hydrologic initial condition, which result in very similar pressure distributions, but very different saturation distributions. Each of the following simulations was run out to  $10^5$  days ( $> 270$  years). Over this long period, it is invalid to assume mechanical salt deformation can be ignored, but this is used to illustrate a point. In both cases (Figures 5.4 and 5.5), the excavation is represented on the left with a low-pressure (0.1 MPa) Type I (prescribed potential) boundary condition, and high-permeability ( $10^{-11} \text{ m}^2$ ) porous medium to represent excavation air. The undisturbed intact salt is represented on the right with a high-pressure (6 MPa) type I boundary condition and low permeability ( $10^{-20} \text{ m}^2$ ).

Figure 5.4 shows the development from the starting condition to the final condition for a scenario with constant 6 MPa gas pressure and 100% brine saturation specified in the intact salt and the DRZ. The upper portion of the figure shows the distribution of materials and intrinsic permeability in the one-dimensional model domain. The second sub-plot shows pressure (gas pressure in the two-phase DRZ, and liquid pressure in the single-phase intact salt). The third sub-plot shows the liquid saturation ( $S_\ell$ ), and the fourth sub-plot shows the relative permeability to brine ( $k_{r,\ell}$ ). The fifth sub-plot shows the liquid Darcy velocity. In this scenario the pressure profile is achieved relatively quickly, but the DRZ remains saturated throughout the full simulation time. Flux in the DRZ is initially high (through  $10^3$  days), but decays down to a constant steady-state value of  $5 \times 10^{-6} \text{ m/day}$ . This is the approach taken in (Stauffer et al., 2012, Fig. IV.4) and (Stauffer et al., 2013, p. 67) in development of initial conditions for TH and THC simulations using FEHM. The brine saturating the DRZ in these simulations is in hydraulic equilibrium (balance of gravitational and capillary forces), but would require a physically unrealistic time to be achieved from an initially mechanically desaturated DRZ using only brine from the low-permeability intact salt beyond the DRZ. Over-saturating the DRZ in the initial conditions for THC simulations of heater tests provides a large physically unrealistic reservoir of brine available to flow into the excavation during heated test conducted in the drift.

Figure 5.5 shows the development from the initial to final conditions for a scenario with constant initial pressure, but low initial saturation in the DRZ (6 MPa gas pressure and 40% brine saturation). The sub-plots in Figure 5.5 represent the same variables as in Figure 5.4 for comparison. In this case, the relative saturation of the DRZ increases with time due to brine flowing into the DRZ from the intact salt. At late time ( $> 10^4$  days or 27 years), the pressure and saturation



profiles are identical to those in the initially saturated scenario in Figure 5.4. Over these long periods of time, the salt creep would have changed the system significantly. These hydrologic-only simulations are not meaningful beyond their use to illustrate the eventual convergence of pressure and brine saturation in both scenarios.

The salt relative permeability to brine is low in the DRZ when the saturation is mechanically reduced. The DRZ acts as a capillary barrier preventing immediate flow of brine to the excavation. The flux in the DRZ is initially lower than in the saturated zone and eventually increases up to its steady-state value.

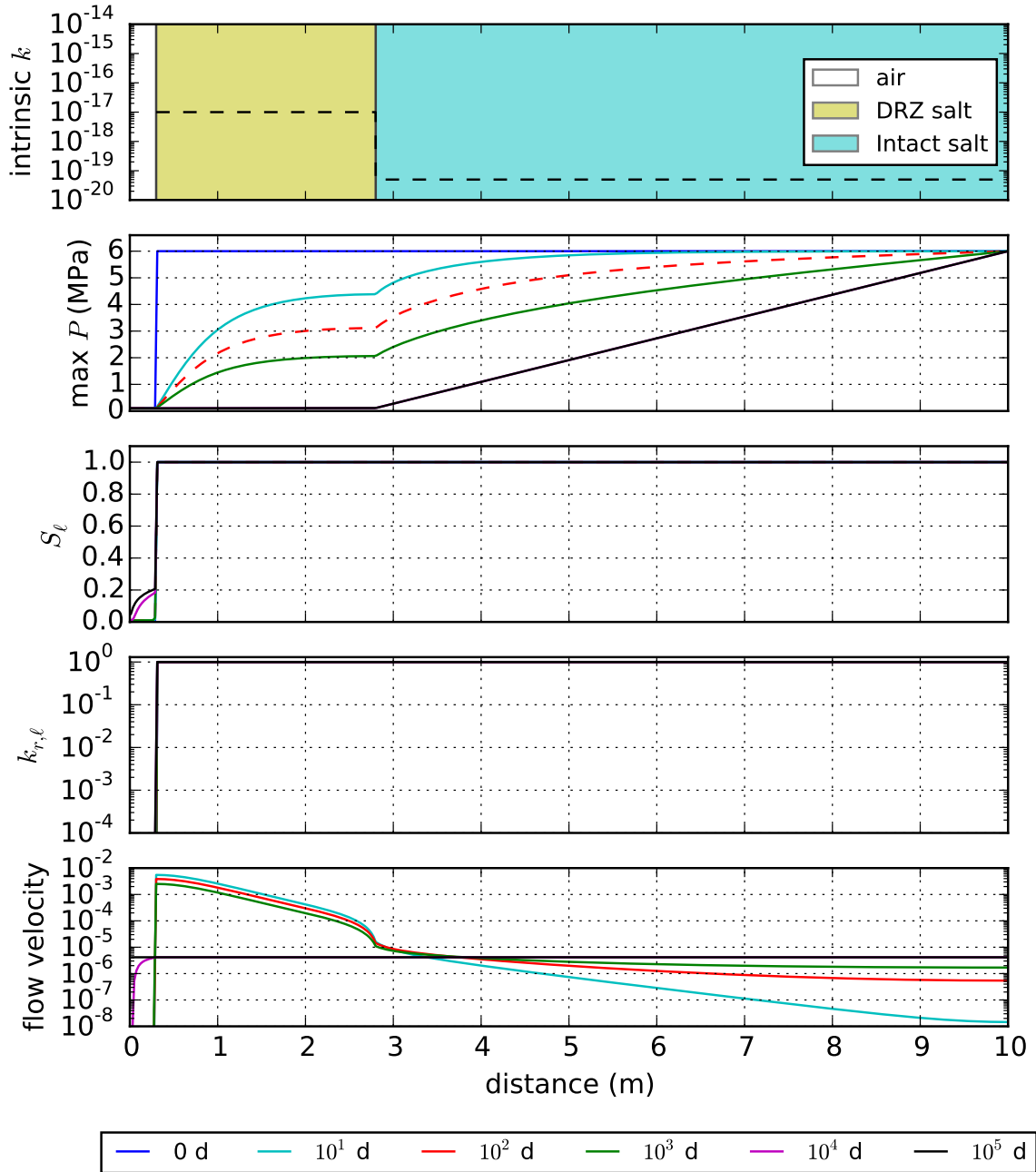


Figure 5.4: One-dimensional two-phase flow modeling in brine using PFLOTTRAN. Initial conditions starting from nearly brine-saturated and hydrostatic (6 MPa) pressure.

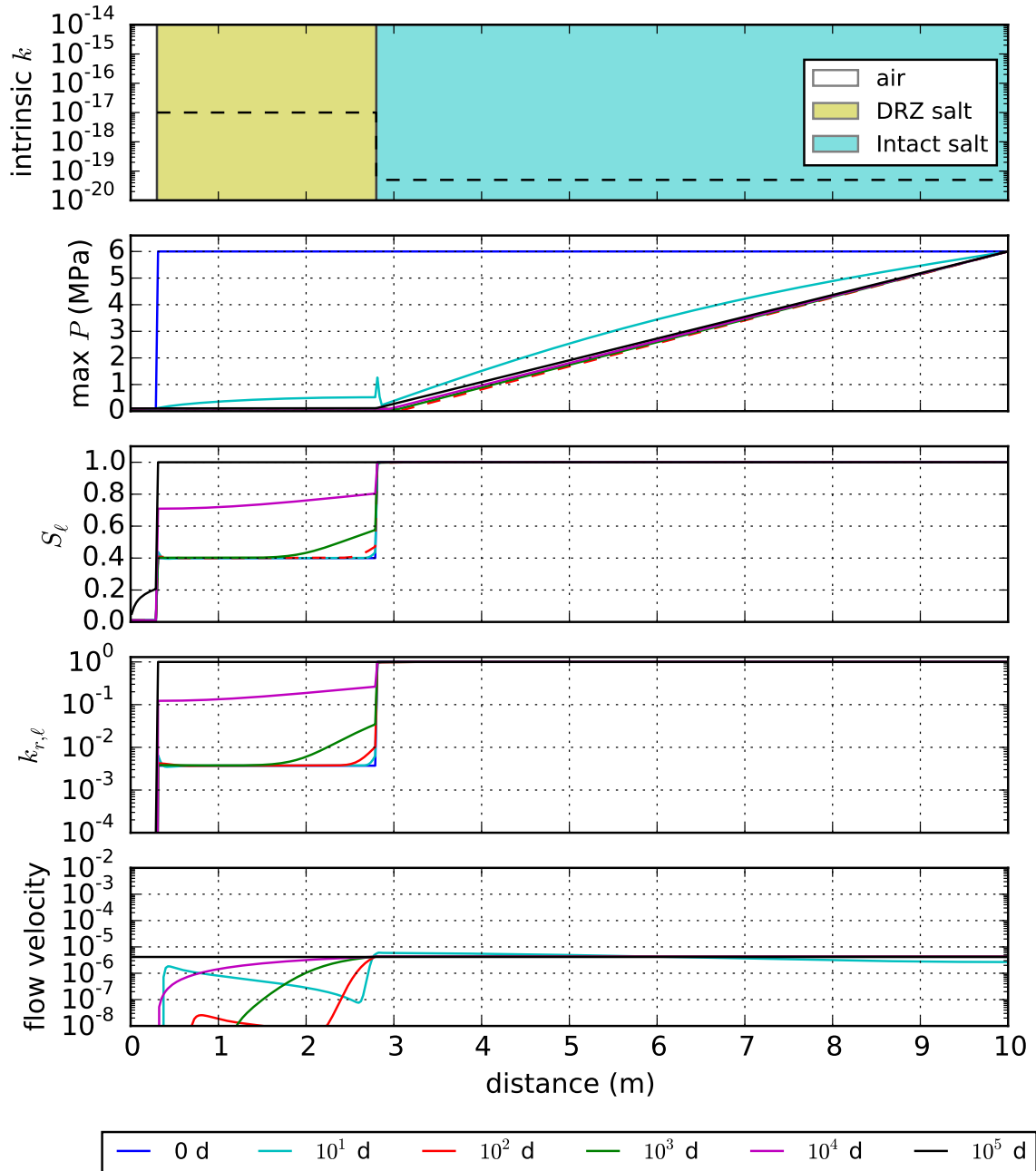


Figure 5.5: One-dimensional two-phase flow modeling in brine using PFLOTTRAN. Initial conditions from 20% brine saturation in DRZ and 100% brine saturation in intact salt, with hydrostatic (6 MPa) pressure.

## 5.3 WIPP Observations of DRZ Dry-out

The following field-scale observations confirm the DRZ is largely desaturated after excavation. These observations could be used for validation of THMC models like TOUGH-FLAC or CODE\_BRIGHT, which include hydraulic and mechanical development of the DRZ or as a realistic initial condition for TH only models (Section 5.2).

### 5.3.1 MB139 water table

At WIPP, Deal et al. (1995) established several sets of shallow monitoring locations in anhydrite, polyhalite, and clay Marker Bed 139 (MB139). A water table was observed at or near the bottom of MB139 (Figure 5.6), and low-flowrate short-duration pumping tests were performed in these boreholes. These observations are consistent with an essentially dry DRZ immediately below the excavation floor and MB139 acting as a sump, collecting brine flowing into the DRZ surrounding rooms via gravity (Kuhlman and Malama, 2014).

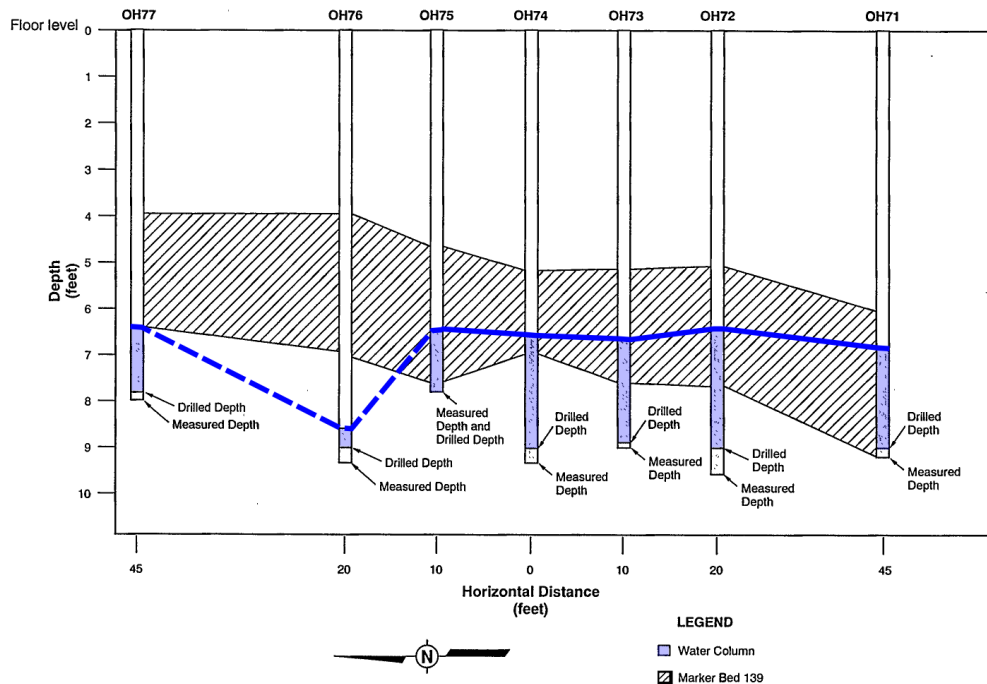


Figure 5.6: Water table observed with shallow MB139 boreholes in the DRZ at WIPP. Modified from (Deal et al., 1995, App. E).

### 5.3.2 WIPP small-scale mine-by

Stormont (1990a), Stormont et al. (1991a), and Stormont (1997a,b) summarized the results of WIPP brine and gas permeability tests, including the Small-scale Mine-by experiment. This experiment measured gas and brine permeability in 4.8-cm diameter boreholes over a 65-cm interval

8-m deep into the floor before, during, and after excavation of a 97-cm diameter central borehole (Figure 5.7).

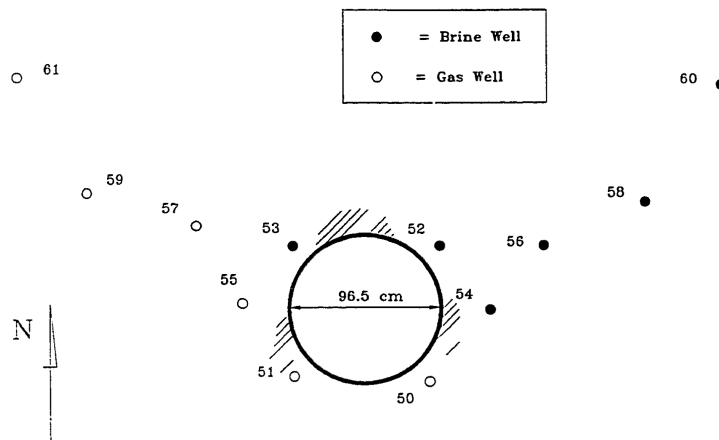


Figure 5.7: WIPP Small-scale Mine-by borehole layout (Stormont et al., 1991a)

A damaged zone was found to propagate into the salt almost immediately upon excavating the large-diameter borehole, with larger effects observed in brine-filled boreholes compared to gas-filled boreholes. Ranges of permeability and porosity were estimated by fitting pressure build-up data before and after mining; model results bracketed observed data, but they did not match it exactly (Stormont et al., 1991a).

The Small-scale Mine-by test produced useful data illustrating the temporal changes in both brine and gas permeability measurements, due to a controlled excavation. The test delineated the presence of a saturation front surrounding the large borehole approximately  $2R/3$  deep into the formation (Figure 5.9). It was assumed the effects of excavating Room L1 were impacting the results at 8 m depth because static formation pressure was only  $\approx 3$  MPa before mining the 1 m borehole, rather than the expected  $\approx 15$  MPa. Figure 3.4 shows 3 MPa static formation pressure corresponds to test intervals 0.5–2 excavation radii into the salt, which is consistent with a test 8 m below the floor of a room. Figure 3.12 also shows results reported from the Small-scale Mine-by experiment, fit to a simplified radial distance power law.

### 5.3.3 WIPP large-scale brine inflow (Room Q)

Room Q was an isothermal brine inflow and mine-by test constructed using a tunnel boring machine in an area isolated from existing WIPP excavations. The final room was a 2.9-m diameter cylinder 109 m long. The Room Q geometry and construction method were chosen to minimize excavation impacts to salt and to reduce stress-concentrations associated with rectangular openings (Figure 5.2). Brine inflow, humidity, pore pressure, permeability, room closure, and disturbed rock zone geophysical properties were collected in Room Q (Jensen et al., 1993a,b).

Room Q sloped uphill away from the access drift following an orange marker band and clay seam, naturally accumulating brine inflow at the room entrance. Different seals (temporary and permanent) were installed at the room entrance to isolate Room Q air from mine ventilation and

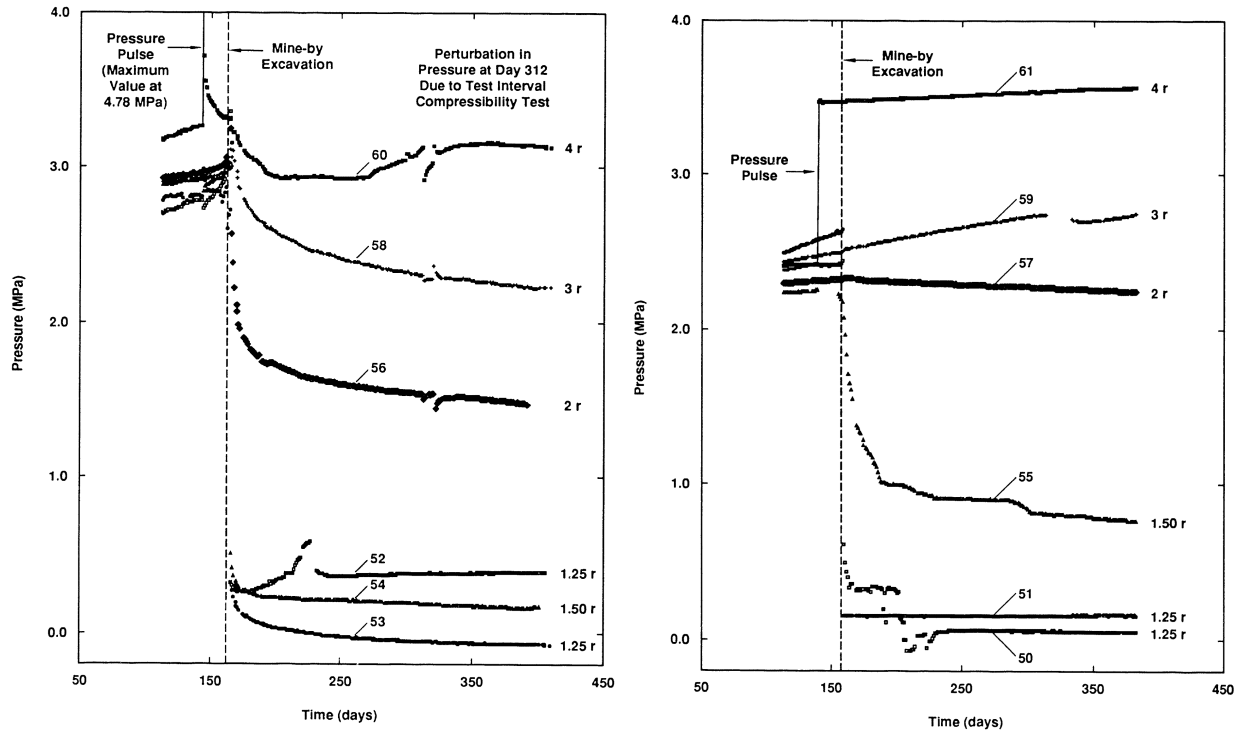


Figure 5.8: WIPP Small-scale Mine-by brine (left) and gas (right) pressures in observation boreholes before, during, and after excavation of the central borehole (Stormont et al., 1991a)

measure total room brine inflow (Figure 5.10). Approximately 5 years after construction, leaks developed through fractures in the salt near the door, which allowed brine to escape unmeasured.

Little brine was initially observed flowing into Room Q, while most numerical and analytical models predicted the highest flowrates occurred immediately after construction of the drift (compare curves and points in Figure 5.10).

Freeze et al. (1997) validated three different modeling approaches against measured inflow to Room Q:

1. A modified form of the TH model TOUGH2 was loosely coupled with a geomechanical model to allow porosity specification at each time step.
2. The isothermal poroelasticity model of McTigue (1993) was used to predict inflow, assuming all flow was due to a thin horizontal anhydrite layer intersecting the room (Freeze et al., 1997, Appendices A2 & A3).
3. Munson et al. (1995a) predicted brine inflow to Room Q using a mechanical damage (“snow plow”) model.

The second and third modeling approaches re-created the typical early peak and decay in inflow; they could not re-create the delay in observed brine inflow due to re-filling of the mechanically dried-out DRZ. These approaches are found in Freeze et al. (1997) and are not discussed further.

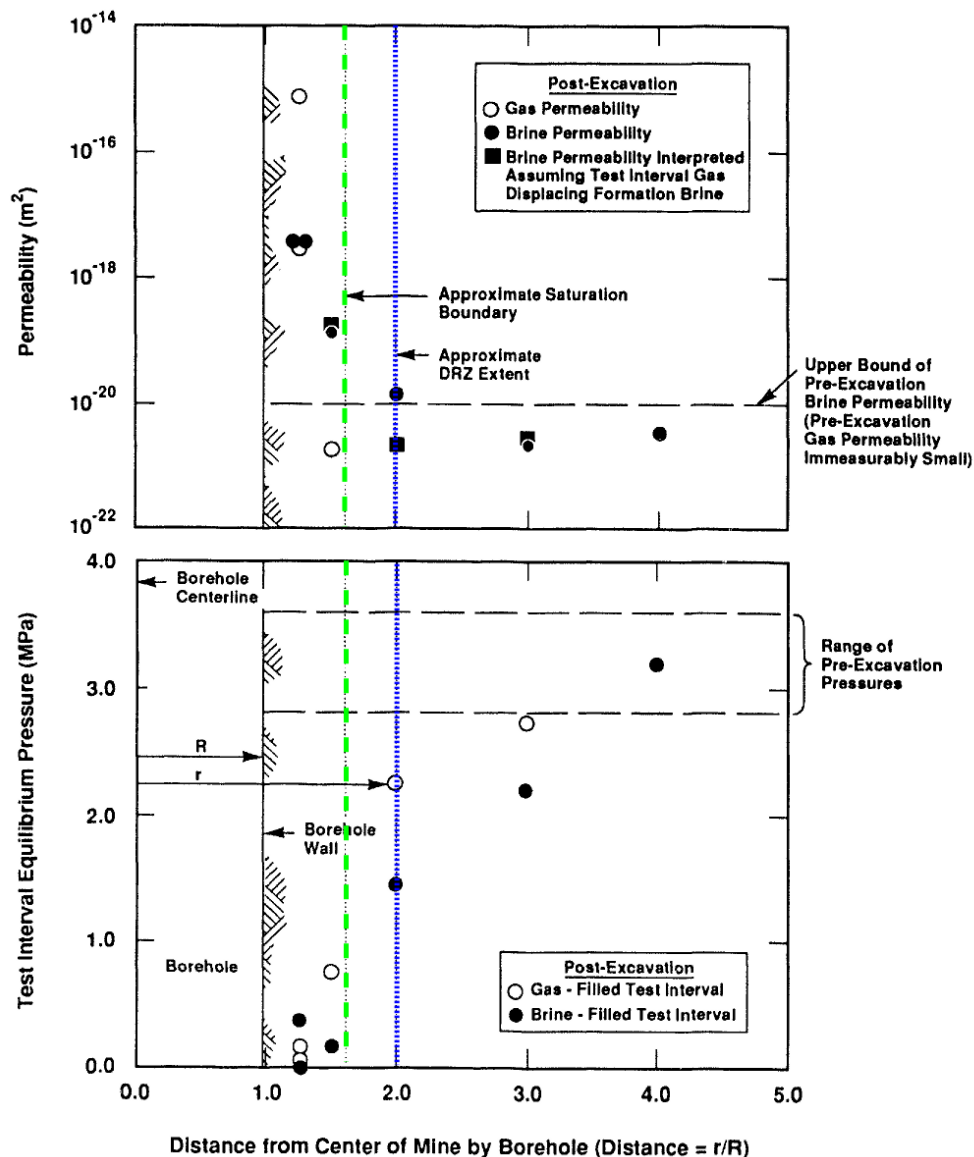


Figure 5.9: WIPP Small-scale Mine-by experiment results showing extent of DRZ (blue dotted line) and desaturated zone (green dashed line); modified from Stormont et al. (1991a)

The loosely coupled TOUGH2 and SPECTROM-32 (Callahan et al., 1989) THM modeling showed results qualitatively similar to those observed could be obtained by increasing the DRZ porosity in the flow model, representing dilatant mechanical deformation (Figure 5.11).

Directly using the results of the SPECTROM-32 simulation in TOUGH2 improved the ability to qualitatively match the observed brine-inflow behavior – a delay with no brine inflow followed by a pulse and decay (Figure 5.12).

Increasing the DRZ porosity used in the TOUGH2 simulation to 5% and 10% greater than SPECTROM-32 predictions resulted in a better model-to-data fit (Figure 5.13), compared to the baseline porosity case. The modeling approach taken by Freeze et al. (1997) is conceptually the same as the one-dimensional PFLOTRAN simulations in the second scenario (Figure 5.5). These

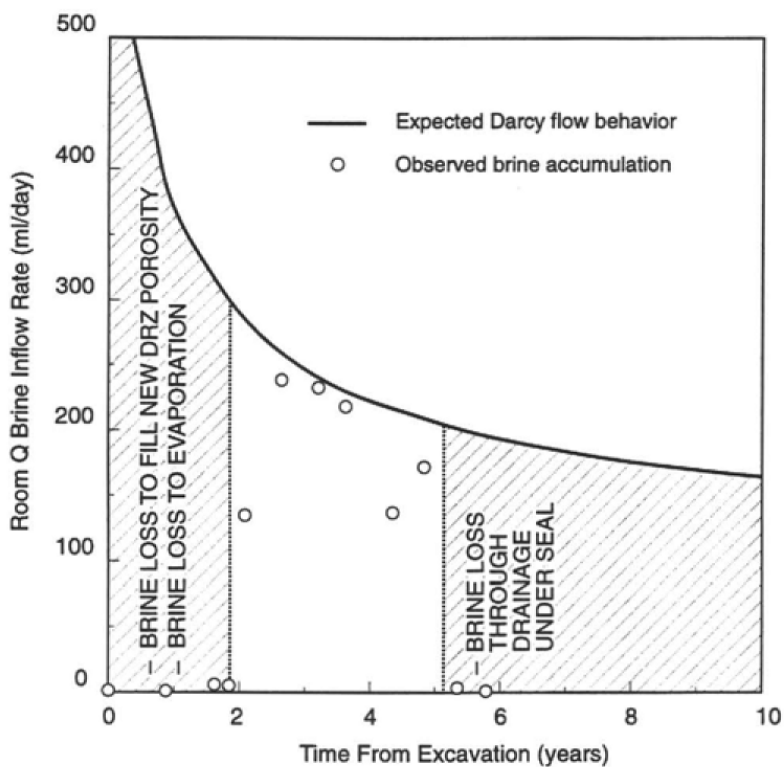


Figure 5.10: WIPP Room Q inflow data (Freeze et al., 1997)

results illustrate it is possible to qualitatively recreate isothermal brine flow using hydrologic models and appropriate boundary and initial conditions, which fully coupled THM models are not available. They also illustrate hydrologic models cannot reproduce the observed delay in initial inflow without modifications to account for mechanical damage and increase in porosity.



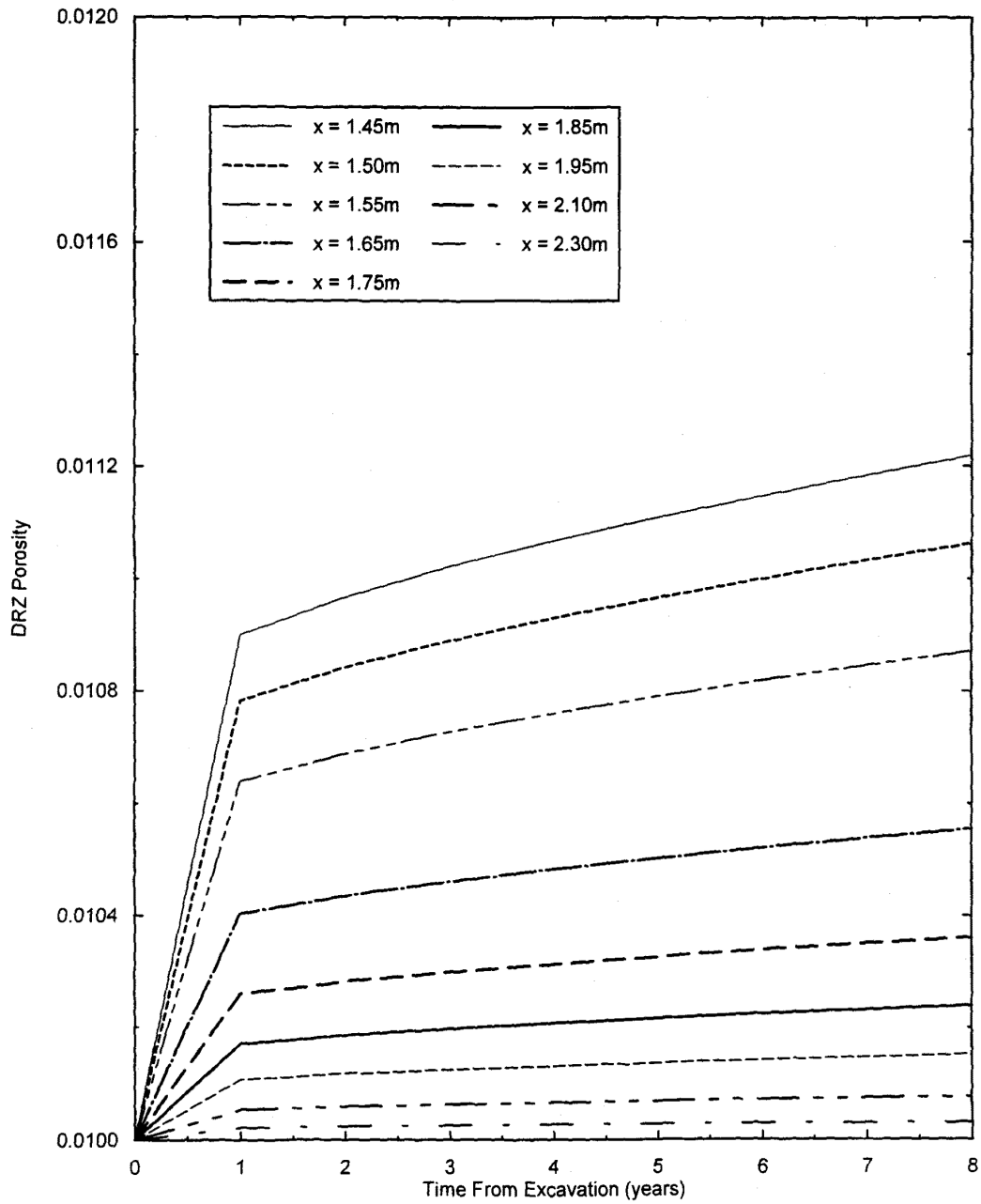


Figure 5.11: Room Q porosity increase predicted by SPECTROM-32 (Freeze et al., 1997)

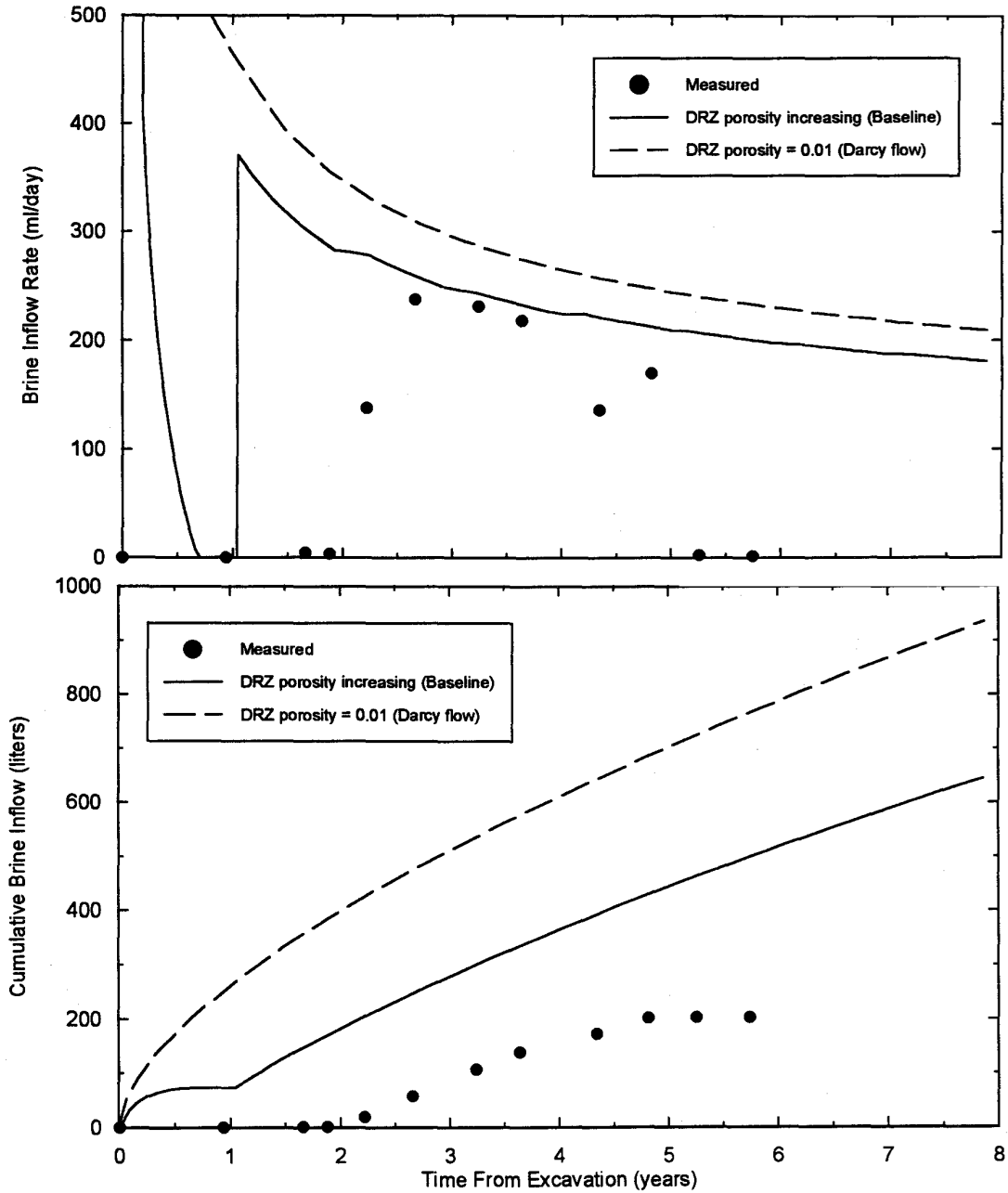


Figure 5.12: Room Q TOUGH2 baseline porosity case inflow predictions, showing constant-porosity model (dashed), variable porosity model (solid) (Freeze et al., 1997)

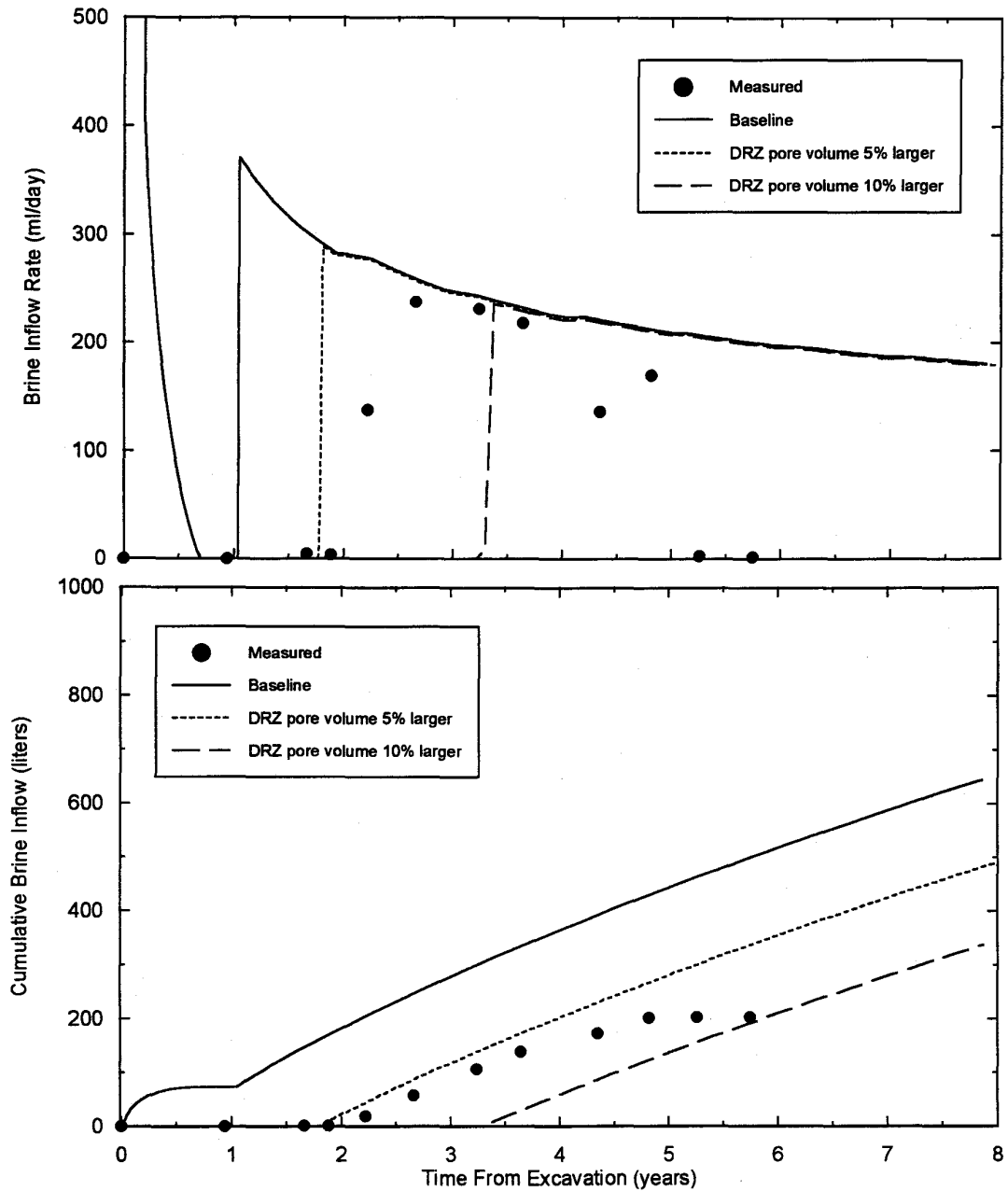


Figure 5.13: Room Q TOUGH2 increased porosity case inflow predictions, showing baseline porosity increase (solid) and 5% and 10% additional DRZ porosity (dashed) (Freeze et al., 1997)

## 6 Summary and Conclusions

We reviewed brine inflow mechanisms and driving forces relevant to a salt repository for heat-generating waste, indicating which numerical models implement or lack different relevant mechanisms and processes. We have reviewed recent numerical model development, modeling exercises, and laboratory experiments that are part of the development of our understanding and “technical basis” for the disposal of heat-generating waste in salt. A great deal is already known about the behavior of salt under repository-like conditions; Kuhlman et al. (2012), Callahan et al. (2012), Kuhlman and Malama (2013), and Kuhlman and Sevougian (2013) summarize many of the large number of laboratory and *in situ* tests conducted in salt. The ongoing development, verification, and validation of coupled THMC models for prediction of salt repository relevant processes is an important part of refinement of the technical basis.

We illustrate the development of appropriate initial conditions for hydrologic modeling of intact and disturbed salt surrounding excavations in a repository or underground research laboratory. Due to the strong coupling between hydraulic and mechanical processes in salt, the DRZ surrounding an excavation cannot be fully saturated. Due to the low permeability of the intact salt and the low saturation of the DRZ salt, the re-wetting process proceeds slowly. We present one-dimensional two-phase PFLOTRAN simulations comparing different conceptualizations of the evolution of the DRZ surrounding an excavation.

Continued model development is needed to bring together different implementations and approaches to numerical modeling of salt. Ideally, before constructing a large-scale field test or licensing a heat-generating waste repository for operation, multiple coupled process models will be used to perform similar simulations to predict the THMC response of the system and better design the repository or test (model verification). Laboratory or field-scale *in situ* tests can provide precious validation data; numerical models can be further compared to the observed responses to determine the adequacy of the conceptualizations embodied in the numerical approaches.

Large open fractures and cavities definitely impact continuum-scale modeling, but are not well-represented in samples or models. Fractures and cavities present at a field site may act as capillary barriers, provide fast-transport pathways, or serve as reservoirs for brine, which will likely not be characterized in data obtained from cores, or predicted by continuum THMC models.

The coupled THM problem can be very difficult to match model and observed data, because the permeability of salt is extremely sensitive to very small levels of dilation and damage (Figure 3.15). For similar reasons, the precipitation and dissolution problem (THC or THMC) in lower-porosity reconsolidated crushed salt ( $\leq 5\%$  porosity) or damaged salt would be difficult to quantitatively match observations (much more than in crushed salt with  $\geq 30\%$  porosity). To validate the non-linear connections between chemical or mechanical processes and hydrologic processes may require additional laboratory or field data for validation purposes. Ideally, experiments

would be designed to isolate individual processes for testing (e.g., hydro-mechanical coupling both with and without thermal effects). Many relevant experiments have already been conducted and their data should be used for benchmarking purposes. Creating validation exercises from existing data also provides insight on designing new experiments to obtain the most impact for the money and time spent on *in situ* and laboratory tests.

---

## Bibliography

- Alkan, H. Percolation model for dilatancy-induced permeability of the excavation damaged zone in rock salt. *International Journal of Rock Mechanics & Mining Sciences*, 46:716–724, 2009.
- Anthony, T. R. and Cline, H. E. The thermal migration of liquid droplets through solids. *Journal of Applied Physics*, 42(9):3380–3387, 1971.
- Anthony, T. R. and Cline, H. E. The thermomigration of biphasic vapor-liquid droplets in solids. *Acta Metallurgica*, 20(2):247–255, 1972.
- Argüello, J. G. Potential use of geologic rock salt for fuel cycle sustainability – a computational modeling perspective. In *48th US Rock Mechanics / Geomechanics Symposium*, number ARMA 14–7040, 2014.
- Argüello, J. G. and Rath, J. S. SIERRA Mechanics for coupled multi-physics modeling of salt repository behavior for NEAMS applications. In *Mechanical Behavior of Salt VII*, number SAND2011–6761C. MINES Paris Tech, Taylor & Francis, 2012.
- Argüello, J. G. and Rath, J. S. Revisiting the 1980’s WIPP Room D and B in-situ experiments: Performing thermo-mechanical simulations of rock salt using an state-of-the-art code suite. In *47th US Rock Mechanics / Geomechanics Symposium*, number ARMA 13–370, 2013.
- Balay, S., Abhyankar, S., Adams, M. F., Brown, J., Brune, P., Buschelman, K., Eijkhout, V., Gropp, W. D., Kaushik, D., Knepley, M. G., McInnes, L. C., Rupp, K., Smith, B. F., and Zhang, H. PETSc users manual. ANL-95/11 - Revision 3.5, Argonne National Laboratory, 2014. URL <http://www.mcs.anl.gov/petsc>.
- Battistelli, A., Calore, C., and Pruess, K. Vapor pressure lowering effects due to salinity and suction pressure in the depletion of vapor-dominated geothermal reservoirs. In *Proceedings, TOUGH Workshop*, volume 95, pages 77–83, 1995.
- Bauer, S. J. and Urquhart, A. Thermophysical properties of reconsolidating crushed salt. SAND2014–2240, Sandia National Laboratories, Albuquerque, NM, March 2014.
- Bauer, S. J., Urquhart, A., Broome, S. T., and Hansen, F. D. Experimental determination of thermophysical properties of reconsolidated crushed salt. In *48th US Rock Mechanics / Geomechanics Symposium*, number ARMA 14–144. American Rock Mechanics Association, 2014.
- Bear, J. *Dynamics of Fluids in Porous Media*. Dover Publications, Inc., New York, 1972.

- 
- Beauheim, R. L. and Roberts, R. M. Hydrology and hydraulic properties of a bedded evaporite formation. *Journal of Hydrology*, 259(1):66–88, 2002.
- Beauheim, R. L., Saulnier, G. J., and Avis, J. D. Interpretation of brine-permeability tests of the Salado Formation at the Waste Isolation Pilot Plant site: First interim report. SAND90–0083, Sandia National Laboratories, Albuquerque, NM, 1991.
- Beauheim, R. L., Howarth, S. M., Vaughn, P., Webb, S. W., and Larson, K. W. Integrated modeling and experimental programs to predict brine and gas flow at the Waste Isolation Pilot Plant. SAND94–0599C, Sandia National Laboratories, Albuquerque, NM, 1994.
- Beauheim, R. L., Ait-Chalal, A., Vouille, G., Tijani, S.-M., McTigue, D. F., Brun-Yaba, C., Hasanzadeh, S. M., van der Gissen, G. M., Holtman, H., and Mollema, P. N. INTRAVAL phase 2 WIPP 1 test case report: Modeling of brine flow through halite at the Waste Isolation Pilot Plant site. SAND97–0788, Sandia National Laboratories, Albuquerque, NM, May 1997.
- Bechthold, W., Rothfuchs, T., Poley, A., Ghoreychi, M., Heusermann, S., Gens, A., and Olivella, S. Backfilling and sealing of underground repositories for radioactive waste in salt (BAMBUS Project). EUR 19124 EN, Nuclear Science and Technology Commission of the European Communities, Brussels, Belgium, 1999.
- Bechthold, W., Smailos, E., Heusermann, S., Bollingerfehr, W., Bazargan-Sabet, B., Rothfuchs, T., Kamlot, P., Grupa, J., Olivella, S., and Hansen, F. D. Backfilling and sealing of underground repositories for radioactive waste in salt (BAMBUS II Project). EUR 20621 EN, Nuclear Science and Technology Commission of the European Communities, Brussels, Belgium, 2004.
- Bejan, A. and Kraus, A. D. *Heat transfer handbook*, volume 1. John Wiley & Sons, 2003.
- Blanco Martín, L., Rutqvist, J., and Birkholzer, J. T. Long-term analysis of thermal-hydraulic-mechanical processes in a generic salt repository for high-level nuclear waste. In *48th US Rock Mechanics / Geomechanics Symposium*, number ARMA 14–7206. American Rock Mechanics Association, June 2014a.
- Blanco Martín, L., Rutqvist, J., Birkholzer, J. T., Wolters, R., Rutenberg, M., Zhao, J., and Lux, K.-H. Comparison of two modeling procedures to evaluate thermal-hydraulic-mechanical processes in a generic salt repository for high-level nuclear waste. In *48th US Rock Mechanics / Geomechanics Symposium*, number ARMA 14–7411. American Rock Mechanics Association, June 2014b.
- Bornemann, O., Behlau, J., Fischbeck, R., Hammer, J., Jaritz, W., Keller, S., Mingerzahn, G., and Schramm, M. Description of the Gorleben site part 3: Results of the geological surface and underground exploration of the salt formation. Bundesanstalt für Geowissenschaften und Rohstoffe (BGR), Hannover, Germany, 2008.
- Borns, D. J. Marker Bed 139: A study of drillcore from a systematic array. SAND85–0023, Sandia National Laboratories, Albuquerque, NM, 1985.

- 
- Borns, D. J. and Stormont, J. C. An interim report on excavation effects studies at the Waste Isolation Pilot Plant: The delineation of the disturbed rock zone. SAND87-1375, Sandia National Laboratories, Albuquerque, NM, 1988.
- Bradshaw, R. L. and McClain, W. C. Project Salt Vault: A demonstration of the disposal of high-activity solidified wastes in underground salt mines. ORNL-4555, Oak Ridge National Laboratory, Oak Ridge, TN, 1971.
- Bradshaw, R. L. and Sanchez, F. Migration of brine cavities in rock salt. *Journal of Geophysical Research*, 74(17):4209-4212, 1969.
- Brodsky, N. S. The effect of brine injection on the creep of WIPP salt during laboratory tests. RSI-0371, RE/SPEC, Inc., Rapid City, SD, 1990.
- Brodsky, N. S. Hydrostatic and shear consolidation tests with permeability measurements on Waste Isolation Pilot Plant crushed salt. SAND93-7058, Sandia National Laboratories, Albuquerque, NM, March 1994.
- Brodsky, N. S. and Munson, D. E. The effect of brine on the creep of WIPP salt during laboratory tests. In Roegiers, editor, *Rock Mechanics as a Multidisciplinary Science*, pages 703-712. Balkema, 1991.
- Brooks, R. H. and Corey, A. T. Properties of porous media affecting fluid flow. *Journal of Irrigation and Drainage division, AMCE*, 92(IR2):61-88, 1966.
- Burdine, N. T. Relative permeability calculations from pore size distribution data. *Journal of Petroleum Technology*, 5(3):71-78, 1953.
- Buscheck, T. A., Rosenberg, N. D., Gansemer, J., and Sun, Y. Thermohydrologic behavior at an underground nuclear waste repository. *Water Resources Research*, 38(3):15, 2002.
- Callahan, G. D. Crushed salt constitutive model. SAND98-2680, Sandia National Laboratories, Albuquerque, NM, 1999.
- Callahan, G. D., Fossum, A. F., and Svalstad, D. K. Documentation of SPECTROM-32: A finite-element thermomechanical stress analysis program (2 volumes). RSI-0269, RE/SPEC, Inc., Rapid City, SD, August 1989.
- Callahan, G. D., Guerin, D. C., Levitt, D. G., Newell, D. L., Robinson, B. A., and Van Sambeek, L. Salt repository synthesis data of non-Delaware Basin and international programs for the storage/disposal of nuclear waste. FCRD-UFD-2012-000312, US Department of Energy Used Fuel Disposition Campaign, October 2012.
- Caporuscio, F. A., Boukhalfa, H., Cheshire, M. C., Jordan, A. B., and Ding, M. Brine migration experimental studies for salt repositories. LA-UR-13-27240, Los Alamos National Laboratory, Los Alamos, NM, September 2013.
- Caporuscio, F. A., Boukhalfa, H., Cheshire, M. C., and Ding, M. Brine migration experimental studies for salt repositories. LA-UR-26603, Los Alamos National Laboratory, Los Alamos, NM, August 2014.



- Carter, N. L., Horseman, S. T., Russell, J. E., and Handin, J. Rheology of rocksalt. *Journal of Structural Geology*, 15(9-10):1257–1271, 1993.
- Castagna, S., Olivella, S., Lloret, A., and Alonso, E. E. *Computational Methods for Flow and Transport in Porous Media*, chapter Experimental and Numerical Investigation of Porosity Variations in Saline Media Induced by Temperature Gradients, pages 327–338. Kluwer Academic Publishers, 2000.
- Chace, D. A., Roberts, R. M., Palmer, J. B., Kloska, M. B., Fort, M. D., Martin, G. J., and Stensrud, W. A. Waste Isolation Pilot Plant Salado hydrology program data report #3. SAND97–1880, Sandia National Laboratories, Albuquerque, NM, January 1998.
- Chan, K. S., Bodner, S. R., and Munson, D. E. Permeability of WIPP salt during damage evolution and healing. *International Journal of Damage Mechanics*, 10(4):347–375, 2001.
- Cinar, Y., Pusch, G., and Reitenbach, V. Petrophysical and capillary properties of compacted salt. *Transport in Porous Media*, 64(2):199–228, 2006.
- Clayton, D. J. and Gable, C. W. 3-D thermal analyses of high-level waste emplaced in a generic salt repository. AFCI-WAST-PMO-MI-DV-2009–000002, US Department of Energy Office of Nuclear Fuel Recycling, February 2009.
- Clayton, D. J., Lee, M. Y., Holcomb, D. J., and Bronowski, D. R. Crushed salt reconsolidation at elevated temperatures. In *44th US Rock Mechanics Symposium and 5th US-Canada Rock Mechanics Symposium*, 2010.
- Clayton, D. J., Argüello, J. G., Hardin, E. L., Hansen, F. D., and Bean, J. E. Thermal-mechanical modeling of a generic high-level waste salt repository. In *Mechanical Behavior of Salt VII*, pages 435–440. MINES Paris Tech, Taylor & Francis, 2012.
- Cole, C. R. Evaluation and status report on HYDROCOIN at midway. PNL-6087, Pacific Northwest National Laboratory, Richland, WA, 1986.
- COMSOL. COMSOL Multiphysics 4.3 users guide, 2012. URL <http://www.comsol.com>.
- Cosenza, Ph. *Coupled Effects Between Mechanical Behavior and Mass Transfer Phenomena in Rock Salt*. PhD thesis, Ecole Polytechnique, 1996.
- Cosenza, Ph. and Ghoreychi, M. Coupling between mechanical behavior and transfer phenomena in salt. In Ghoreychi, M., editor, *3rd Conference on Mechanical Behavior of Salt*, pages 271–293. Trans Tech Publications, 1993.
- Cosenza, Ph., Ghoreychi, M., and Su, K. Modeling of chemo-mechanical coupled effects in halitic porous media. In Thimus, editor, *Poromechanics*, pages 385–390, Rotterdam, 1998. Balkema.
- Cristescu, N. and Gioda, G. *Visco-plastic behavior of geomaterials*, volume 350. Springer, 1994.
- Czaikowski, O., Wiczorek, K., and Kröhn, K. P. Compaction of salt backfill – new experiments and numerical modelling. In *Mechanical Behavior of Salt VII*, pages 155–160. MINES Paris Tech, Taylor & Francis, 2012.

- 
- Davies, C. and Bernier, F., editors. *Impact of the Excavation Disturbed or Damaged Zone (EDZ) on the Performance of Radioactive Waste Geological Repositories*, number EUR 21028 EN, Brussels, Belgium, 2005.
- Davies, P. B. Evaluation of the role of threshold pressure in controlling flow of waste generated gas into bedded salt at the Waste Isolation Pilot Plant. SAND90-3246, Sandia National Laboratories, Albuquerque, NM, 1991.
- Dawson, P. R. Benchmark computation for WIPP creep analysis (reissued 3/29/79 to incorporate current material properties). (Memo to Distribution), March 1979.
- Deal, D. E., Abitz, R. J., Belski, D. S., Case, J. B., Crawley, M. E., Givens, C. A., Lipponer, P. P. J., Milligan, D. J., Myers, J., Powers, D. W., and Valdivia, M. A. Brine sampling and evaluation program 1992-1993 report and summary of BSEP data since 1982. DOE-WIPP 94-011, Westinghouse Electric Corporation, Carlsbad, NM, 1995.
- Desbois, G., Uraï, J. L., Schmatz, J., Zavada, P., and de Bresser, H. The distribution of fluids in natural salt rock to understand deformation mechanisms. In *Mechanical Behavior of Salt VII*, pages 3-12. MINES Paris Tech, Taylor & Francis, 2012.
- DOE. A conceptual plan for salt disposal investigations with a field scale heater test at WIPP. DOE/CBFO-11-3470, US Department of Energy Office of Environmental Management Carlsbad Field Office, Carlsbad, NM, June 2011.
- DOE. Test specifications for the salt defense disposal investigations thermal test in WIPP. DOE/CBFO-12-3485, US Department of Energy Office of Environmental Management Carlsbad Field Office, Carlsbad, NM, June 2012.
- Doeven, I., Soullié, P. P., and Vons, L. H. Convergence measurements in the dry-drilled 300 m borehole in the Asse-II saltmine. *European Applied Research Reports – Nuclear Science and Technology Section*, 5(2):267-324, 1983.
- Dullien, F. A. L. *Porous Media: Fluid Transport and Pore Structure*. Academic Press, second edition, 1992.
- Fallah, N. A., Bailey, C., Cross, M., and Taylor, G. A. Comparison of finite element and finite volume methods application in geometrically nonlinear stress analysis. *Applied Mathematical Modelling*, 24(7):439-455, 2000.
- Finlayson, B. A. *The Method of Weighted Residuals and Variational Principles*. Academic Press, 1972.
- Finley, S. J., Hanson, D. J., and Parsons, R. Small-scale brine inflow experiments – data report through 6/6/91. SAND91-1956, Sandia National Laboratories, Albuquerque, NM, 1992.
- Francis, J. Nicholas D., Webb, S. W., Itamura, M. T., and James, D. L. CFD modeling of natural convection heat transfer and fluid flow in Yucca Mountain Project (YMP) enclosures. SAND2002-4179, Sandia National Laboratories, Albuquerque, NM, March 2003.

- 
- Freeze, G. A., Christian-Frear, T. L., and Webb, S. W. Modeling brine inflow to Room Q: A numerical investigation of flow mechanisms. SAND96-0561, Sandia National Laboratories, Albuquerque, NM, 1997.
- Fuenkajorn, K. and Daemen, J. J. K. Borehole closure in salt. NUREG/CR-5243, US Nuclear Regulatory Commission, Washington, DC, 1988.
- Gloyna, E. F. and Reynolds, T. D. Permeability measurements of rock salt. *Journal of Geophysical Research*, 66(11):3913-3921, 1961.
- Gnirk, P. S., Krause, W. B., and Fossum, A. S. State-of-the-art review of brine migration studies in salt. SAND81-7054, Sandia National Laboratories, Albuquerque, NM, 1981.
- Gramberg, J. and Roest, J. P. A. Cataclastic effects in rock salt laboratory and in situ measurements. EUR 9258 EN, European Commission on Nuclear Science and Technology, Brussels, Belgium, 1984.
- Guyer, J. E., Wheeler, D., and Warren, J. A. FiPy: Partial differential equations with Python. *Computing in Science & Engineering*, 11(3):6-15, 2009. URL <http://www.ctcms.nist.gov/fipy>.
- Hadley, G. R. Theoretical treatment of evaporation front drying. *International Journal of Heat and Mass Transfer*, 25(10):1511-1522, 1982.
- Hammond, G. E. and Lichtner, P. C. Field-scale modeling for the natural attenuation of uranium at the Hanford 300 Area using high performance computing. *Water Resources Research*, 46: W09527, 2010. doi: 10.1029/2009WR008819.
- Hammond, G. E., Lichtner, P. C., and Mills, R. T. Evaluating the performance of parallel sub-surface simulators: An illustrative example with PFLOTRAN. *Water Resources Research*, 50, 2014. doi: 10.1002/2012WR013483.
- Hampel, A., Salzer, K., Günther, R. M., Minkley, W., Pudewills, A., Leuger, B., Zapf, D., Staudtmeister, K., Rokahr, R., Herchen, K., Wolters, R., and Lux, K.-H. Joint projects on the comparison of constitutive models for the mechanical behavior of rock salt – II. overview of the models and results of 3-D benchmark calculations. In *Mechanical Behavior of Salt VII*, pages 231-240. MINES Paris Tech, Taylor & Francis, 2012.
- Hampel, A., Argüello, J. G., Hansen, F. D., Günther, R. M., Salzer, K., Minkley, W., Lux, K.-H., Harchen, K., Düsterloh, U., Pudewills, A., Yildirim, S., Staudtmeister, K., Rokahr, R., Zapf, D., Gährken, A., Missal, C., and Stahlmann, J. Benchmark calculations of the thermo-mechanical behavior of rock salt – results from a US-German joint project. In *47th US Rock Mechanics / Geomechanics Symposium*, number ARMA 13-456. American Rock Mechanics Association, 2013.
- Hansen, F. D. The disturbed rock zone at the Waste Isolation Pilot Plant. SAND2003-3407, Sandia National Laboratories, Albuquerque, NM, 2003.

- 
- Hansen, F. D., Steininger, W., and Biurrun, E. 2nd US/German workshop on salt repository research, design and operation. SAND2012–1245C, Sandia National Laboratories, March 2012.
- Hansen, F. D., Kuhlman, K. L., Steininger, W., and Biurrun, E. Proceedings of 3rd US/German workshop on salt repository research, design and operation. FCRD-UFD-2013–000100, US Department of Energy Used Fuel Disposition Campaign, Albuquerque, NM, February 2013a.
- Hansen, F. D., Steininger, W., and Biurrun, E. Proceedings of 4th US/German salt repository workshop. FCRD-UFD-2014–000335, US Department of Energy Used Fuel Disposition Campaign, Albuquerque, NM, December 2013b.
- Hansen, F. D., Pop, T., Wiczorek, K., and Stührenberg, D. Granular salt summary: Reconsolidation principles and applications. SAND2014–16141R, US Department of Energy Used Fuel Disposition Campaign, Albuquerque, NM, July 2014a.
- Hansen, G., Salinger, A., Phipps, E., Ostien, J., Muller, R., Mota, A., Sun, W., Chen, Q., Gao, X., Nielsen, E., Kalashnikova, I., Littlewood, D., Parks, M., Cortial, J., Seol, S., and Granzow, B. Albany: A multiphysics application based on Trillinos. SAND2014–0426P, Sandia National Laboratories, Albuquerque, NM, 2014b. URL <https://github.com/gahansen/Albany>.
- Harp, D. R., Stauffer, P. H., Mishra, P. K., Levitt, D. G., and Robinson, B. A. Thermal modeling of high-level nuclear waste disposal in a salt repository. *Nuclear Technology*, 187(3):294–307, 2014.
- Herrera, I. and Pinder, G. F. *Mathematical modeling in science and engineering: An axiomatic approach*. John Wiley & Sons, 2012.
- Hess, H. H., Adkins, J. N., Heroy, W. B., Benson, W. E., Hubbert, M. K., Frye, J. C., Russell, R. J., and Theis, C. V. The disposal of radioactive waste on land, report of the committee on waste disposal of the division of earth sciences. Publication 519, National Academy of Sciences - National Research Council, Washington, DC, 1957.
- Hohlfelder, J. J. Salt Block II: Description and results. SAND79–2226, Sandia National Laboratories, Albuquerque, NM, 1980.
- Hohlfelder, J. J., Beattie, A. G., and Shefelbine, H. C. Water release and mechanical failure in heated geologic salt. SAND81–1488, Sandia National Laboratories, Albuquerque, NM, 1981.
- Holcomb, D. J., Zeuch, D. H., Morin, K., Hardy, R., and Tormey, T. V. Field and laboratory investigations of coring-induced damage in core recovered from Marker Bed 139 at the Waste Isolation Pilot Plant underground facility. SAND94–2757, Sandia National Laboratories, Albuquerque, NM, September 1995.
- Holcomb, D. J., MacDonald, T., and Hardy, R. D. Using ultrasonic waves to assess the disturbed rock zone (DRZ) in an alcove corner excavated in salt at the WIPP (Waste Isolation Pilot Plant). SAND2001–3055C, Sandia National Laboratories, Albuquerque, NM, 2002.

- Hou, Z., Wolters, R., Rokahr, R., Zapf, D., Salzer, K., Günther, R. M., Minkley, W., Pudewills, A., Heemann, U., Schulze, O., Zetsche, F., and Hampel, A. Comparison of advanced constitutive models for the mechanical behavior of rock salt – results from a joint research project II. numerical modeling of two in situ case studies and comparison. In *6th Conference on the Mechanical Behavior of Salt: Understanding of THMC Processes in Salt Rocks*. Federal Institute for Geosciences and Natural Resources (BGR), Germany, Taylor & Francis, May 2007.
- Howarth, S. M. and Christian-Frear, T. Porosity, single-phase permeability, and capillary pressure data from preliminary laboratory experiments on selected samples from Marker Bed 139 at the Waste Isolation Pilot Plant (3 volumes). SAND94-0472, Sandia National Laboratories, Albuquerque, NM, 1997.
- Isherwood, D. J. Geoscience data base handbook for modeling a nuclear waste repository: Final report. NUREG/CR-0912-V1, Lawrence Livermore Laboratory, Livermore, CA, 1981.
- Jaeger, J. C., Cook, N. G. W., and Zimmerman, R. W. *Fundamentals of Rock Mechanics*. Blackwell Publishing, fourth edition, 2007.
- Jenks, G. H. Effects of temperature, temperature gradients, stress, and irradiation on migration of brine inclusions in a salt repository. ORNL-5526, Oak Ridge National Laboratory, Oak Ridge, TN, 1979.
- Jensen, A. L., Howard, C. L., Jones, R. L., and Peterson, T. P. Room Q data report: Test borehole data from April 1989 through November 1991. SAND92-1172, Sandia National Laboratories, Albuquerque, NM, 1993a.
- Jensen, A. L., Jones, R. L., Lorusso, E. N., and Howard, C. L. Large-scale brine inflow data report for Room Q prior to November 25, 1991. SAND92-1173, Sandia National Laboratories, Albuquerque, NM, 1993b.
- Jockwer, N. and Wiczorek, K. ADDIGAS: Advective and diffusive gas transport in rock salt formations, Final Report. GRS-234, Gesellschaft für Anlagen- und Reaktorsicherheit (GRS), Cologne, Germany, 2008.
- Johnson, K. S. and Gonzales, S. Salt deposits in the United States and regional geologic characteristics important for storage of radioactive waste. Y/OWI/SUB-7414/1, Office of Waste Isolation, Oak Ridge, TN, 1978.
- Kast, W. and Hohenthanner, C. R. Mass transfer within the gas-phase of porous media. *International Journal of Heat and Mass Transfer*, 43:807–823, 2000.
- Kazan, Y. and Ghoreychi, M. Essais in situ CPPS: Étude thermomécanique du champ proche d'un puits de stockage de déchets radioactifs dans le sel [CPPS in situ test: Thermo-mechanical study of the near-field surrounding a radioactive waste disposal borehole in salt]. EUR 16946 FR, European Commission, Luxembourg, 1996.
- Kim, J. *Sequential Methods for Coupled Geomechanics and Multiphase Flow*. PhD thesis, Stanford University, 2010.

- 
- Kitagawa, Y. An aspect of the water in clay minerals: An application of nuclear magnetic resonance spectroscopy to clay mineralogy. *American Mineralogist*, 57:751–764, 1972.
- Klinge, H., Boehme, J., Grisseman, C., Houben, G., Ludwig, R.-R., Rübél, A., Schelkes, K., Schildknecht, F., and Suckow, A. Description of the Gorleben site part 1: Hydrogeology of the overburden of the Gorleben salt dome. Bundesanstalt für Geowissenschaften und Rohstoffe (BGR), Hannover, 2007.
- Knowles, M. K., Borns, D., Fredrich, J., Holcomb, D., an David Zeuch, R. P., Dale, T., and Van Pelt, R. S. Testing the disturbed zone around a rigid inclusion in salt. In *Proceedings of the 4th Conference on the Mechanical Behavior of Salt*, pages 1–17, Rotterdam, 1996. A.A. Balkema.
- Konikow, L. F., Sanford, W. E., and Campbell, P. J. Constant-concentration boundary condition: Lessons from the HYDROCOIN variable-density groundwater benchmark problem. *Water Resources Research*, 33(10):2253–2261, 1997.
- Kostka, T. D. and Templeton, J. A. Coupled thermomechanical modeling using dissimilar geometries in Arpeggio. SAND2010–7746, Sandia National Laboratories, Albuquerque, NM, November 2010.
- Krause, W. B. Avery Island brine migration tests: Installation, operation, data collection, and analysis. ONWI-190(4), Office of Nuclear Waste Isolation, Columbus, OH, 1983.
- Krause, W. B. and Brodsky, N. S. Intracrystalline brine inclusion motion for Palo Duro unit 5 salt from the Mansfield no. 1 borehole in Oldham County, Texas. BMI/ONWI-663, Office of Nuclear Waste Isolation, Columbus, OH, 1987.
- Krieg, R. D., Morgan, H. S., and Hunter, T. O. Second benchmark problem for WIPP structural computations. SAND80–1331, Sandia National Laboratories, Albuquerque, NM, 1980.
- Krumhansl, J. L., Stein, C. L., Jarrell, G. D., and Kimball, K. M. Summary of WIPP Room B heater test brine and backfill material data. SAND90–0626, Sandia National Laboratories, Albuquerque, NM, 1991.
- Kuhlman, K. L. and Malama, B. Brine flow in heated geologic salt. SAND2013–1944, Sandia National Laboratories, Albuquerque, NM, March 2013.
- Kuhlman, K. L. and Malama, B. Assessment of contaminated brine fate and transport in MB139 at WIPP. SAND2014–16153, Sandia National Laboratories, Albuquerque, NM, 2014.
- Kuhlman, K. L. and Sevougian, S. D. Establishing the technical basis for disposal of heat-generating waste in salt. FCRD-UFD-2013–000233, US Department of Energy Used Fuel Disposition Campaign, Albuquerque, NM, 2013.
- Kuhlman, K. L., Wagner, S., Kicker, D., Kirkes, R., Herrick, C., and Guerin, D. Review and evaluation of salt R&D data for disposal of nuclear waste in salt. FCRD-UFD-2012–000380, US Department of Energy Used Fuel Disposition Campaign, Carlsbad, NM, September 2012.

- 
- Lai, C. S. *Fluid Flow through Rock Salt Under Various Stress States*. PhD thesis, Michigan State University, East Lansing, MI, 1971.
- Larsson, A. The international projects INTRACOIN, HYDROCOIN, and INTRAVAL. *Advances in Water Resources*, 15(1):85–87, 1992.
- Larsson, A., Pers, K., Skagius, K., and Dverstorp, B. The international INTRAVAL project: Phase 2, summary report. Swedish Nuclear Power Inspectorate (SKI), 1997.
- Lichtner, P. C., Hammond, G. E., Lu, C., Karra, S., Bisht, G., Andre, B., Mills, R. T., and Kumar, J. PFLOTRAN user manual: A massively parallel reactive flow and transport model for describing surface and subsurface processes. 2014.
- Lomenick, T. F. The siting record. ORNL/TM-12940, Oak Ridge National Laboratory, Oak Ridge, TN, 1996.
- Lowe, M. J. S. and Knowles, N. C. The community project COSA: Comparison of geo-mechanical computer codes for salt. EUR 10760 EN, Commission of the European Communities, 1986.
- Lowe, M. J. S. and Knowles, N. C. COSA II: Further benchmark exercises to compare geomechanical computer codes for salt. EUR 12135 EN, Commission of the European Communities, 1989.
- Lyly, M., Ruokolainen, J., and Järvinen, E. Elmer—a finite element solver for multiphysics. *CSC-report on scientific computing*, 2000:156–159, 1999. URL <http://www.csc.fi/english/pages/elmer>.
- Makedonska, N., Painter, S. L., Karra, S., and Gable, C. W. Numerical experiments on advective transport in large three-dimensional discrete fracture networks. In *American Geophysical Union Fall Meeting*, number H53A-1398, 2013.
- Martinez, M. J., Stone, C. M., Notz, P. K., Turner, D. Z., Hopkins, P. L., Subia, S., Jove-Colon, C., Moffat, H. K., Bean, J. E., Dewers, T., Klise, K., Red-Horse, J., Field, R., Mesh, M., Davidson, S., Yoon, H., Carnes, B., Alger, N., Bishop, J., and Newell, P. Computational thermal, chemical, fluid, and solid mechanics for geosystems management. SAND2011–6643, Sandia National Laboratories, Albuquerque, NM, September 2011.
- McTigue, D. F. Thermoelastic response of fluid-saturated rock. *Journal of Geophysical Research*, 91(B9):9533–9542, 1986.
- McTigue, D. F. Flow into a heated borehole in porous, thermoelastic rock: Analysis. *Water Resources Research*, 26(8):1763–1774, 1990.
- McTigue, D. F. Permeability and hydraulic diffusivity of Waste Isolation Pilot Plant repository salt inferred from small-scale brine inflow experiments. SAND92–1911, Sandia National Laboratories, Albuquerque, NM, June 1993.
- Morgan, H. S., Wallner, M., and Munson, D. E. Results of an international parallel calculations exercise comparing creep responses predicted with three computer codes for two excavations in rock salt. SAND87–2125, Sandia National Laboratories, Albuquerque, NM, 1987.

- 
- Morgan, K. Z. Health physics division annual progress report for period ending July 31, 1959. ORNL-2806, Oak Ridge National Laboratory, Oak Ridge, TN, 1959.
- Moridis, G. J., Freeman, C. M., Webb, S., and Finsterle, S. The REALGAS and REALGASH2O options of the TOUGH+ code for the simulation of coupled fluid and heat flow in tight/shale gas systems. In *Proceedings, TOUGH Symposium*, Berkeley, CA, September 2012. Lawrence Berkeley National Laboratory.
- Mualem, Y. A new model for predicting the hydraulic conductivity of unsaturated porous media. *Water Resources Research*, 12(3):513–521, 1976.
- Müller-Lyda, I., Birthler, H., and Fein, E. Ableitung von permeabilitäts-porositätsrelationen für salzgrus [Derivation of permeability-porosity relations for crushed salt]. GRS-148, Gesellschaft für Anlagen- und Reaktorsicherheit (GRS), Braunschweig, Germany, 1999.
- Munson, D. E. and Dawson, P. R. Constitutive model for the low temperature creep of salt (with application to WIPP). SAND79–1853, Sandia National Laboratories, Albuquerque, NM, 1979.
- Munson, D. E. and Morgan, H. S. Methodology for performing parallel design calculations (nuclear waste repository application). SAND85–0324, Sandia National Laboratories, Albuquerque, NM, 1986.
- Munson, D. E., Jones, R. L., Hoag, D. L., and Ball, J. R. Mining development test (Room D): In situ data report (March 1984 – May 1988) Waste Isolation Pilot Plant (WIPP) thermal/structural interactions program. SAND88–1460, Sandia National Laboratories, Albuquerque, NM, 1988.
- Munson, D. E., Fossum, A. F., and Senseny, P. E. Advances in resolution of discrepancies between predicted and measured in situ Waste Isolation Pilot Plant (WIPP) room closures. SAND88–2948, Sandia National Laboratories, Albuquerque, NM, 1989.
- Munson, D. E., Jones, R. L., Ball, J. R., Clancy, R. M., Hoag, D. L., and Petney, S. V. Overtest for simulated Defense High-Level Waste (Room B): In situ data report (May 1984–February 1988) Waste Isolation Pilot Plant (WIPP) Thermal/Structural Interactions program. SAND89–2671, Sandia National Laboratories, Albuquerque, NM, 1990.
- Munson, D. E., Christian-Frear, T. L., Baird, G. T., Labreche, D. A., Ball, J. R., Jones, R. L., and Northrop-Salazar, C. L. Intermediate scale borehole (Room C): in situ data report (January 1989–June 1993). SAND92–2470, Sandia National Laboratories, Albuquerque, NM, 1994.
- Munson, D. E., DeVries, K. L., Jensen, A. L., and Webb, S. W. Brine release based on structural calculations of damage around an excavation at the Waste Isolation Pilot Plant (WIPP). SAND95–1704C, Sandia National Laboratories, Albuquerque, NM, 1995a.
- Munson, D. E., Hoag, D. L., Ball, J. R., Baird, G. T., and Jones, R. L. Air intake shaft performance tests (shaft 5): in situ data report (May 1988–July 1995). SAND94–1311, Sandia National Laboratories, Albuquerque, NM, 1995b.
- Nield, D. A. and Bejan, A. *Convection in porous media*. Springer, third edition, 2006.



- 
- Notz, P. K., Subia, S. R., Hopkins, M. M., Moffat, H. K., and Noble, D. R. Aria 1.5: User manual. SAND2007–2734, Sandia National Laboratories, Albuquerque, NM, April 2007.
- Nowak, E. J. Preliminary result of brine migration studies in the Waste Isolation Pilot Plant (WIPP). SAND86–0720, Sandia National Laboratories, Albuquerque, NM, 1986.
- Nowak, E. J. and McTigue, D. F. Interim result of brine transport studies in the Waste Isolation Pilot Plant (WIPP). SAND87–0880, Sandia National Laboratories, Albuquerque, NM, 1987.
- Nowak, E. J., McTigue, D. F., and Beraun, R. Brine inflow to WIPP disposal rooms: Data, modeling, and assessment. SAND88–0112, Sandia National Laboratories, Albuquerque, NM, 1988.
- Olander, D. R. A model of brine migration and water transport in rock salt supporting a temperature gradient. *Nuclear Technology*, 58:256–270, 1982.
- Olander, D. R., Machiels, A. J., Balooch, M., and Yagnik, S. K. Thermal gradient migration of brine inclusions in synthetic alkali halide single crystals. *Journal of Applied Physics*, 53(1): 669–681, 1982.
- Olivella, S. and Gens, A. A constitutive model for crushed salt. *International Journal for Numerical and Analytical Methods in Geomechanics*, 26:719–746, 2002.
- Olivella, S., Carrera, J., Gens, A., and Alonso, E. E. Nonisothermal multiphase flow of brine and gas through saline media. *Transport in Porous Media*, 15:271–293, 1994.
- Olivella, S., Gens, A., Carrera, J., and Alonso, E. E. Numerical formulation for a simulator (CODE\_BRIGHT) for the coupled analysis of saline media. *Engineering Computations*, 13 (7):87–112, 1995.
- Olivella, S., Carrera, J., Gens, A., and Alonso, E. E. Porosity variations in saline media caused by temperature gradients coupled to multiphase flow and dissolution/precipitation. *Transport in Porous Media*, 25:1–25, 1996.
- Olivella, S., Castagna, S., Alonso, E. E., and Lloret, A. Porosity variations in saline media induced by temperature gradients: Experimental evidences and modelling. *Transport in Porous Media*, 90:763–777, 2011.
- Owen, L. B. and Schwendiman, L. Laboratory testing of salt samples for water content/loss of weight on heating, thermal fracture, insoluble residue, and clay and bulk mineralogy. BMI/ONWI/C-297, Office of Nuclear Waste Isolation, Columbus, OH, 1987.
- Parkhurst, D. L. and Appelo, C. A. J. Description of input and examples for PHREEQC version 3 – a computer program for speciation, batch-reaction, one-dimensional transport, and inverse geochemical calculations. Techniques and Methods Book 6, Chapter A43, US Geological Survey, Denver, CO, 2013.
- Peach, C. J. *Influence of Deformation on the Fluid Transport Properties of Salt Rocks*. PhD thesis, University of Utrecht, Netherlands, 1991.

- 
- Popielak, R. S., Beauheim, R. L., Black, S. R., Coons, W. E., Ellingson, C. T., and Olen, R. L. Brine reservoirs in the Castile Formation, Waste Isolation Pilot Plant (WIPP) project, southeastern New Mexico. WTSD-TME-3153, US Department of Energy, Albuquerque, NM, 1983.
- Potukuchi, S. and Wexler, A. S. Identifying solid-aqueous phase transitions in atmospheric aerosols – I. neutral-acidity solutions. *Atmospheric Environment*, 29(14):1663–1676, 1995.
- Powers, D. W., Lambert, S. J., Shaffer, S.-E., Hill, L. R., and Weart, W. D. Geologic characterization report, Waste Isolation Pilot Plant (WIPP) site, southeastern New Mexico. SAND78–1596 (2 Volumes), Sandia National Laboratories, Albuquerque, NM, 1978.
- Prevost, J. H. Two-way coupling in reservoir-geomechanical models: Vertex-centered Galerkin geomechanical model cell-centered and vertex-centered finite volume reservoir models. *International Journal for Numerical Methods in Engineering*, 98:612–624, 2014.
- Pruess, K. ECO2N: A TOUGH2 fluid property module for mixtures of water, NaCl, and CO<sub>2</sub>. LNL-57952, Lawrence Berkeley National Laboratory, Berkeley, CA, August 2005.
- Pruess, K., Oldenburg, C., and Moridis, G. TOUGH2 user's guide, version 2. LBNL-43134, Lawrence Berkeley National Laboratory, Berkeley, CA, September 2012.
- Pudewills, A. Numerical simulation of coupled thermo-hydro-mechanical processes in rock salt. In *Mechanical Behavior of Salt VII*, pages 115–122. MINES Paris Tech, Taylor & Francis, 2012.
- Rashed, M. G. Development and evaluation of an open source finite element analysis framework. In *Proceedings of the 1st International Conference on Civil Engineering for Sustainable Development*, Khulna: KUET, Bangladesh, 2012. URL <http://sfepy.org>.
- Ratigan, J. L. A finite element formulation for brine transport in rock salt. *International Journal for Numerical and Analytical Methods in Geomechanics*, 8:225–241, 1984.
- Reynolds, T. D. and Gloyna, E. F. Reactor fuel waste disposal project: Permeability of rock salt and creep of underground salt cavities. TID-12383, Atomic Energy Commission Division of Technical Information, Oak Ridge, TN, 1960.
- Roedder, E. and Bassett, R. L. Problems in determination of the water content of rock-salt samples and its significance in nuclear-waste storage siting. *Geology*, 9:525–530, 1981.
- Roest, J. P. A. Acoustic P-wave velocity measurements of cataclastic effects in rock salt. EUR 10857 EN, Nuclear Science and Technology Commission of the European Communities, Brussels, Belgium, 1987.
- Rothfuchs, T., Wiczorek, K., Feddersen, H. K., Stupendahl, G., Coyle, A. J., Kalia, H., and Eckert, J. Brine migration test, Asse salt mine, Federal Republic of Germany: Final report. GSF-Bericht 6/88, Office of Nuclear Waste Isolation (ONWI) and Gesellschaft für Strahlen- und Umweltforschung München (GSF), Munich, Germany, 1988.
- Rübel, A., Buhmann, D., Meleshyn, A., Mönig, J., and Spiessl, S. Aspects on the gas generation and migration in repositories for high level waste in salt formations. GRS-303, Gesellschaft für Anlagen- und Reaktorsicherheit (GRS), 2013.

- Rutqvist, J. Status of the TOUGH-FLAC simulator and recent applications related to coupled fluid flow and crustal deformations. *Computers & Geosciences*, 37:739–750, 2011.
- Rutqvist, J. and Tsang, C.-F. TOUGH-FLAC: A numerical simulator for analysis of coupled thermal-hydrological-mechanical processes in fractured and porous geologic media under multi-phase flow conditions. In *Proceedings, TOUGH Symposium*, 2003.
- Rutqvist, J., Blanco Martín, L., Kim, J., and Birkholzer, J. T. Modeling coupled THMC processes and brine migration in salt at high temperatures. FCRD-UFD-2013-000262, US Department of Energy Used Fuel Disposition Campaign, 2013.
- Rutqvist, J., Blanco Martín, L., Mukhopadhyay, S., Houseworth, J., and Birkholzer, J. Modeling coupled THMC processes and brine migration in salt at high temperatures. FCRD-UFD-2014-000341, US Department of Energy Used Fuel Disposition Campaign, August 2014.
- Salari, K. and Knupp, P. Code verification by the method of manufactured solutions. SAND2000-1444, Sandia National Laboratories, Albuquerque, NM, June 2000.
- Salzer, K., Popp, T., and Böhnel, H. Mechanical and permeability properties of highly pre-compacted granular salt bricks. In Lux, K.-H., Minkley, W., Wallner, M., and Hardy, H. R. Jr., editors, *Proceedings of the Sixth Conference on the Mechanical Behavior of Salt*, pages 239–248, Hannover, 2007. Francis & Taylor (Balkema).
- Salzer, K., Günther, R. M., Minkley, W., Popp, T., Wiedemann, M., Hampel, A., Pudewills, A., Leuger, B., Zapf, D., Staudtmeister, K., Rokahr, R., Herchen, K., Wolters, R., and Lux, K.-H. Joint projects on the comparison of constitutive models for the mechanical behavior of rock salt – I. overview of the projects, reference mine for 3-D benchmark calculations, in-situ measurements and laboratory tests. In *Mechanical Behavior of Salt VII*, pages 221–230. MINES Paris Tech, Taylor & Francis, 2012.
- Sassani, D. C., Jové Colón, C. F., Weck, P., Jerden, J. L. Jr., Frey, K. E., Cruse, T., Ebert, W. L., Buck, E. C., Wittman, R. S., Skomusrski, F. N., Cantrell, K. J., McNamara, B. K., and Soderquist, C. Z. Integration of EBS models with generic disposal system models. FCRD-UFD-2012-000277, US Department of Energy Used Fuel Disposition Campaign, September 2012.
- Sassani, D. C., Jové Colón, C. F., Weck, P., Jerden, J. L. Jr., Frey, K. E., Cruse, T., Ebert, W. L., Buck, E. C., and Wittman, R. S. Used fuel degradation: Experimental and modeling report. FCRD-UFD-2013-000404, US Department of Energy Used Fuel Disposition Campaign, October 2013.
- Satterfield, C. N. *Mass Transfer in Heterogeneous Catalysis*. MIT Press, 1970.
- Saulnier, G. J. Jr., Domski, P. S., Palmer, J. B., Roberts, R. M., Stensrud, W. A., and Jensen, A. L. Waste Isolation Pilot Plant Salado hydrology program data report #1. SAND90-7000, Sandia National Laboratories, Albuquerque, NM, May 1991.
- Schenk, O. and Urai, J. L. The migration of fluid-filled grain boundaries in recrystallizing synthetic bischofite: first results of in-situ high-pressure, high-temperature deformation experiments in transmitted light. *Journal of Metamorphic Geology*, 23:695–709, 2005.

- 
- Schlich, M. and Jockwer, N. Simulation of water transport in heated rock salt. In *MRS Proceedings - Symposium STOCKHOLM - Scientific Basis for Nuclear Waste Management IX*, volume 50, pages 577–585, 1985.
- Schneider, A. Enhancement of the codes d<sup>3</sup>f and r<sup>3</sup>t. GRS-292, Gesellschaft für Anlagen- und Raktosicherheit (GRS), March 2012.
- Schneider, A., Kröhn, K.-P., and Püschel, A. Developing a modelling tool for density-driven flow in complex hydrogeological structures. *Computing and Visualization in Science*, 15(4):163–168, 2012.
- Schulze, O., Heemann, U., Zetsche, F., Hampel, A., Pudewills, A., Günther, R. M., Minkley, W., Salzer, K., Hou, Z., Wolters, R., Rokahr, R., and Zapf, D. Comparison of advanced constitutive models for the mechanical behavior of rock salt – results from a joint research project I. modeling of deformation processes and benchmark calculations. In *6th Conference on the Mechanical Behavior of Salt: Understanding of THMC Processes in Salt Rocks*. Federal Institute for Geosciences and Natural Resources (BGR), Germany, Taylor & Francis, May 2007.
- Senseny, P. E., Hansen, F. D., Russell, J. E., Carter, N. L., and Handin, J. W. Mechanical behavior of rock salt: Phenomenology and micromechanisms. *International Journal of Rock Mechanics and Mining Sciences & Geomechanics Abstracts*, 29(4):363–378, 1992.
- Serata, S. and Gloyna, E. F. Reactor Fuel Waste Disposal Project: Development of design principle for disposal of reactor fuel into underground salt cavities. Sanitary Engineering Research Laboratory, Civil Engineering Department, University of Texas, Austin, TX, 1959.
- Shelfbine, H. C. Brine migration: A summary report. SAND82–0152, Sandia National Laboratories, Albuquerque, NM, 1982.
- Sherer, N. M., editor. *Proceedings of Salt Repository Project's Workshop on Brine Migration, University of California-Berkeley, April 17–19, 1985*, number PNL/SRP-SA 14341, 1987. Pacific Northwest National Laboratory.
- SIERRA Solid Mechanics Team. Adagio 4.20 user's guide. SAND2011–1825, Sandia National Laboratories, Albuquerque, NM, March 2011.
- SKI. INTRACOIN, final report level 1, code verification. SKI 84:3, Swedish Nuclear Power Inspectorate (SKI), Stockholm, Sweden, 1984.
- SKI. INTRACOIN, final report levels 2 and 3, model validation and uncertainty analysis. SKI 86:2, Swedish Nuclear Power Inspectorate (SKI), Stockholm, Sweden, 1986.
- SKI. The international HYDROCOIN project. groundwater hydrology modelling strategies for performance assessment of nuclear waste disposal: Summary report. OECD Nuclear Energy Agency, Paris, France, 1992.
- SNL. Evaluation of options for permanent geologic disposal of spent nuclear fuel and high-level radioactive waste in support of a comprehensive national fuel cycle strategy (2 volumes). FCRD-UFD-2013–000371 Rev 1, US Department of Energy Used Fuel Disposition Campaign, Albuquerque, NM, April 2014.

- 
- Spiers, C. J., Urai, J. L., Lister, G. S., Boland, J. N., and Zwart, H. J. The influence of fluid-rock interactions on the rheology of salt rock. EUR 10399 EN, Nuclear Science and Technology, Commission of the European Communities, Brussels, Belgium, 1986.
- Spiers, C. J., Peach, C. J., Brzesowsky, R. H., Schutjens, P. M. T. M., Liezenberg, J. L., and Zwart, H. J. Long-term rheological and transport properties of dry and wet salt rocks. EUR 11848 EN, Nuclear Science and Technology, Commission of the European Communities, Brussels, Belgium, 1988.
- Stauffer, P. H., Harp, D. R., and Robinson, B. A. Model development and analysis of the fate and transport of water in a salt-based repository. LA-UR-12-25050, Los Alamos National Laboratory, Los Alamos, NM, September 2012.
- Stauffer, P. H., Harp, D. R., Jordan, A. B., Lu, Z., Kelkar, S., Kang, Q., Ten Cate, J., Boukhalfa, H., Labyed, Y., Reimus, P. W., Caporuscio, F. A., Miller, T. A., and Robinson, B. A. Coupled model for heat and water transport in a high level waste repository in salt. LA-UR-13-27584, Los Alamos National Laboratory, Los Alamos, NM, September 2013.
- Stein, C. L. Mineralogy in the Waste Isolation Pilot Plant (WIPP) facility stratigraphic horizon. SAND85-0321, Sandia National Laboratories, Albuquerque, NM, 1985.
- Steininger, W. US-German workshop on salt repository research, design, and operation. KIT-SR 7569, Karlsruhe Institute of Technology, Karlsruhe, Germany, 2010.
- Stensrud, W. A., Dale, T. F., Domski, P. S., Palmer, J. B., Roberts, R. M., Fort, M. D., Saulnier, G. J. Jr., and Jensen, A. L. Waste Isolation Pilot Plant Salado hydrology program data report #2. SAND92-7072, Sandia National Laboratories, Albuquerque, NM, December 1992.
- Stephens, D. B. *Vadose Zone Hydrology*. CRC Press, 1996.
- Stewart, J. R. and Edwards, H. C. *Large-Scale PDE-Constrained Optimization*, chapter The SIERRA framework for developing advanced parallel mechanics applications, pages 301–315. Springer, 2003.
- Stone, C. M., Holland, J. F., Bean, J. E., and Arguello, J. G. Coupled thermal-mechanical analyses of a generic salt repository for high level waste. In *44th US Rock Mechanics / Geomechanics Symposium and 5th US-Canadian Rock Mechanics Symposium*, number ARMA 10-180, 2010.
- Stormont, J. C. *Gas Permeability Changes in Rock Salt During Deformation*. PhD thesis, University of Arizona, 1990a.
- Stormont, J. C. Discontinuous behavior near excavations in a bedded salt formation. *International Journal of Mining and Geological Engineering*, 8:35–56, 1990b.
- Stormont, J. C. Conduct and interpretation of gas permeability measurements in rock salt. *International Journal of Rock Mechanics and Mining Sciences*, 34(3–4):303.e1–303.e11, 1997a.
- Stormont, J. C. In situ gas permeability measurements to delineate damage in rock salt. *International Journal of Rock Mechanics, Mineral Science & Geomechanics Abstracts*, 34(7): 1055–1064, 1997b.

- 
- Stormont, J. C. and Daemen, J. J. K. Laboratory study of gas permeability changes in rock salt during deformation. *International Journal of Rock Mechanics, Mineral Science & Geomechanics Abstracts*, 29(4):325–342, 1992.
- Stormont, J. C. and Fuenkajorn, K. Dilation-induced permeability changes in rock salt. SAND93–2670C, Sandia National Laboratories, Albuquerque, NM, 1993.
- Stormont, J. C., Peterson, E. W., and Lagus, P. L. Summary of and observations about WIPP facility flow measurements through 1986. SAND87–0176, Sandia National Laboratories, Albuquerque, NM, 1987.
- Stormont, J. C., Howard, C. L., and Daemen, J. J. K. In situ measurements of rock salt permeability changes due to nearby excavation. SAND90–3134, Sandia National Laboratories, Albuquerque, NM, 1991a.
- Stormont, J. C., Howard, C. L., and Daemen, J. J. K. Changes in rock salt permeability due to nearby excavation. SAND91–0269, Sandia National Laboratories, Albuquerque, NM, 1991b.
- Stormont, J. C., Daemen, J. J. K., and Desai, C. S. Prediction of dilation and permeability changes in rock salt. *International Journal for Numerical and Analytical Methods in Geomechanics*, 16: 545–569, 1992.
- Sutherland, H. J. and Cave, S. P. Argon gas permeability of New Mexico rock salt under hydrostatic compression. *International Journal of Rock Mechanics, Mineral Science & Geomechanics Abstracts*, 17:281–288, 1980.
- Tsang, C.-F. Introductory editorial to the special issue on the DECOVALEX-THMC project. *Environmental Geology*, 57:1217–1219, 2009.
- Tyler, L. D., Matalucci, R. V., Molecke, M. A., Munson, D. E., Nowak, E. J., and Stormont, J. C. Summary report for the WIPP technology development program for isolation of radioactive waste. SAND88–0844, Sandia National Laboratories, Albuquerque, NM, April 1988.
- UFD Campaign. Used Fuel Disposition (UFD) campaign disposal research and development roadmap. FCR&D-USED-2011–000065 REV 1, US Department of Energy Used Fuel Disposition Campaign, September 2012.
- Urai, J. L., Spiers, C. J., Zwart, H. J., and Lister, G. S. Weakening of rock salt by water during long-term creep. *Nature*, 324:554–557, 1986.
- Urai, J. L., Schléder, Z., Spiers, C. J., and Kukla, P. A. *Dynamics of Complex Intracontinental Basins*, chapter Flow and Transport Properties of Salt Rocks. Springer-Verlag, Berlin, Germany, 2008.
- van Genuchten, M. T. A closed-form equation for predicting the hydraulic conductivity of unsaturated soils. *The Soil Science Society of America Journal*, 44(5):892–898, 1980.
- Van Sambeek, L. L. Measurements of humidity-enhanced salt creep in salt mines: proving the Joffe effect. In *Mechanical Behavior of Salt VII*, pages 315–326. MINES Paris Tech, Taylor & Francis, 2012.

- Van Sambeek, L. L., Luo, D. D., Lin, M. S., Ostrowski, W., and Oyenuga, D. Seal design alternatives study. SAND92-7340, Sandia National Laboratories, Albuquerque, NM, 1993a.
- Van Sambeek, L. L., Ratigan, J. L., and Hansen, F. D. Dilatancy of rock salt in laboratory tests. *International Journal of Rock Mechanics and Mining Sciences & Geomechanics Abstracts*, 30 (7):735-738, 1993b.
- van Weert, F. H. A. and Hassanizadeh, S. M. INTRAVAL phase 2, Gorleben test case. interpretation of the Weisses Moor pumping test. RIVM-715206004, Rijksinstituut voor Volksgezondheid en Milieuhygiene (RIVM), February 1994.
- Wang, H. F. *Theory of linear poroelasticity with applications to geomechanics and hydrogeology*. Princeton University Press, 2000.
- Warrick, A. W. *Soil water dynamics*. Oxford University Press, 2003.
- Wawersik, W. R. and Stone, C. M. A characterization of pressure records in inelastic rock demonstrated by hydraulic fracturing measurements in salt. *International Journal of Rock Mechanics and Mining Sciences & Geomechanics Abstracts*, 26(6):613-627, 1989.
- Wawersik, W. R., Carlson, L. W., Henfling, J. A., Borns, D. J., Beauheim, R. L., Howard, C. L., and Roberts, R. M. Hydraulic fracturing tests in anhydrite interbeds in the WIPP, Marker Beds 139 and 140. SAND95-0596, Sandia National Laboratories, Albuquerque, NM, 1997.
- Webb, S. W. EOS7C-ECBM version 1.0: Additions for enhanced coal bed methane including the dusty gas model. CRC2011-0002, Canyon Ridge Consulting, Sandia Park, NM, 2011.
- Wieczorek, K., Förster, B., Rothfuchs, T., Zhang, C.-L., Olivella, S., Kamlot, P., Günther, R.-M., and Lerch, C. THERESA subproject MOLDAU: Coupled thermal-hydrological-mechanical-chemical processes in repository safety assessment. GRS-262, Gesellschaft für Anlagen- und Reaktorsicherheit (GRS), 2010.
- Wigley, M. R. and Russell, J. E. Comparison of solutions to benchmark problems in salt using different numerical methods. In *National Waste Terminal Storage Program Information Meeting*, number ONWI-212, pages 320-325, December 1980.
- Wilcox, W. R. Removing inclusions from crystals by gradient techniques. *Industrial & Engineering Chemistry*, 60(3):12-23, 1968.
- Wilcox, W. R. Anomalous gas-liquid inclusion movement. *Industrial & Engineering Chemistry*, 61:76-77, 1969.
- Wolters, R., Lux, K.-H., and Düsterloh, U. Evaluation of rock salt barriers with respect to tightness: Influence of thermomechanical damage, fluid infiltration and sealing/healing. In *Mechanical Behavior of Salt VII*, pages 435-440. MINES Paris Tech, Taylor & Francis, 2012.
- Xu, T., Sonnenthal, E., Pycher, N., and Pruess, K. TOUGHREACT user's guide: A simulation program for non-isothermal multiphase reactive geochemical transport in variably saturated geologic media. LBNL-55460 V1.2, Lawrence Berkeley National Laboratory, Berkeley, CA, December 2006.

Zhang, K., Wu, Y.-S., and Pruess, K. User's guild for TOUGH2-MP - a massively parallel version of the TOUGH2 code. LBNL-315E, Lawrence Berkeley National Laboratory, Berkeley, CA, May 2008.

Zienkiewicz, O. C., Chan, A. H. C., Pastor, M., Schrefler, B. A., and Shiomi, T. *Computational geomechanics*. Wiley Chichester, 1999.

Zoback, M. *Reservoir Geomechanics*. Cambridge, 2007.

Zyvoloski, G. A., Robinson, B. A., Dash, Z. V., and Trease, L. L. Models and methods summary for the FEHM application. SC-194, Los Alamos National Laboratory, Los Alamos, NM, July 1999.

Zyvoloski, G. A., Robinson, B. A., Dash, Z. V., Kelkar, S., Viswanathan, H. S., Pawar, R. J., and Stauffer, P. H. *Software Users Manual (UM) for the FEHM Application Version 3.1–3.X*. Los Alamos National Laboratory, Los Alamos, NM, 2011.



# Appendix A PFLOTRAN input files

## A.1 Saturated Initial Condition

```
1 ! uniform initial condition for DRZ, based on 1D calculation
2
3 !===== flow mode
4 MODE GENERAL MORE
5   TWO_PHASE_ENERGY_DOF TEMPERATURE
6   MAXIMUM_PRESSURE_CHANGE 1e5
7 END
8
9 FLUID_PROPERTY
10  DIFFUSION_COEFFICIENT 1.d-9
11 END
12
13 EOS WATER
14  VISCOSITY CONSTANT 8.5077d-4
15 END
16
17 EOS GAS
18  VISCOSITY CONSTANT 9.0829d-6
19 END
20
21 TIMESTEPPER FLOW
22  TS_ACCELERATION 10
23  DT_FACTOR 2.d0 2.d0 1.8d0 1.6d0 1.4d0 1.2d0 1.d0 0.8d0 0.6d0 0.5d0
24 END
25
26 NEWTON_SOLVER FLOW
27  RTOL 1.d-30
28  ATOL 1.d-30
29  STOL 1.d-30
30  ITOL_RES 1.d-5
31  ITOL_SCALED_RESIDUAL 1.d-6
32  ITOL_RELATIVE_UPDATE 1.d-6
33  MAXIT 20
34 END
35
36 !===== discretization
37 GRID
38  TYPE structured
39  NXYZ 400 1 1
40  DXYZ
41    2.5D-2
42    1.0D0
43    1.0D0
44  END
45 END
46
47 !===== material properties
48 !===== saturation functions
49
50 MATERIAL_PROPERTY AIR
```

```
51 ID 1
52 SATURATION_FUNCTION air_sf
53 POROSITY 0.99
54 TORTUOSITY 1.0
55 ROCK_DENSITY 1.2
56 THERMAL_CONDUCTIVITY_DRY 14.0
57 THERMAL_CONDUCTIVITY_WET 14.0
58 SPECIFIC_HEAT 1012.0
59 SOIL_REFERENCE_PRESSURE 1.0132e+05
60 PERMEABILITY
61   PERM_ISO 1.0E-11
62 END
63 END
64
65 SATURATION_FUNCTION air_sf
66 SATURATION_FUNCTION_TYPE BROOKS_COREY
67 PERMEABILITY_FUNCTION_TYPE BURDINE
68 RESIDUAL_SATURATION GAS 0.0
69 RESIDUAL_SATURATION LIQUID 0.0
70 LAMBDA 0.7
71 ALPHA 0.35 ! 3E-5 atm air-entry pressure
72 END
73
74
75 MATERIAL_PROPERTY HALITE
76 ID 2
77 POROSITY 0.01
78 TORTUOSITY 1.0
79 ROCK_DENSITY 2163.0
80 THERMAL_CONDUCTIVITY_DRY 5.4
81 THERMAL_CONDUCTIVITY_WET 5.4
82 SPECIFIC_HEAT 862.8
83 SOIL_REFERENCE_PRESSURE 1.0132e+05
84 SATURATION_FUNCTION HALITE_sf
85 PERMEABILITY
86   PERM_ISO 5.0E-20
87 END
88 END
89
90 SATURATION_FUNCTION HALITE_sf ! SAND94-0472 v.1 fig 39
91 SATURATION_FUNCTION_TYPE BROOKS_COREY
92 PERMEABILITY_FUNCTION_TYPE BURDINE
93 RESIDUAL_SATURATION GAS 0.2
94 RESIDUAL_SATURATION LIQUID 0.2
95 MAX_CAPILLARY_PRESSURE 1.0E+8
96 LAMBDA 0.7
97 ALPHA 0.65E-6
98 END
99
100
101 MATERIAL_PROPERTY DRZ ! using MB139 core data SAND94-0472 Table 12
102 ID 3
103 POROSITY 0.05
104 ROCK_DENSITY 2190.0
105 THERMAL_CONDUCTIVITY_DRY 4.21
106 THERMAL_CONDUCTIVITY_WET 4.21
107 SPECIFIC_HEAT 862.8
108 SOIL_REFERENCE_PRESSURE 1.0132e+05
109 SATURATION_FUNCTION DRZ_sf
110 PERMEABILITY
111   PERM_ISO 1.0E-17
112 END
113 END
114
115 SATURATION_FUNCTION DRZ_sf
116 SATURATION_FUNCTION_TYPE BROOKS_COREY
117 PERMEABILITY_FUNCTION_TYPE BURDINE
118 RESIDUAL_SATURATION GAS 0.0
```

```
119 RESIDUAL_SATURATION LIQUID 0.0
120 MAX_CAPILLARY_PRESSURE 1.0E+8
121 LAMBDA 0.644
122 ALPHA 9.8692e-6 ! 1 atm air-entry pressure
123 END
124
125
126 !===== output options
127 OUTPUT
128   FORMAT HDF5
129   PERIODIC TIME 1.0 d between 0.0 d and 10.0 d
130   PERIODIC TIME 10.0 d between 10.0 d and 100.0 d
131   PERIODIC TIME 100.0 d between 100.0 d and 1000.0 d
132   PERIODIC TIME 1000.0 d between 1000.0 d and 100000.0 d
133   PERIODIC_OBSERVATION timestep 1
134   VARIABLES
135     GAS_PRESSURE
136     GAS_SATURATION
137     LIQUID_PRESSURE
138     LIQUID_SATURATION
139     GAS_MOBILITY
140     LIQUID_MOBILITY
141     THERMODYNAMIC_STATE
142   END
143   VELOCITY_AT_FACE
144   MASS_BALANCE
145 END
146
147 !===== times
148 TIME
149   FINAL_TIME 100000.0 d
150   INITIAL_TIMESTEP_SIZE 1.0E-7 d
151   MAXIMUM_TIMESTEP_SIZE 100.0 d
152 END
153
154 !===== regions
155 REGION all
156   COORDINATES
157     0.0d0 0.0d0 0.0d0
158     1.0d+1 1.0d0 1.0d0
159   END
160 END
161
162 ! end of 1D domain in far field
163 REGION farfield_face
164   FACE EAST
165   COORDINATES
166     1.0d+1 0.0d0 0.0d0
167     1.0d+1 1.0d0 1.0d0
168   END
169 END
170
171 ! end of 1D domain in excavation
172 ! this isn't the air/salt interface (x=0.3 m)
173 REGION room_face
174   FACE WEST
175   COORDINATES
176     0.0d0 0.0d0 0.0d0
177     0.0d0 1.0d0 1.0d0
178   END
179 END
180
181 REGION excavation_air
182   COORDINATES ! first 0.3 m of domain
183     0.0d0 0.0d0 0.0d0
184     0.3d0 1.0d0 1.0d0
185   END
186 END
```

```
187
188 REGION drz_salt
189   COORDINATES   ! next 2.5 m of domain
190     0.3d0 0.0d0 0.0d0
191     2.8d0 1.0d0 1.0d0
192   END
193 END
194
195 REGION intact_salt
196   COORDINATES   ! from 2.5 m to end of domain (10m)
197     2.8d0 0.0d0 0.0d0
198     1.0d+1 1.0d0 1.0d0
199   END
200 END
201
202 !===== flow conditions
203
204 FLOW_CONDITION atmospheric
205   TYPE
206     GAS_PRESSURE DIRICHLET
207     LIQUID_SATURATION DIRICHLET
208     TEMPERATURE DIRICHLET
209   END
210   GAS_PRESSURE 0.101325E+6
211   LIQUID_SATURATION 0.01
212   TEMPERATURE 27.0
213 END
214
215 FLOW_CONDITION hydrostatic
216   TYPE
217     LIQUID_PRESSURE DIRICHLET
218     MOLE_FRACTION DIRICHLET
219     TEMPERATURE DIRICHLET
220   END
221   LIQUID_PRESSURE 6.0E+6
222   MOLE_FRACTION 1.d-10
223   TEMPERATURE 27.0
224 END
225
226 !===== condition couplers
227 INITIAL_CONDITION
228   FLOW_CONDITION hydrostatic
229   REGION drz_salt
230 END
231
232 INITIAL_CONDITION
233   FLOW_CONDITION hydrostatic
234   REGION intact_salt
235 END
236
237 INITIAL_CONDITION
238   FLOW_CONDITION atmospheric
239   REGION excavation_air
240 END
241
242 BOUNDARY_CONDITION far_field
243   FLOW_CONDITION hydrostatic
244   REGION farfield_face
245 END
246
247 BOUNDARY_CONDITION room
248   FLOW_CONDITION atmospheric
249   REGION room_face
250 END
251
252 !===== stratigraphy couplers
253 STRATA
254   MATERIAL AIR
```

```

255 REGION excavation_air
256 END
257
258 STRATA
259 MATERIAL DRZ
260 REGION drz_salt
261 END
262
263 STRATA
264 MATERIAL HALITE
265 REGION intact_salt
266 END

```

## A.2 Nonuniform Saturation Initial Condition

```

1 ! nonuniform initial condition for DRZ, based on 1D calculation
2
3 !===== flow mode
4 MODE GENERAL MORE
5 TWO_PHASE_ENERGY_DOF TEMPERATURE
6 MAXIMUM_PRESSURE_CHANGE 1e5
7 END
8
9 FLUID_PROPERTY
10 DIFFUSION_COEFFICIENT 1.d-9
11 END
12
13 EOS WATER
14 VISCOSITY CONSTANT 8.5077d-4
15 END
16
17 EOS GAS
18 VISCOSITY CONSTANT 9.0829d-6
19 END
20
21 TIMESTEPPER FLOW
22 TS_ACCELERATION 10
23 DT_FACTOR 2.d0 2.d0 1.8d0 1.6d0 1.4d0 1.2d0 1.d0 0.8d0 0.6d0 0.5d0
24 END
25
26 NEWTON_SOLVER FLOW
27 RTOL 1.d-30
28 ATOL 1.d-30
29 STOL 1.d-30
30 ITOL_SCALED_RESIDUAL 1.d-6
31 ITOL_RELATIVE_UPDATE 1.d-6
32 MAXIT 20
33 END
34
35 !===== discretization
36 GRID
37 TYPE structured
38 NXYZ 400 1 1
39 DXYZ
40 2.5D-2
41 1.0D0
42 1.0D0
43 END
44 END
45
46 !===== material properties
47 !===== saturation functions
48
49 MATERIAL_PROPERTY AIR
50 ID 1
51 SATURATION_FUNCTION air_sf

```

```
52 POROSITY 0.99
53 TORTUOSITY 1.0
54 ROCK_DENSITY 1.2
55 THERMAL_CONDUCTIVITY_DRY 14.0
56 THERMAL_CONDUCTIVITY_WET 14.0
57 SPECIFIC_HEAT 1012.0
58 SOIL_REFERENCE_PRESSURE 1.0132e+05
59 PERMEABILITY
60     PERM_ISO 1.0E-11
61 END
62 END
63
64 SATURATION_FUNCTION air_sf
65     SATURATION_FUNCTION_TYPE BROOKS_COREY
66     PERMEABILITY_FUNCTION_TYPE BURDINE
67     RESIDUAL_SATURATION GAS 0.0
68     RESIDUAL_SATURATION LIQUID 0.0
69     LAMBDA 0.7
70     ALPHA 0.35 ! 3E-5 atm air-entry pressure
71 END
72
73
74 MATERIAL_PROPERTY HALITE
75     ID 2
76     POROSITY 0.01
77     TORTUOSITY 1.0
78     ROCK_DENSITY 2163.0
79     THERMAL_CONDUCTIVITY_DRY 5.4
80     THERMAL_CONDUCTIVITY_WET 5.4
81     SPECIFIC_HEAT 862.8
82     SOIL_REFERENCE_PRESSURE 1.0132e+05
83     SATURATION_FUNCTION HALITE_sf
84     PERMEABILITY
85         PERM_ISO 5.0E-20
86     END
87 END
88
89 SATURATION_FUNCTION HALITE_sf
90     SATURATION_FUNCTION_TYPE BROOKS_COREY
91     PERMEABILITY_FUNCTION_TYPE BURDINE
92     RESIDUAL_SATURATION GAS 0.2
93     RESIDUAL_SATURATION LIQUID 0.2
94     MAX_CAPILLARY_PRESSURE 1.0E+8
95     LAMBDA 0.7
96     ALPHA 0.65E-6
97 END
98
99
100 MATERIAL_PROPERTY DRZ
101     ID 3
102     POROSITY 0.05
103     ROCK_DENSITY 2190.0
104     THERMAL_CONDUCTIVITY_DRY 4.21
105     THERMAL_CONDUCTIVITY_WET 4.21
106     SPECIFIC_HEAT 862.8
107     SOIL_REFERENCE_PRESSURE 1.0132e+05
108     SATURATION_FUNCTION DRZ_sf
109     PERMEABILITY
110         PERM_ISO 1.0E-17
111     END
112 END
113
114 SATURATION_FUNCTION DRZ_sf
115     SATURATION_FUNCTION_TYPE BROOKS_COREY
116     PERMEABILITY_FUNCTION_TYPE BURDINE
117     RESIDUAL_SATURATION GAS 0.0
118     RESIDUAL_SATURATION LIQUID 0.0
119     MAX_CAPILLARY_PRESSURE 1.0E+8
```

```
120 LAMBDA 0.644
121 ALPHA 9.8692e-6 ! 1 atm air-entry pressure
122 END
123
124
125 !===== output options
126 OUTPUT
127   FORMAT HDF5
128   PERIODIC TIME 1.0 d between 0.0 d and 10.0 d
129   PERIODIC TIME 10.0 d between 10.0 d and 100.0 d
130   PERIODIC TIME 100.0 d between 100.0 d and 1000.0 d
131   PERIODIC TIME 1000.0 d between 1000.0 d and 100000.0 d
132   PERIODIC_OBSERVATION timestep 1
133   VARIABLES
134     GAS_PRESSURE
135     GAS_SATURATION
136     LIQUID_PRESSURE
137     LIQUID_SATURATION
138     GAS_MOBILITY
139     LIQUID_MOBILITY
140     THERMODYNAMIC_STATE
141   END
142   VELOCITY_AT_FACE
143   MASS_BALANCE
144 END
145
146 !===== times
147 TIME
148   FINAL_TIME 100000.0 d
149   INITIAL_TIMESTEP_SIZE 1.0E-7 d
150   MAXIMUM_TIMESTEP_SIZE 20.0 d
151 END
152
153 !===== regions
154 REGION all
155   COORDINATES
156     0.0d0 0.0d0 0.0d0
157     1.0d+1 1.0d0 1.0d0
158   END
159 END
160
161 ! end of 1D domain in far field
162 REGION farfield_face
163   FACE EAST
164   COORDINATES
165     1.0d+1 0.0d0 0.0d0
166     1.0d+1 1.0d0 1.0d0
167   END
168 END
169
170 ! end of 1D domain in excavation
171 ! this isn't the air/salt interface (x=0.3 m)
172 REGION room_face
173   FACE WEST
174   COORDINATES
175     0.0d0 0.0d0 0.0d0
176     0.0d0 1.0d0 1.0d0
177   END
178 END
179
180 REGION excavation_air
181   COORDINATES ! first 0.3 m of domain
182     0.0d0 0.0d0 0.0d0
183     0.3d0 1.0d0 1.0d0
184   END
185 END
186
187 REGION drz_salt
```

```

188 COORDINATES ! next 2.5 m of domain
189 0.3d0 0.0d0 0.0d0
190 2.8d0 1.0d0 1.0d0
191 END
192 END
193
194 REGION intact_salt
195 COORDINATES ! from 2.5 m to end of domain (10m)
196 2.8d0 0.0d0 0.0d0
197 1.0d+1 1.0d0 1.0d0
198 END
199 END
200
201 !===== flow conditions
202
203 FLOW_CONDITION atmospheric
204 TYPE
205 GAS_PRESSURE DIRICHLET
206 LIQUID_SATURATION DIRICHLET
207 TEMPERATURE DIRICHLET
208 END
209 GAS_PRESSURE 0.101325E+6
210 LIQUID_SATURATION 0.01
211 TEMPERATURE 27.0
212 END
213
214
215 FLOW_CONDITION farfield
216 TYPE
217 LIQUID_PRESSURE DIRICHLET
218 MOLE_FRACTION DIRICHLET
219 TEMPERATURE DIRICHLET
220 END
221 LIQUID_PRESSURE 6.0E+6
222 MOLE_FRACTION 1.d-6
223 TEMPERATURE 27.0
224 END
225
226 FLOW_CONDITION hydrostatic_intact
227 TYPE
228 LIQUID_PRESSURE DIRICHLET
229 MOLE_FRACTION DIRICHLET
230 TEMPERATURE DIRICHLET
231 END
232 LIQUID_PRESSURE 6.0E+6
233 MOLE_FRACTION 1.d-6
234 TEMPERATURE 27.0
235 END
236
237 FLOW_CONDITION hydrostatic_drz
238 TYPE
239 GAS_PRESSURE DIRICHLET
240 LIQUID_SATURATION DIRICHLET
241 TEMPERATURE DIRICHLET
242 END
243 GAS_PRESSURE 6.0E+6
244 LIQUID_SATURATION 0.4
245 TEMPERATURE 27.0
246 END
247
248
249 !===== condition couplers
250
251 INITIAL_CONDITION
252 FLOW_CONDITION hydrostatic_drz
253 REGION drz_salt
254 END
255

```



---

```
256 INITIAL_CONDITION
257   FLOW_CONDITION hydrostatic_intact
258   REGION intact_salt
259 END
260
261 INITIAL_CONDITION
262   FLOW_CONDITION atmospheric
263   REGION excavation_air
264 END
265
266
267 BOUNDARY_CONDITION far_field
268   FLOW_CONDITION farfield
269   REGION farfield_face
270 END
271
272 BOUNDARY_CONDITION room
273   FLOW_CONDITION atmospheric
274   REGION room_face
275 END
276
277 !===== stratigraphy couplers
278 STRATA
279   MATERIAL AIR
280   REGION excavation_air
281 END
282
283 STRATA
284   MATERIAL DRZ
285   REGION drz_salt
286 END
287
288 STRATA
289   MATERIAL HALITE
290   REGION intact_salt
291 END
```